5-2011

Impacts of climate change and weather modification on hydrologic characteristics of watersheds in the western United States

Anil Acharya
University of Nevada, Las Vegas

IMPACTS OF CLIMATE CHANGE AND WEATHER MODIFICATION ON HYDROLOGIC CHARACTERISTICS OF WATERSHEDS IN THE WESTERN UNITED STATES

by

Anil Acharya

Bachelor of Science in Civil Engineering
Institute of Engineering, Tribhuvan University, Nepal
2003

Master of Science in Water Engineering and Management
Asian Institute of Technology, Thailand
2006

A dissertation submitted in partial fulfillment
of the requirements for the

Doctor of Philosophy in Engineering
Department of Civil and Environmental Engineering
Howard R. Hughes College of Engineering

Graduate College
University of Nevada, Las Vegas
May 2011

THE GRADUATE COLLEGE

We recommend the dissertation prepared under our supervision by

Anil Acharya

entitled

Impacts of Climate Change and Weather Modification on Hydrologic Characteristics of Watersheds in the Western United States

be accepted in partial fulfillment of the requirements for the degree of

Doctor of Philosophy in Engineering
Department of Civil and Environmental Engineering

Thomas C. Piechota, Committee Chair

Sajjad Ahmad, Committee Member

Jacimaria R. Batista, Committee Member

Kumud Acharya, Committee Member

Anton Westveld, Graduate Faculty Representative

Ronald Smith, Ph. D., Vice President for Research and Graduate Studies
and Dean of the Graduate College

May 2011

ABSTRACT

Impacts of Climate Change and Weather Modification on Hydrologic Characteristics of Watersheds in the Western United States

by

Anil Acharya

Dr. Thomas C. Piechota, Examination Committee Chair
Director of Sustainability and Multidisciplinary Research
Professor, Civil and Environmental Engineering
University of Nevada, Las Vegas

This research quantifies the impacts of climate change and weather modification (WM) on hydrologic characteristics of watersheds in the arid regions of the western United States. This research performs a long-term simulation of streamflow for present and future climate conditions in the North Platte (NP) Watershed, Wyoming; a shorter duration simulation is then performed to observe the likely impacts of event based changes in an urban watershed in Las Vegas, Nevada.

First, a study is carried out in Chapter 3 that evaluates the impacts of WM on water supply by developing a hydrologic model for the NP Watershed. The variable infiltration capacity (VIC) model is calibrated using daily meteorological forcings and monthly streamflow data. An average increase of 0.3% to 1.5% in annual streamflow is simulated from the Wyoming area of the watershed for a 1% to 5% increase in precipitation. The centralwest and southwest regions of the watershed, which consist of higher percent coverage of evergreen needleleaf and woodland forest, are found to be more effective for cloud seeding operations. For proposed WM programs or programs that are claimed effective based on precipitation augmentation, the hydrological impacts can be evaluated based on this analysis.

Second, Chapter 4 develops streamflow projections to assess water availability in the NP watershed under anthropogenic climate change conditions. The multi-model multi-scenario climate data available from the World Climate Research Programme's (WCRP's) are utilized. The simulated streamflows are compared using an inter-model inter-scenario approach. Average streamflow shows an increasing pattern over this century with maximum streamflow during 2085-2090. The simulated streamflows for future periods (2011-2040, 2041-2070, and 2071-2100) vary from -20% to 62% with respect to the baseline period (1971-2000). The wet months are getting wetter, while the dry months are found to become dryer under changing climatic conditions. The streamflow projections and the range of streamflow can be utilized by decision makers in future water supply and demand management study.

Finally, the research is extended in the urban Las Vegas area (Flamingo-Tropicana watershed) that utilizes the Master Plan Update (MPU) model and the WCRP's multi-model data to observe the impacts of climate change on extreme storm events. The summer storms, which are considered as extreme storms, are expected to be more intense in future. A larger change in peak streamflow and total runoff volume is simulated for the extreme storm under different climate scenarios and time periods; the simulated increase in peak streamflow varies from 40% to more than 150%. These results can be utilized for various design purposes in the watershed to mitigate runoff impacts of intense storms under changing climatic conditions.

This research assesses water availability for the NP watershed and evaluates the vulnerability of existing flood control system for the FT watershed. These results can be utilized by water managers in regional water resources development and management.

ACKNOWLEDGEMENTS

The author expresses his profound gratitude and appreciation to his advisor Dr. Thomas Piechota for providing his consistent support, encouragement, valuable assistance and personal guidance throughout the study period. His continuous effort has developed confidence and motivation inside the author and towards completion of this dissertation and future works.

The author is grateful to all members of his dissertation committee, Dr. Jacimaria Batista, Dr. Sajjad Ahmad, Dr. Kumud Acharya and Dr. Anton Westveld for providing their valuable time, instructions and suggestions throughout the research period. Special thanks go to Dr. Haroon Stephen, Dr. Andy Wood and Dr. Glenn Tootle for providing great help to complete this research. The author wishes to extend his special thanks to his colleagues Dr. Kenneth Lamb and Dr. William P. Miller for providing help and suggestions throughout the course of the study. The author likes to thank Timothy E. Sutko, Environmental Mitigation Manager for Clark County Regional Flood Control District, for providing necessary data and information. The author also likes to thank all his friends whom he met at the University of Nevada Las Vegas, for their continuous support, encouragement and friendship during his school life.

The author feels proud to express his profound gratitude to his parent (Mr. Trailokya Ram Acharya and Ms. Bhawani Acharya), sisters (Anu Acharya and Anita Acharya) and brother in law (Amit Karki). Without their unconditional love, continuous moral support and inspiration, it was not possible for the author to come this long. Finally, the author expresses his love and appreciation to his wife (Alisha Paudel) for her sacrifices, endless love, patience, encouragement, invaluable suggestions and aid. The author would like to thank her for being a part of his life.

TABLE OF CONTENTS

LIST OF TABLES

LIST OF FIGURES

CHAPTER 1

INTRODUCTION

1.1 Background

The impact of climate change on water resources is a major issue for the world. Climate change and increasing temperature trends are likely due to increasing anthropogenic activities (IPCC, 2007). In scenarios where carbon dioxide (CO_2) is doubled, the increase in global temperature, as simulated by Global Climate Models (GCMs) UKH1, was 3.5ºC (Houghton et al, 1990); 4ºC for CSIRO4 (Gordon et al., 1992) and 4.8ºC for CSIRO9 (Watterson et al, 1995). Although various uncertainties exist in climate modeling, the conclusion that the average temperature of the Earth is rising is provided by International Panel on Climate Change (IPCC) with a high level of certainty. National Aeronautics and Space Administration (NASA, 2008) has reported that, almost 90% of the observed changes on physical and biological systems on a global scale are much more likely due to increased warming with the remaining due to other driving forces such as landuse (urbanization).

Variability over the Earth's climate has been observed by paleoclimate reconstructions. Past climatic shifts such as glacial and interglacial cycles and the variations in the global ocean circulation can significantly affect the climate (Stute et al., 2001). Changes observed in interannual to interdecadal teleconnections in the ocean atmosphere climate variability such as the El Niño Southern Oscillation (ENSO), North Pacific Decadal Oscillation (PDO) and North Atlantic Oscillation (NAO) may cause drastic change in climatic conditions around the globe; ENSO and PDO have a strong effect in the United States (U.S.) regions (Iorio et. al, 2004). El Niño is the warming

phase while La Niña is the cold phase of Southern Oscillation; El Niño represents the largest natural variation in climate (Mantua et al, 1997). The increase in El Niño intensity has been documented from 7000 years ago; it increased the temperature in West Antarctica by 5 to 7°C during 1939-1942 (Rodbell et al, 1999). These types of irregular and natural variations in climate affect the sea level pressure, sea surface temperature, air temperature, streamflow and other hydrological phenomenon (Mantua et al, 1997). It has been documented that the extreme weather events such as droughts, intense rainfalls, hurricanes, cold temperatures, change in the amount of snow and storms could be the result of these natural variations in climate (e.g. Hidalgo and Dracup, 2003).

There is a high probability of unequal distribution of water throughout the world. Climate change has increased the risk of floods and droughts in many regions (IPCC, 2001). The likely impacts of climate change are already documented by various studies in different parts of the world (e.g. Arnell and Reynard, 1996; Strzepek and Yates, 1997; Leung and Wigmosta, 1999; Pfister et al, 2004; Li et al, 2008). The major impacts are observed on the hydrological cycle and regional water availability for industry, domestic use, flood control, irrigation and agriculture, aquatic life survival, reservoir operation and navigation. The hydrologic response due to climate change further affects the strategies and polices of water resources management (Liu et al, 2007; Barontini et al, 2009).

Climate change is occurring due to natural variability as well as human induced activities, the later is attributing for additional impacts. There still exist uncertainties while evaluating the impacts due to human induced climate change alone. It is necessary to quantify the impacts of climate change attributed to human activities which include anthropogenic activities and land use changes. However, weather modification is also a

major concern at some regions of the world including the western United States. The overall goal of the proposed research is to assess the possible impacts of climate change and weather modification on the regional hydrologic characteristics of watersheds in the western United States.

1.2 Weather Modification and its Impact on Water Supply

Snowpack augmentation and runoff enhancement are considered an integral part of regional water management in many arid and semi arid regions. The longer droughts in the arid regions have caused the necessity of weather modification (WM), or cloud seeding programs, so as to increase precipitation by utilizing the clouds in the sky. WM modifies the local weather conditions to alter or improve the unpleasant and disastrous variations of the weather (Kethley, 1970). With increasing water demand, the WM projects, which are also known as the precipitation enhancement projects, are expected to increase in different parts of the world.

Most of the cloud seeding activities inside the U.S. have been operating in the western region since the 1950s to fulfill the increasing water demand in these regions. Reconstructed climate data has indicated the occurrence of very lengthy and severe droughts in the arid western U.S. in the past (USGS, 2004). The 2000-2004 Colorado River drought resembles one of those droughts which is most common for the western United States (Ryan et al, 2005). The Colorado River Basin, a major source of water supply for the western U.S., has been in a drought since 1999 (BOR, 2006). Snowmelt runoff is the major source of water supply in the western U.S. but a significant decrease in the mountain snowpack is noticed in the last century in these regions (Mote et al.,

2005). In California, there is a need of at least two million more acre feet of water to sustain urban growth by 2030 (Shaw, 2006). The United States Department of Interior (U.S. DoI, 2003) has also reported the continuous increase in the consumptive use of water in the West to sustain urban growth. It could create serious water conflicts in the future while meeting the higher water demand. In addition, decreased snowpack runoff may impact production of hydroelectric power, thus creating adverse impacts on the power demand of California and other western States (Griffith and Solak, 2006; Hunter, 2007). The trend of increasing water demand and declining snowpack could worsen the situation even more if no significant action is taken (U.S. DoI, 2003). WM programs have been considered the most attractive option for increasing water availability.

Many cloud seeding projects has been ongoing in the headwater watersheds of the Colorado River Basin. A properly designed and implemented WM program are considered to increase snowpack in the range of 5% to 15% (average 10%) (AMS, 1998; WMA, 2005). Cloud seeding is supposed to contribute from 0.8 to 1.8 million acre-feet (MAF) of water for Colorado River Basin, which could result in a favorable benefit cost ratio for the program (Ryan et al, 2005; WMA, 2005; Griffith and Solak, 2006). The feasibility study of the operational cloud seeding program in the Salt River and the mountains of Wyoming have shown an average increase of 10% in November through March precipitation (Griffith et al, 2007). The Wyoming Water Development Commission (WWDC) through the Wyoming Weather Modification Pilot Project (WYMPP) has conducted the silver iodide based cloud seeding during the winter period (60-80 days) in between the months of November and March (WWDC, 2005). Most of the cloud seeding for the WYMPP is done in the North Platte watershed (Sierra Madre

and Medicine Bow ranges) in south central Wyoming and Wind Range River in west central Wyoming. Around 250 storm events are estimated in the target areas to attain a 15% increase in precipitation (Breed, 2008). The present available water resources in the Platte River basin in Wyoming are fully allocated (WWDC, online accessed 2010). Under a moderate population growth, the water demand in Green River Basin is expected to increase from 73 to 82 percent of its allocation given in the Colorado River and up to 88 percent in the Wind River (Big Horn) Basin. WWDC (2010) has estimated an additional 130,000 to 260,000 acre-feet (AF) of water each spring for a 10% increase in precipitation from the proposed pilot projects. However there is a need to further evaluate this and quantify the impacts. Snowpack augmentation in the basin through WM programs is expected to increase the water availability to meet increasing water demand and improve the water level of the reservoirs.

The WM programs are operating based on cost versus probabilistic benefit analysis (NRC, 2003). Although various improvements and advance technologies have been utilized since the start of the WM programs, there still exist uncertainties which restrict the verification of the direct impacts of these activities. Additional experiments are needed to reduce the existing uncertainties associated with the impacts of WM programs. It is necessary to evaluate the possible impacts of the ongoing WM programs which will determine whether and to what extent the implemented programs could produce the claimed results.

1.3 Impacts of Climate Change on the North Platte Basin, Wyoming

The IPCC (2007b) suggests the general trend of increasing temperature (and drier conditions) in mid latitudes. Saunders and Maxwell (2005) have suggested that the continuous climate disruption in the western U.S. is likely to result in higher temperatures, declining snowpack, lower snow water content, earlier snowmelt and shift in streamflow timing (Hunter, 2007). Several past studies have documented the similar types of hydroclimatic changes in the western United States (Hidalgo et al, 2009). As mentioned earlier, the trend of declining snowpack and increasing water demand is primarily driven by an increase in temperature (Mote et al, 2005). The increase in temperature and the observed reduction in snowpack (1950-1999) are attributed to higher anthropogenic input of GHGs, ozone and aerosols (Pierce et al, 2008). The U.S. Global Change Research Program (2009) has reported a strong seasonal climatic variation in the arid western regions of U.S. in the past. The greatest seasonal change was observed during the winter months. With projected temperature changes over this century, a maximum rise in temperature is observed for the regions with the summer changes (more than 10^{o}F) being larger than the winter. The North Platte Basin in Wyoming is a region in the western U.S. and the temperature and precipitation are projected to change in the future.

The dominant affect of anthropogenic climate change could continue into the future which may induce additional changes in the hydrology and discharge regime of the basin and several other indirect consequences. The human induced anthropogenic activities might lead to increased flood risk in the future (Bronstert et al, 2002). Research

is necessary at a regional scale that could quantify the future impacts of anthropogenically forced climate change on the hydrologic characteristics of the basin.

Most studies have utilized output from GCMs to evaluate the impacts of climate change under increased greenhouse conditions (e.g. Chiew et. al, 1995; Cameron et al, 2000; Bergstrom et al., 2001; Li et al, 2008). Various climate scenarios and GCMs for regional analysis have simulated different results. Research on climate change with more reliable methods is necessary to reduce the uncertainties observed in the past results. Recently, the statistically downscaled high resolution data (12km) for 112 contemporary climate projections of 3 major climate scenarios (from IPCC) and 16 robust climate models are available through the World Climate Research Programme's (WCRP's) Coupled Model Intercomparison Project phase 3 (CMIP3) multi model dataset for the whole contiguous United States. There is a need to quantify the changes in hydrologic characteristics of the North Platte River basin under future anthropogenic activities by incorporating the WCRP's multi-model climate projection dataset.

1.4 Climate Change and Extreme Precipitation Events

The above studies are important as they assess water availability in the future at a monthly to annual timescale. The simulation of the extreme precipitation events is also important, since the increase in the frequency and intensity of extreme rainfall events may cause serious impacts on both environmental and human systems in terms of increased frequency and severity of floods. The extreme flows are predicted to increase more than mean flows under different climate change conditions (Arnell et al, 2003). Under the enhanced greenhouse conditions, the possibility of significant increases in the

frequency and magnitude of extreme daily precipitation both at global and regional scale is supported by various studies (Fowler and Hennessey, 1995; Hennessey et al, 1997; Zwiers and Kharin, 1998; Groisman et al, 1999; McGuffie, 1999; Kharin and Zwiers, 2000; Frich et al, 2002; Semenov and Bengtsson, 2002; Fowler and Kilsby, 2003b). The warmer temperature due to enhanced greenhouse gas increases the moisture holding capacity; thus the amount of rainfall as well as the percentage of convective rainfall events increases (Gordon et al., 1992). Easterling et al. (1999) have suggested the higher occurrence of various extremes in the U.S. since the 1970s. The increase in extreme precipitation events is contributing to increasing number of days of higher precipitation (>50 mm) and the frequency of occurrence of events in the United States (Karl et al., 1996; Karl and Knight 1998). An increase of at least 5% in mean summer precipitation is documented in the past century and an increase of 20% of summer daily precipitation is suggested in future in the northern countries (Canada, Norway, Russia, Poland) and mid latitude countries (U.S., Mexico, China, Australia) for the same increase in mean summer precipitation (Groisman et al, 1999).

The evaluation of extreme events requires either the use of regional climate models (RCMs), high resolution GCMs, or the downscaling of data to a smaller time scale to improve the analysis and accuracy of the GCM results (Mearns et al. 1995; Kim et al, 2002). The use of coarser GCMs in the past century did not simulate the extreme rainfall events well (Rind et al, 1989; Mearns et al, 1990; Cubasch et al, 1995). The GCMs were also running under the scenario of doubling of CO_2 or using only a few climate projections. This restricted the full range of scenarios thus increasing the uncertainty related to future climate change. The multi-model or multi-scenario approach

with the inclusion of high resolution simulation at present addresses some uncertainties in the impact studies of extreme precipitation events at global scale (McGuffie et al, 1999; Palmer and Ra¨isa¨nen, 2002; Semenov and Bengtsson, 2002; Voss et al, 2002; Watterson and Dix, 2003; Tebaldi et al, 2006; Buonomo et al, 2007). The summer is expected to dry further, while the increase in the intensity and decrease in the return period for both shorter and longer duration extreme precipitation events is expected in most areas based on the results from climate models (Christensen and Christensen, 2003; Fowler and Kilsby, 2003a). There are, however, some uncertainties while analyzing the results at a regional scale (May et al, 2002; Voss et al, 2002; Huntingford et al, 2003; Kiktev et al, 2003).

The change in the intensity of extreme storm events, which are likely to occur as summer monsoon storms, are found disproportionately very large as compared to changes in precipitation during other seasons (Zwiers and Kharin, 1998; Groisman et al, 1999). The types of runoff producing storms in arid regions are mainly local, high intensity, convective thunderstorms and occur for very short periods over small areas (Pilgrim et al., 1988). The response of streamflow to changes in precipitation may range from a double in wet and temperate areas to more than 5 times in arid areas (Chiew et. al, 1995). The semi arid areas of southwestern Nevada such as Las Vegas are of particular interest as the summer storms, which are mostly developed by convective storms and rapid thunderstorms and occurring only for a short duration, have caused heavy damages to life and the property in the past (CCRFCD, 2006). The intense thunderstorms occur during the summer months and are localized. The projection of changes in extreme precipitation has shown the greatest increase in the precipitation intensity for the most intense storms

(i.e. extreme short duration storms) (Ra¨isa¨nen and Joelsson, 2001; Buonomo et al, 2007).

As mentioned earlier, the statistically downscaled high resolution data for 3 major climate scenarios (from IPCC SRES report) and 16 robust GCMs can be retrieved from WCRP's CMIP3 dataset. Research is needed to quantitatively assess the watershed level impacts for event based changes under different climate conditions by utilizing the WCRP's downscaled multi model dataset.

1.5 Research Goals and Research Questions

This research presents the quantitative assessment of the hydrological impacts due to weather modification and climate change that are mostly attributable to human activities**.** The proposed research will incorporate hydroclimatic modeling as tools for answering the research questions below.

Research Question 1. How would a hydrologic model be utilized to evaluate the possible impacts of weather modification on water supply of a watershed?

Hypothesis 1. Based on the feasibility study, the operational cloud seeding programs in the North Platte watershed is expected to increase precipitation (snowpack) by 10%. This increase of snowpack may augment annual and seasonal streamflow and reduce the impact of declining streamflow during dry periods.

Research Question 2. How would a robust downscaling technique and the use of a suitable land surface hydrologic model be utilized to quantitatively assess the long term response of streamflow based on forecasted global climate change scenarios?

Hypothesis 2. Based on complex topography and diverse climate regime of the western U.S., the use of higher resolution climate data and hydrological model may simulate more realistic hydrological changes. The climate parameters such as temperature and precipitation are expected to change under anthropogenic climate change conditions. The long term streamflow projections, which are based on bias corrected and statistically downscaled WCRP CMIP3 multi-model dataset, may be used to determine the future water availability in the basin under changing climatic conditions.

Research Question 3. How would an urban basin respond to the most intense storm under projected climate change conditions?

Hypothesis 3. The intensity of extreme storm events is expected to increase under anthropogenic climate change conditions. The impacts of intense storms on streamflow are expected to be more in arid urban areas. The higher resolution and downscaled WCRP CMIP3 data can be used to determine the change in intensity of extreme storms, which may contribute to changes in peak runoff and total runoff volume for the basin.

1.6 Research Tasks

Task 1 develops a hydrologic model for the North Platte watershed. Further, 'what if' scenarios are run to quantify the significant changes in streamflow (annual and seasonal) for an increase of precipitation due to cloud seeding operations in the watershed. Additionally, this analysis identifies the most favorable region and landcover for cloud seeding operations in the watershed. Task 1 creates a continuous simulation by using the Variable Infiltration Capacity (VIC) macro-scale semi distributed land surface hydrologic model.

Task 2 utilizes the model from Task 1 and develops long term streamflow projections for the watershed by incorporating output from multiple climate emission scenarios and GCMs. Statistically downscaled WCRP's CMIP3 multi-model dataset are used to quantify the impacts of anthropogenic climate change conditions on hydrologic response of the basin. The inter-model inter-scenario comparisons are performed to observe the changes in streamflow for future climate, which are a result of changes in precipitation, temperature (min and max), wind speed, type of vegetation and soil classification. A Kolmogorov Smirnov (KS) goodness of fit test is applied to test if there exists any significant difference in streamflow distributions in between the emission scenarios and for different time periods. Both tasks provide an idea of water availability for different climate change conditions attributed to human activities.

Task 3 utilizes the Master Plan Update (MPU) model and WCRP's CMIP3 multi-model dataset to observe the impacts of climate change on extreme storm events in the urban Las Vegas area. Various climate scenarios based on multi-model data are forced into the MPU model. The changes in streamflow (peak runoff and total runoff volume) are quantified with respect to changes in rainfall intensity for the intense storms. This allows for the evaluation of vulnerability of existing flood control system under forced anthropogenic climatic conditions.

A proper understanding of the impacts of climate change at a regional scale is important for local impact analysis. Overall, this research helps to better understand and estimate the impacts of climate change which could be beneficial for further planning, management and implementation of water resources projects.

1.7 Dissertation Outline

This dissertation is comprised of six major chapters. Chapter 1 provides an overall introduction, problem statements and the major objectives of this research. Chapter 2 reviews the literatures and technical reports related to climate change and weather modification. Chapter 3, 4 and 5 corresponds to a separate analysis performed for Tasks 1, 2 and 3 respectively. Each of these chapters is comprised of a journal article, which incorporates the introduction, objective, methodology, results and conclusion for each task. Chapter 6 provides the contributions from this research and recommendations for future work.

CHAPTER 2

REVIEW OF RELATED LITERATURE

Overall, this research assesses the impacts of climate change on regional hydrology. This chapter first reviews literature of climate change studies and then reviews weather modification (WM) studies. The major areas under the climate change section include the various methods and the major uncertainties included in past studies. The major areas covered under the WM section are the various methods, the environmental impacts, uncertainties and the evaluation criteria.

2.1 Climate Change

The Earth's climate has seen major changes over its history (Stute et al, 2001). The major drivers of climate change prior to industrial era are considered to be the result of changes in the Earth's orbit, sun's intensity, volcanic eruptions (aerosol and carbon dioxide emissions), greenhouse gas (GHG) concentrations and ocean currents (EPA, 2009). Present climate change is described as the combination of natural and human induced changes. Climate change, especially the increase in temperature, is mostly likely due to increasing anthropogenic activities (IPCC, 2007a, 2007b). The concentration of anthropogenic gases (especially the emission of CO_2) could nearly double by 2100 if the 1990 level of emissions continues at the same rate (Loaiciga et al, 1996 adopted from Xu, 1999). The greenhouse gases trap the heat in the atmosphere, thus warming the Earth's climate, which is known as global warming. Climate change could affect the hydrologic response of watersheds as well as their water quality aspects. It could intensify the

frequency and intensity of rainfall which results in increased runoff, more pollution and sedimentation (IPCC, 2007b).

2.1.1 Climate Emission Scenarios

The Synthesis Report from International Panel on Climate Change (IPCC, 2007b) has reported a more than 70% increase in the emissions of greenhouse gases due to human activities during the period of 1970-2004. The annual emission of CO_2 alone represents almost 77% of this total increase. GHG emissions, measured in terms of CO_2 equivalent emission, have more than doubled during this period. The increase in global mean surface and ocean temperatures have impacted sea level rise and melting of ice in the past. These impacts are likely to continue into the future if natural and anthropogenic emissions also continue to increase. If the future GHG emissions are stabilized, the total emission at present is likely to increase mean global temperatures and sea levels to a certain degree. As CO_2 concentrations double, due to GHG emission at or higher than the current rate, the temperature is expected to increase in the range of 2 ºF to 4.5ºF until the end of this century.

The model control runs (i.e. no change in future emission) and the idealized assumption of 1% CO_2 increment per year represent the most scientific climate change scenario with no other external effects. These model runs are collected and archived at the Program for Climate Model Diagnosis and Intercomparison (PCMDI) for public access (Meehl et al, 2007). Six illustrative emission scenarios included in the IPCC Special Report on Emissions Scenarios (SRES) act as a basis for most of the climate change research at present. These scenarios act as ‘marker’ scenarios for future GHG emissions representing the CO_2 emissions projections produced by a range of integrated

assessment models based on a range of socio-economic storylines. The projected CO_2 emission scenarios consider the demographic, socio-economic and technological changes. However, no additional changes are assumed in future climate policies. The emission scenarios are identified as A2 (higher emission), A1B (moderate emission), B2 and B1 (lower emission) which are discussed in detail as follows;

A1 Emission Scenario: This scenario assumes the world of global population growth that peaks in mid century. It considers very rapid economic growth and rapid introduction of new and more efficient technology. It is categorized into three types based on the three directions of technological change: fossil intensive (A1F1), non fossil source (A1T), and balance of all sources (A1B).

A2 Emission Scenario: This scenario assumes a very heterogeneous world of high population growth with less concern for rapid economic development and technological change. It assumes uneven economic growth and income gap between industrialized and developing parts of the world. It gives less emphasis on economic, social and cultural interactions between regions, and more emphasis on self reliance of the resources.

B1 Emission Scenario: This scenario assumes a convergent world (unlike in A2) with high population growth that peaks in mid century. It considers rapid changes in economic structures towards service and information. It emphasizes more on environmental and social aspects of development for a more sustainable future.

B2 Emissions Scenario: This scenario assumes a heterogeneous world with less rapid but more diverse technological change. The higher emphasis is given on community initiative and social innovation to find local rather than global solutions for economic, social and environmental sustainability.

2.1.2 Climate Models

A full climate model consists of the Earth's various components (atmosphere, hydrosphere, land surface, cryosphere, geosphere, and biosphere) along with the coupled interactions and feedback mechanisms in between each component. The climate transitions during the past, present and future is modeled based on the dynamics and interactions between the Earth's components. Climate modeling started in the 1980's with limited number of models, data, experiments and model accessibility. Global Climate Models (GCMs) are the only available tools to help understand the climate and the impacts of climate change at a global scale. GCMs run under the scenarios that consider the effect of GHGs and their projection into the future. A number of GCMs exist that simulate hundreds of constructed scenarios of past and future climate change. Table 2.1 provides a list of the most robust GCMs along with the emission scenarios collected through the WCRP CMIP3 effort (Meehl et. al, 2007). The downscaled data for these GCMs can be accessed through the Lawrence Livermore National Laboratory (LLNL) Program for Climate Model Diagnosis and Intercomparison (PCMDI). The dataset consists of the runs from 3 scenarios: SRES B1 (low forcing, CO_2 concentration ~ 550 ppm by 2100); SRES A1B (medium forcing, CO_2 concentration ~ 700 ppm by 2100); and SRES A2 (high forcing, CO_2 concentration ~ 820 ppm by 2100). All GCMs model future climate based on the similar boundary conditions for atmosphere, ocean and land surface. GCMs are assumed to simulate temperature trend better than precipitation (Pierce et. al, 2009). Some earlier projects (such as ENSEMBLE, PRUDENCE, NARCCAP) have produced ensemble results from multi-model GCMs to better understand the uncertainty in present and future estimates of extremes (Fowler et al, 2007). The ensemble of

Table 2.1 Model abbreviations, emission pathways, projection run and primary reference

Modeling Group, Country	WCRP CMIP3 I.D.	SRES A2 runs	SRES A1B runs	SRES B1 runs	Primary Reference
Bjerknes Centre for Climate Research	BCCR-BCM2.0	1	1	1	Furevik et al., 2003
Canadian Centre for Climate Modeling & Analysis	CGCM3.1 (T47)	1...5	1...5	1...5	Flato and Boer, 2001
Meteo-France / Centre National de R. Meteorologiques, France	CNRM-CM3	1	1	1	Salas-Melia et al., 2005
CSIRO Atmospheric Research, Australia	CSIRO-Mk3.0	1	1	1	Gordon et al., 2002
US Dept. of Commerce / NOAA / Geophysical Fluid Dynamics Laboratory, USA	GFDL-CM2.0	1	1	1	Delworth et al., 2006
(Same as above)	GFDL-CM2.1	1	1	1	Delworth et al., 2006
NASA / Goddard Institute for Space Studies, USA	GISS-ER	1	2, 4	1	Russell et al., 2000
Institute for Numerical Mathematics, Russia	INM-CM3.0	1	1	1	Diansky and Volodin, 2002
Institut Pierre Simon Laplace, France	IPSL-CM4	1	1	1	IPSL, 2005
Center for Climate Sys. Res. (U. of Tokyo), Nat. I. for Env. Stu., and Frontier Res. C. for Global Change (JAMSTEC), Japan	MIROC3.2 (medres)	1...3	1...3	1...3	K-1 model developers, 2004
Met. Ins. of the U. of Bonn, Met. Research Institute of KMA	ECHO-G	1...3	1...3	1...3	Legutke and Voss, 1999
Max Planck Institute for Meteorology, Germany	ECHAM5/ MPI-OM	1...3	1...3	1...3	Jungclaus et al., 2006
Meteorological Research Institute, Japan	MRI-CGCM2.3.2	1...5	1...5	1...5	Yukimoto et al., 2001
National Center for Atmospheric Research, USA	CCSM3	1...4	1...3, 5...7	1...7	Collins et al., 2006
National Center for Atmospheric Research, USA	PCM	1...4	1...4	2...3	Washington et al., 2000
Hadley Center for Climate Pred. and Res./ Met Office, UK	UKMO-HadCM3	1	1	1	Gordon et al., 2000

(source: http://gdo-dcp.ucllnl.org/downscaled_cmip3_projections)

multiple GCMs is assumed to improve the model performance during simulation (Pierce et. al, 2009). There are various uncertainties (e.g. human induced changes, natural processes, interactions and feedback mechanism, cloud effects, oceanic overflow) in the prediction of future climate change and the degree of uncertainty is not known fully. Regardless, GCMs are the most current way to look, understand and predict the likely future climate change.

2.1.3 Downscaling Techniques

Most of the GCMs are designed to run globally at a coarser spatial resolution (e.g. 2°, 5°) and longer time scale (such as monthly or yearly). The same resolution may not accurately represent the local climate and hydrological processes for the impact models operating at a smaller scale (McCabe and Ayers, 1989). Therefore, the coarser resolution model output must be downscaled to a finer resolution for local impact analysis. The various models used for downscaling utilize parameters such as sea level pressure and geosynthetic heights to predict temperature and precipitation (Cavazos and Hewitson, 2002). No universal method of downscaling is available that is suitable for all situations; all methods available at present are still under study and testing (Xu, 1999). Downscaling can be applied to the spatial and temporal domains.

2.1.3.1 Spatial Downscaling

Spatial downscaling methods are developed to represent the local sub-grid scale features and dynamics such as convective cloud processes (Joubert and Hewitson, 1997). The spatial downscaling methods include simple interpolation, statistical downscaling and dynamical downscaling (Prudhomme et al, 2002). The interpolation method does not consider any correction for GCM output. The statistical methods establish an empirical

relationship between the predictor variable and the observed parameters based on the present climate observations (Xu, 1999). The simple statistical method includes the fitting of a linear regression model between the observed and modeled dataset. But the established physical relationship underlying the statistical relation is not without uncertainty and is therefore, difficult to justify in the climate change studies. Dynamic methods consider and solve the physical dynamics of the system. They are computationally expensive but they are assumed to produce more homogenous results than the statistical methods. They use the GCM output and higher resolution regional climate models (RCMs) embedded in the GCM, which runs regionally at a much smaller space scale (Fowler et al, 2007).

The statistically downscaled climate projections data available through WCRPs CMIP3 multi-model dataset follows two major steps to spatially downscale the data from 2º to 1/8º: Bias Correction and Spatial Disaggregation (BCSD). While comparing the hydrologic impacts, the BCSD method is considered to have the capabilities in comparable to other statistical and dynamical downscaling approaches (Wood et al., 2002, 2004; Maurer and Hidalgo, 2008). The bias between the GCM monthly data (average temperature and precipitation) and the observed data is corrected using a quantile based mapping technique. The bias corrected temperature and precipitation are then interpolated into a finer grid by using additive anomalies for temperature and multiplicative factor for precipitation.

2.1.3.2 Temporal Downscaling

Temporal resolution is considered more important for shorter duration storms (Bronstert et al, 2002). The temporal downscaling methods include dynamic temporal

downscaling and weather generator techniques (Prudhomme et al, 2002). The dynamic temporal downscaling uses the atmospheric variables that are compatible with the resolution of GCM output to statistically downscale the data (e.g. monthly to daily). Among various types of statistical methods, the weather generator techniques use stochastic models to generate the daily data from the monthly data (Wilby et al, 1998). The stochastic rainfall generator technique considers the changes in model parameters and modeling of extreme rainfall events in the future. The stochastic model uses a resampling procedure (such as Monte Carlo) and generates random rain storms from the available data; however, the capacity of GCM is limited to ensure the effectiveness of this approach (Wilks, 1999; Cameron et al, 2000). The perturbation method is widely used by hydrologists for temporal downscaling due to its simplicity and lack of complete reliability on other sophisticated downscaling methods (Chiew et al, 1995; Arnell and Reynard, 1996; Tucker and Slingerland, 1997; Wood et al, 1997; Reynard et al, 2001; Loukas et al, 2002). It expresses the difference between modeled and observed data as a percentage change or scale factor.

Prudhomme et al. (2003) applied three methods of temporal downscaling which are categorized as ‘proportional method’, ‘change in day’s method’ and ‘enhanced storm method’. The monthly percentage change in rainfall is applied to each day’s rainfall (only to those days with a rainfall total above a certain threshold value) in the ‘proportional method’. The number of rain days in each month is increased or decreased based on the monthly increase or decrease in rainfall in the ‘change in day’s method’. The monthly change in rainfall is applied to an enhanced storm in the ‘enhanced storm method’. The BCSD data available through WCRP CMIP3 multi-model dataset possess monthly

average of precipitation and temperature. The monthly data are downscaled to daily data via random sampling and the bias correction and temporal downscaling (BCTD) technique (Wood et al, 2002, 2004). During the bias correction, temperatures are shifted by a certain quantity and precipitations are assigned a scaling factor similar to the BCSD method.

Most of the climate change studies (including those listed in the current proposal), which perform at a regional scale and use the GCM output, have adopted a downscaling technique based on the hydrologic input data requirements (Bronstert et al, 1999; Miller et al, 1999; Widmann et al, 2002; Arnell et al, 2003; Zhang et al, 2005; Wetterhall et al, 2005; Tripathi et al, 2006; Spak et al, 2007). Among the various types of downscaling methods, the application of RCMs and the statistical downscaling are considered the most important for hydroclimatic model applications (Bronstert et al, 2002). The major limitation of the statistical method is the assumption of stationary conditions for future climate. The bias present in historical GCM output are transferred to future simulations while applying the bias correction methods (Wood et al, 2004). The BCTD and perturbation method assume a change only in the future rainfall intensity. However, land use and other watershed characteristics along with the distribution and frequency of events remain unchanged. The coarser resolution from RCMs still need spatial and temporal downscaling to observe the impact at a local scale or for short duration events. The biases present in coarser scale GCM output are likely to get transferred to future climate predictions for all available downscaling methods.

2.1.4 Assessment of Hydrological Impacts of Climate Change

A proper understanding of climate change and its hydrological impacts at a regional scale are important for water resources management (Barontini et al, 2009). The common way of to assess future climate is based on historic climate change patterns. Temperature and precipitation are considered the most important parameters that influence hydrologic response of a watershed. The IPCC Third Assessment Report (TAR) has reported the likely decrease of rainfall in subtropics during the 21st century, but extreme precipitation events are likely to increase possibly contributing to severe flooding conditions (Cubasch et al, 2000). The occurrence and duration of extreme hot events are likely to increase, and the frequency and severity of extreme cold events are likely to decrease throughout the United States (Diffenbaugh et al, 2005).

The impacts of climate change are considered to be region specific (Leung and Wigmosta, 1999). A significant shift in floods both in terms of magnitude and frequency is observed during climate change studies (Prudhomme et al., 2002). A significant change in annual runoff (almost 20 to 50%) is observed in the northeast, southeast and western coast of Australia by the year 2030 (Chiew et al, 1995). This same study reported a two times increase for wet and temperate areas to more than five times increase in arid regions. For 21 catchments in Great Britain, prior to 2050, the annual runoff shows an increase or decrease over 20% for the wettest or driest scenarios respectively (Arnell and Reynard, 1996). Another study identified 10% to 20% change in annual runoff across Southern Africa. The extreme storms show larger change in runoff when compared with the mean runoff (Arnell et al, 2003). The runoff for the head waters region of the Yellow River indicates a slight change in runoff before 2020, 10% decrease in the next 50 years,

and more than 5% decrease per year after 2050 due to greater enhancement of temperature (Li et al, 2008). The impacts of climate change on Belgian catchments are found positive or negative depending on the catchment characteristics and climate change scenarios. Most of the scenarios show an increase in flood frequency during winter months and for catchments with prevailing surface runoff (Gellens and Roulin, 1998). Except for some regions which show a decrease, the frequency of extreme events are increased through most of the tropics in south central Africa (Walsh and Pittock, 1998).

Climate change has resulted in an increase of the magnitude and frequency of flood events in southeastern Australia and the U.K. (Schreider et al., 2000; Reynard et al, 2001; Prudhomme et al, 2003). The peak flow depends on extreme precipitation and land use, with more significant effect of the land cover on increasing flood pattern (Reynard et al, 2001). Strzepek and Yates (1997) has reported a runoff reduction of more than 23% in Central and Eastern Europe for most of the future climate scenarios; the GISS scenario resulted in almost a 12% increase in runoff. Middelkoop et al. (2001) has reported a rise in winter flow due to intensified snow melt and higher precipitation, and reduction in summer flow due to reduced snow storage and higher evapo-transpiration in the Rhine basin. The increase in the probability of flooding in the Rhine and Meuse basins are attributed to an increase in the total rainfall and intensity (Pfister et al, 2004). A reduction in snowpack of nearly 60% and a shift in seasonal streamflow observed at the American River are attributed to less snowfall and more rainfall in warmer climate conditions (Leung and Wigmosta, 1999). Several studies are carried out in other regions of the world which relate the hydrological impacts to climate change (Bates et al, 1994; Aizen et al, 1997; Arnell, 1999; Bronstert et al, 1999; Hamlet and Lettenmaier, 1999; Miller et al,

1999; Braun et al, 2000; Arora and Boer, 2001; Bergstrom et al., 2001; Loukas et al, 2002; Jian and Shuo, 2006; Kay et al, 2006; Hayhoe et al, 2007; Liu et al, 2007; Minville et al, 2008; Barontini et al 2009; Gerbaux et al, 2009). Most of these studies have demonstrated similar increasing or decreasing trends, whatever the case may be, across a wide variety of climate change scenarios. The obvious discrepancy between these studies is in the magnitude of the change, not the direction.

2.1.4.1 Hydro-Climatic Change in the Western U.S.

The natural hydroclimatic variability in the western U.S. is most often defined as a function of the ENSO and PDO (Mantua et al, 1997). The major changes are observed in terms of higher or lower temperature and precipitation than the normal conditions (Hamlet and Lettenmaier, 1999). ENSO and PDO are also interconnected with each other. When both the climate indicators are in same phase, there is a strong possibility of higher or lower streamflow anomalies (Hamlet and Lettenmaier, 1998). The regional warming and changes in atmospheric circulation of the North Pacific are also related (Dettinger and Cayan 1995). Most of the studies (from 1991 to 2000) that relate to natural variability of the Pacific climate conditions and its effect on hydroclimatology of North America are documented by Hidalgo and Dracup (2003). Other studies also verified the effects of natural variability on the hydroclimatology of North America (e.g. Chao et al, 2000; Barlow et al., 2001; Papineu, 2001; Gutzler et al, 2002; Hidalgo and Dracup, 2003; Newmann et al, 2003; Westerling and Swetnam 2003; Beebee and Manga, 2004; Schoennagel et al, 2005; Yu and Zwiers, 2007; Tootle and Piechota 2006; Tootle et al, 2008; Timilsena et al, 2009; Aziz et al, 2010; Lamb et al, 2010).

The trend of declining snowpack over the western U.S. is primarily driven by an increase in temperature rather than change in precipitation (Mote et al, 2005; Hamlet et al, 2005; Mote, 2006; Maurer et al, 2007; Miller and Piechota, 2008). A study of Jan-March (JFM) minimum surface temperatures, precipitation, ENSO, and PDO data confirmed the anthropogenically forced temperature change over the western United States (Pierce et al, 2009). The winter snowpack acts as a reservoir which stores more water than is stored by man made reservoirs in most of the western United States (Mote et al, 2005). The accumulated snowpack during the winter storms gradually melts and serves as the major source of water supply during the dry periods. The expected increase in the greenhouse gas induced warming in the coming century could contribute significantly on the decline of snowpack in the west (Pierce et al, 2008).

Some studies have utilized the detection and attribution analysis (D&A) technique to study the human induced changes in hydrology along with temperature variability in the mountain ranges, and the shifts in streamflow timing as a result of climate change impacts in the western United States (Barnett et al, 2008; Bonfils et al., 2008; Pierce et al, 2008; Hidalgo et al, 2009). These studies also found the effects of anthropogenic climate forcing to dominate over the natural internal climate variability from the recent historical record. Barnett et al. (2008) has identified that almost 60% of the climate related change (e.g. snowpack reduction) during the period of 1950-1999 is attributed to human induced changes. Pierce et al. (2008) has identified that the reduction in April 1 snow water equivalent (SWE) to precipitation ratio is higher for anthropogenic climate simulations rather than the natural internal climate variability alone. Hidalgo et al. (2009) has identified that the shift in the timing of spring snowmelt (streamflow) along the

California region, the Upper Colorado River basin and the Columbia River basin (since 1950) is also attributed to increasing anthropogenic activities. The linear regression between SWE, temperature and precipitation shows an increase in the SWE (during 1930-1950) which is attributed to the increase in precipitation; the reduction in the SWE since 1950's is attributed to regional warming in the western United States (Mote, 2003, 2006). These studies indicated a serious water crisis in the western U.S. in future decades.

Cayan et al. (2006) has showed an increase in temperature (2 to 6 ºC) in California during the period of 2000 to 2100. The relatively small change in temperature is shown to have negative impacts on the state's water supply, hydroelectric power, agriculture, recreation, and ecosystems. Groisman et al. (2004) reported a reduction in the spring and summer snowpack during the period of 1972-92. A decrease in April 1 SWE was observed (except in southern Sierra Nevada) during the period of 1950-2000 (Mote et al, 2005). As an exception, the higher precipitation overcomes the warming effect in the Southwest, thus leading to higher SWE (Mote et. al, 2005; Udall and Bates, 2007). The trend of higher rainfall rather than snow in terms of total precipitation is observed over the period of 1949-2004. This attributed to a decrease in total snowpack in the region (Knowles et al., 2006).

The observed daily records (from 1950-1999) showed more precipitation for stations located on the south of Wyoming and less for stations located on the north (Regonda et. al, 2005). An increase in precipitation (almost 6.3%) is observed over western Washington, Orlando and British Columbia, during the period of 1920-2000. A decreasing precipitation trend of 4.8% is observed during 1950-2000 for the same regions (Hamlet et al., 2005). Similar earlier studies also showed the hydroclimatic changes in the

western U.S. in terms of declining snowpack, lower snow water content, earlier snowmelt, and shift in spring runoff timing (Roos 1987, 1991; Wahl 1992; Aguado et al. 1992; Pupacko, 1993; Dettinger and Cayan 1995; Leung et al, 2004; Vanrheenen et al, 2004; Stewart et al, 2005). Although the impacts are visible, no significant changes in annual streamflow volume was observed during the past 50 years; this indicates the regional warming induced changes mainly contributed to the seasonal distribution of streamflow (Hidalgo et al., 2009).

2.1.4.2 Application of GCMs for Hydrologic Assessment

GCM data was initially incorporated by Environmental Protection Agency (EPA) in 1984 to study the impacts of climate change on the regions of North America (Gleick, 1986). However, climate models do not provide short term time scale projections needed for hydrologic modeling. The coarser resolution data obtained from climate models are downscaled to desired spatial and temporal scale to observe hydrologic impacts due to climate change. The climate change impact studies based on GCM output are mainly oriented to areas where higher resolution data are available. At present, this means most of these studies are focused in the regions of North America. The two common steps adopted by most of the studies related to hydrological impacts of climate change include:

- Climate modeling based on projected climate scenarios (IPCC scenarios); and
- Perform simulation under present and future conditions by using climate model output and a suitable hydrological model.

Past studies have utilized a number of GCMs and climate projections to study the impacts of climate change. Based on the multi-models future climate projections, the dry subtropics are likely to dry further while the wet, higher latitude regions are likely to be

wetter in the future (Held and Sodden, 2006). A study over the continental U.S. based on 18 CMIP models has showed the normalized annual mean temperature at more than one; and less than one for normalized mean precipitation (Covey et al, 2003). A study on the large River basins throughout the U.S. based on 24 climate projections has showed an increase in runoff of 5-10% in the Ohio River basin and 2-5% in the upper Mississippi River during the period of 2041-2060. No significant increase in runoff is observed in the Great Lakes region during that period (Milly et al, 2005). The simulation based on 19 climate models participating in IPCC (AR4) report has resulted in more arid southwestern U.S. in 21st century (Seager et al, 2007).

The application of a number of GCMs, RCMs and multiple projections over the western U.S. shows an increase in the future temperature pattern. Precipitation shows an increase or decrease pattern based on the type of models, regions and seasons. The Pacific Northwest (PNW) is likely to have somewhat wetter winters and dryer summers (Hamlet et al, 2005). Giorgi et al (1994) has reported an increase in temperature and precipitation (except for a period of April to Oct in southwestern U.S.) under doubled CO_2 concentration levels. An increase in temperature (0-4.5ºC) and an increase or decrease in precipitation is observed at Washington, Oregon, Idaho and Montana (Leung and Ghan, 1999). An increase in temperature and precipitation is observed for the western U.S., except for spring and summer precipitation which shows both increasing and decreasing patterns (Kim et al., 2002). Snyder et al. (2002) and Coquard et al. (2004) also confirmed the positive response for temperature for all seasons, and positive or negative response for precipitation for different regions. The existing research demonstrates how difficult it is to predict the precipitation response in the western United

States. Precipitation data show increasing or decreasing patterns based on results from different climate models applied to the same region. McGuffie (1999) pointed out that careful consideration is needed when drawing conclusions from a single GCM output, since the observed changes are very likely prone to errors.

2.1.4.3 Effect of GCMs Resolution in Impact Studies

Based on various climate change studies performed using GCMs, no single climate models are considered the best for all climate variables. The simulated results showed different levels of success from using different models and parameters. Some studies have found no significant difference in the model results when altering the model resolution, performance, quality or projections (Lambert and Boer, 2001; Pierce et al, 2009). Other studies have shown the GCM results in close agreement with observed data for higher resolution simulation in compared to coarser resolution simulation (Giorgi et al, 1998; Iorio et al, 2004). Due to the lack of high quality data, it has become difficult to simulate the seasonal cycle amplitude of precipitation in the western United States (Coquard et al, 2004; Pierce et al, 2009). In a study by Mearns et al. (1995), the rainfall intensity is simulated accurately while the mean precipitation is over estimated by GCM in the northeast U.S. The frequency and magnitude of extreme events are not simulated quite well using coarser resolution models and sometimes even with higher resolution models (Gordon et al, 1992; Giorgi et al, 1998; Iorio et al, 2004). Coarser resolution models consider the average rainfall in small catchments which diminishes the importance of extreme events. The natural climate variability (e.g. ENSO, PDO) are also not represented well in coarser resolution GCMs. More descriptions on the sensitivity of

the simulated response of climate change to model resolution can be found in Duffy et al. (2003) and Govindasamy et al. (2003).

The results also vary for studies which incorporate both higher resolution regional climate models (RCMs) and coarser GCMs. The mean precipitation for the U.S. is over predicted by GCMs while it's under predicted (almost 20%) by MM4 RCM (Giorgi et al., 1994). The spatial and temporal biases present in the coarser resolution models are reduced with the use of higher resolution models and provide more detailed, accurate and realistic simulations (Giorgi et al. 1994, 1998; Mearns et al. 1995). As discussed in Iorio et al (2004), the coarser resolution models depend more on the semi-empirical parameterizations which lacks higher quality output of simulated precipitation. The ability to simulate convective storms and extreme precipitation events mainly occurring in summer, which attributes to larger biases in the model results and increased reliance on parameterizations, are also improved by higher resolution simulation. This occurs despite the fact that the model relies less on these parameterization mechanisms at higher resolution. The extreme precipitation events are more accurately represented and simulated by the super parameterization model "SP-CAM" in which the higher resolution cloud system resolving model (CSRM) are embedded within the GCM.

2.1.4.4 Extreme Precipitation Events

The frequency and intensity of heavy precipitation events have increased in many regions during the past 50 years (Frich et al, 2002; IPCC, 2007). The increase in the precipitation intensity under the warmer climate is supported by various studies (Cubasch et al, 2001; Palmer and Ra¨isa¨nen, 2002; Semenov and Bengtsson, 2002; Voss et al, 2002; Milly et al, 2002; Watterson and Dix, 2003; Wehner, 2004; Meehl et al, 2005;

Ra¨isa¨nen, 2005; Goswami et al, 2006). The anticipated increase in convective activity due to increased radiative energy under enhanced GHG conditions could result in an increase of the intensity and frequency of heavy rainfall events (Noda and Tokioka, 1989; Gordon et al., 1992). Along with the increase in extreme events, the uncertainties for estimating the average recurrence interval for more extreme flood events are expected to increase under changed climatic conditions (Mearns et al., 1984; Schreider et al, 2000). The analysis of extreme rainfall events and their variability with the use of GCMs in the past century have simulated larger changes in the frequency of extreme daily precipitation (e.g. Mearns et al, 1990; Gordon et al. 1992; Cubasch et al, 1995; Mearns et al, 1995; Jones et al, 1997; Hennessy et al, 1997; Zwiers and Kharin, 1998; McGuffie et al, 1999; Kharin and Zwiers, 2000). However the available resolution of GCMs is not considered well enough to draw a conclusion on extreme events in most of these studies.

The evaluation of extreme events requires the use of RCMs, high resolution GCMs, or downscaling of data to a smaller time scale (Brown and Katz, 1995). Although RCMs possess restricted boundary conditions, they can simulate local fine-scale feedback processes which were not possible in the past (Maurer et al, 2007). The high resolution simulation improves the analysis and accuracy of the GCM results (Kim et al, 2002). Including these recommendations, several studies (most of which are from Europe) have been done using multi-models, multi-scenarios, or both along with high resolution simulations to address the various uncertainties in the impact studies of extreme precipitation events (e.g. McGuffie et al, 1999; Durman et al, 2001; Jones and Reid, 2001; Ra¨isa¨nen and Joelsson, 2001**;** Prudhomme et al, 2002; Huntingford et al., 2003; Watterson and Dix, 2003; Ekstro¨m et al, 2005; Fowler et al, 2005; Frei et al, 2006;

Tebaldi et al, 2006; Beniston et al, 2007; Buonomo et al, 2007; Fowler et al, 2007; Dankers and Feyen, 2009; Dankers et al, 2009; Fowler and Ekstro¨m, 2009; Kyselý and Beranová, 2009; Mailhot et al, 2010).

The summer is expected to dry further, while an increase in intensity and decrease in return period for both shorter and longer duration extreme precipitation events is expected in most areas based on the results from climate models (Christensen and Christensen, 2003; Fowler and Kilsby, 2003a).The projection of changes in extreme precipitation has shown the greatest increase in precipitation intensity for extreme short duration events (Ra¨isa¨nen and Joelsson, 2001**;** Buonomo et al, 2007). There are, however, some uncertainties while analyzing the results at a regional scale. Some areas showed decrease in total precipitation in warmer climates (May et al, 2002; Voss et al, 2002); results of some models are not statistically significant in some regions, while, in other areas, they are not simulated properly (Huntingford et al, 2003; Kiktev et al, 2003).

2.1.5 Uncertainties in Climate Change Studies

Existing research based on assumption of a stationary climate are not supported at present due to the occurrence of significant changes in the Earth's hydrological cycle over time. These changes occur due to natural variability, human activities and regional warming (Bonfils et al, 2008). The answer on "Will global warming be 'warm and wet' or 'warm and dry'?" is still inconclusive. At this point, any of the above situations could occur (Hamlet et al, 2005). The available GCMs possess different abilities to model current and future climate trends. Climate change study results vary for different catchment scales and climate scenarios. Most of the studies assume that good climate models can reproduce present climate. On the other hand, Coquard et al (2004) has

reported that better models do not necessarily provide improved predictions of precipitation, and to some extent, temperature as a response to increased CO_2 concentration. Uncertainty in the development of future climate conditions is also a big issue (Braun et al, 2000). The uncertainty arises from various sources such as the method of downscaling, incorporating natural variability in the developed models, the number of GCMs available, GCM inter-model variability, choice of SRES scenarios, and the selection, calibration and validation of a hydrologic model for a future climate conditions (Prudhomme et al, 2003; Minville et al, 2008). The model simulated results are considered comparable with observational data, even though it does not capture all the processes in the Earth's system (Lambert and Boer, 2001).

Efforts should be focused on reducing uncertainty for better predictions. A number of GCMs and scenarios are used by several studies to reduce the uncertainty to some extent (Merritt et al, 2006; Maurer, 2007; Vicuna et al, 2007). A minimum of three different GCMs are considered as the useful ensemble size, when analyzing the changes in precipitation extremes (Kendon et al, 2008). There is a considerable difference between the results simulated with different models. The mean model result, which is obtained by averaging all the ensemble model results, is considered to provide the best comparison to observations for climatological mean fields (Lambert and Boer, 2001; Coquard et al, 2004). Various studies have suggested the non-uniform weighting of model results due to different capacity of each model to simulate climate conditions (Giorgi and Mearns, 2003; Tebaldi et al, 2004, 2005; Lopez et al, 2006). The future hydrologic impacts such as percent increase or decrease in streamflow are also compared with respect to a common baseline period for different models. The Bayesian approach of

probabilistic analysis of ensemble multi-model multi-scenario results, and the generation of probability density functions (pdfs) of change are considered to better represent the uncertainty of climate variability (Tebaldi et al, 2004, 2005; Lopez et al, 2006). Seasonal analysis, calculation of mean, median and percentiles, and the analysis of variance (ANOVA) are suggested by some other studies as a way to quantify model uncertainty (e.g. Fowler et al, 2007; Seager et al, 2007; Pierce et al, 2008; Dankers and Feyen, 2009; Fowler and Ekstro¨m, 2009).

There are several criteria (such as coefficient of determination, r^2; Nash-Sutcliffe efficiency, E; index of agreement, d; Nash-Sutcliffe efficiency with logarithmic values, ln E; modified forms of E and d, relative efficiency criteria E_{rel} and d_{rel}) that can be used to evaluate the performance of a hydrologic model (Krause et al, 2005). It is possible that a precisely calibrated model parameter at present may not perform well when predicting future conditions. The use of the same optimized parameter for the past and the future also ignores the potential feedback between the surface and the atmospheric processes (Chiew et al, 1995).The use of more physically based hydrologic models including the multi-model, multi-scenario approach, and the probabilistic analysis could quantify the uncertainty to some extent and provide the likelihood of occurrence of future hydrologic changes (Georgakakos et al., 2004; Minville et al, 2008).

The integrated climate hydrology model is required to quantitatively access the impacts of climate change on runoff (Bronstert et al, 2002). Most of the past studies utilized GCM output and a suitable hydrologic model to see the impacts of climate change on runoff response of a basin (e.g. Chiew et. al, 1995; Gellens and Roulin, 1998; Cameron et al, 2000; Bergstrom et al., 2001; Middelkoop et al, 2001; Reynard et al,

2001; Li et al, 2008). All information related to hydrologic variations, soil variations, artificial storage, snowfall, snowmelt, and climate change should be included for a realistic regional hydrologic evaluation. Additionally the availability and accuracy of data, the inherent accuracy, flexibility, and compatibility (with the existing GCMs) of the hydrologic model represent major criteria for evaluating the applicability of hydrologic model to climate change studies (Gleick, 1986).

2.2 Weather Modification (Cloud Seeding)

2.2.1 Concepts on Weather Modification

Weather Modification (WM) is also called an 'atmospheric water resources management technology', or 'cloud seeding', or 'precipitation enhancement' project. WM represents an artificial stimulation of clouds to increase natural rainfall (snowfall) or hail suppression. Runoff augmentation is an alternative to meet the need of increasing water demand. Cloud condensation nuclei, which are present as a particulate matter in the atmosphere, are not always sufficient for natural precipitation. An introduction of ice nuclei (e.g. silver iodide (AgI), dry ice, liquid propane, salt compounds) in the cloud increases the freezing of the super cooled liquid at a higher temperature than natural and forms precipitation (WMA, 2005). Super cooled liquid water attaches to the AgI crystals and freeze to form droplets of super cooled liquid water. These droplets form snow crystals and fall as snow flakes. During this process, heat is released into the atmosphere which boosts updrafts and pulls more moist air into the cloud for more precipitation. Static and dynamic mode represents two modes of cloud seeding. The scientific basis for static mode is an increase in precipitation efficiency. The scientific basis for dynamic

mode is to enhance cloud development to increase the productivity of clouds (Kauser et al, 2008). Two types of cloud seeding are hygroscopic seeding (warm or mixed phase clouds) and glaciogenic seeding (cold based and continental). Ice producing materials (e.g. silver iodide, dry ice) or large hygroscopic particles (e.g. salt powder) is dispersed into the cloud during glaciogenic and hygroscopic seeding respectively. Cloud seeding is done by using ground based cloud seeding generators or special equipped aircraft. Depending on the type of cloud seeded and seeding delivery method, seeding effect takes place from immediate to almost 30 minutes (NAIWMC, 2010). Timing and targeting are two critical determinants in cloud seeding. It could decrease rainfall if the seeding time and place are not suitable (Kauser et al, 2008).

Silver Iodide (AgI) is a major component used for cloud seeding. Past studies have documented the release concentration of AgI aerosols through snowpack, rainwater, soil and lake sediment samples to be very low to cause any environmental and human health impacts (Cooper & Jolly 1970; Dennis, 1980; Warburton et al, 1996; McGurty, 1999; Sanchez et al, 1999; Tsiouris et al. 2002a, 2002b; ASCE, 2006; Williams & Denholm 2009; WMA, 2009). Eisler (1996) reported that the amount of AgI aerosols released by cloud seeding activities in 1978 was almost 0.1% of total release of silver in the environment; the same release amount is considered at present in U.S. and Canada. AgI is recommended for use because it can produce higher number of ice crystal seeds to produce more ice crystals (10^{15} ice forming nuclei per gram of AgI expended); it is considered water insoluble ($<10^{-9}$ g of Ag per g of water), and it is not freely bioavailable to the environment (ASCE 2004, 2006; WMA, 2009).

2.2.2 Previous Studies on Weather Modification

WM programs have existed since the early 1950s (NRC, 2003). Most of these activities have been in operation in the western parts of the U.S., Canada and some other regions of the world (e.g. China, Thailand). The World Meteorological Organization (WMO, 2000) reported about 74 operational cloud seeding projects all over the world in the year 2000. The National Oceanic and Atmospheric Administration (NOAA) identified almost 66 projects in the semi arid western U.S. by the year 2001; some projects have been running for more than 50 years (NRC, 2003; Ryan et al, 2005). The WM programs are in operation for water supply enhancement in western U.S. and hail suppression in the High Plains of U.S. and Canada (Cotton, 2007). The production of additional supply through cloud seeding is inexpensive in compared to building of new infrastructures (Grant, 1983; Breed, 2008). The WM programs are considered as "cost benefit and environmental friendly" technology, which are also viewed as a long-term water management tool (WWDC, 2005; Kauser et al, 2008).

A properly designed cloud seeding project can increase precipitation by more than 10% (AMS, 1998; WMA, 2005). WM programs are assumed to be effective in target areas with no adverse effects on surrounding areas. A feasibility study of operational cloud seeding program in the Salt River and the Wyoming ranges in Wyoming has reported an average increase of 10% in November through March precipitation (Griffith et al, 2007). This project also recommended the months of November to March for cloud seeding since a majority of seedable storms are present in this period. Since 1972, glaciogenic seeding of winter orographic clouds is in practice in the Colorado River Basin. The projects are in operation to prevent water shortage, reduce the impact of

drought, and enhance reservoir storage (Ryan et al, 2005; Cotton, 2007). The headwater regions of Colorado River Basin for wintertime cloud seeding include the Central Colorado Rockies, the Vail and Upper Arkanas region, the Grand Mesa, the San Juan (Delores) River Basins, the Gunnison Basin, and the Southern ranges of Wyoming. Cloud seeding is supposed to contribute from 0.8 to 1.8 million acre-feet (MAF) of water for the Colorado River Basin with a favorable benefit cost ratio for the program (Ryan et al, 2005; Griffith and Solak, 2006). The WYMPP is planned to run from 15 November to 31 March, for five consecutive years, starting from 2005/06 season (Boe, 2008). Around 250 storm events are estimated in the target areas to attain a 15% increase in precipitation (Breed, 2008).

Higher production of hydroelectric power at a cheaper cost, through increase in snowpack, is the major objective of the cloud seeding projects which are operating in the Upper Snake River Basin, Idaho. An increase in snowpack of about 7 % and a higher reservoir level is already observed in the Basin (Barker, 2009). Some studies identified higher agricultural yield and hail damage reduction in North Dakota (Smith et al, 1992b; Smith et al., 1997; Pandil, 2009). Out of 11 operational cloud seeding programs in the watersheds of Sierra Nevada, the statistical evaluation showed positive effect for 6 watersheds on the western side of Sierra Nevada Mountain Range (Silverman, 2010).

In terms of monetary evaluation, KWO (2001) estimated a cost in the range of $1 to $15 per AF of additional runoff from snowpack in Kansas. Utah Department of Natural Resources (2005) has reported an increase in between 2 to 18 percent in April 1 snowpack water content due to WM projects from Utah. This same project has estimated an annual runoff increase (~ 7% of the study area) at a cost less than $2.0 per AF. The

recorded benefit cost ratio, which also includes the applications of increased runoff from the WM projects, ranges from 20 to 40 for most of the WM projects (Sell and Leistritz, 1998; Griffith and Solak, 1999; Stauffer and Williams, 2000; ASCE, 2006; Kauser et al, 2008). WM programs (hygroscopic or glaciogenic cloud seeding) that were implemented in different regions and evaluated for rainfall enhancement have shown increases in rainfall in most cases (Kethley, 1970; Kahan, 1972; Osborn, 1972; Seely and DeCoursey, 1975; Zovne and Koelliker, 1979; Johnson, 1985; Rosenfeld and Woodley, 1989,1993; Holroyd et al, 1995; Mather et al, 1997; Bruintjes, 1999; Medina, 2000; Murty et al, 2000; Silverman and Sukarnjanaset, 2000; Terblanche et al, 2000; Fowler et al, 2001; Stauffer, 2001; Griffith et al, 2005a,2005b; Hunter et al, 2005; Super and Heimbach, 2005; Heggli et al, 2007; Huggins, 2007; Hunter, 2007; Kang and Ramirez, 2007; Huggins et al., 2008; Woodley and Rosenfeld, 2008; Griffith et al, 2009; Levin, 2009; Chen and Xiao, 2010).

Some cloud seeding projects showed controversial results for different categories of rainfall and weather conditions (Sharon et al, 2008; Levin et al, 2010). Despite the increase in precipitation, the cloud seeding contributed less on the days with higher natural rainfall and made the program insignificant. During the drought condition, few clouds are available for seeding; during the rainfall above normal conditions, seeding is not effective as plenty of rain is available (WWDC, 2010). The decrease in precipitation is also attributed to physical factors such as increasing urban and industrial air pollution (Givati and Rosenfeld, 2004). Some related studies on cloud seeding are listed here (Hastay and Gladwell, 1969; Benjamini and Harpez, 1986; Zvi, 1988; Smith et al, 1992a;

Zvi and Langerman, 1993; Bigg, 1997; Woodley et al, 2000; Yin et al, 2000, 2001; Segal et al, 2004; Gao et al, 2006; Curie et al, 2007; Rasch et al, 2009; Drofa et al, 2010).

2.2.3 Uncertainties and Evaluation Criteria

Most of the past and ongoing researches have mainly focused on winter WM (winter seeding) for snowpack augmentation. The major goal is to increase soil moisture level and reservoir storage during dry periods. Research funding on cloud seeding has been limited over past years due to the lack of proper evidence on the positive effects of cloud seeding (NRC, 2003). The changes in rainfall and snowfall are not accurately verified as changes due to WM programs alone. Various uncertainties such as natural continuous variability of rainfall and runoff, accurate measurement of climate variables, critical questions related to the microphysical processes leading to precipitation, need of randomize and replicate experiments, adverse effects on underlying areas, bias in model results, evaluation of benefits, complications due to environmental factors, restrict while drawing conclusions to verify seeding effects scientifically. WM programs to augment rainfall and snowpack are still operating based on cost versus probabilistic benefit analysis.

The inclusion of uncertainties makes an evaluation of effectiveness of WM programs more challenging. Evaluation is based on data from SNOTEL target sites (precipitation and runoff), measurement of super cooled liquid water, crop yield, and regression equations for precipitation and snow water content (Warburton et al, 1995; Breed, 2008; Griffith et al, 2007). A long period of data is required to establish this type of relation. Snow trace-chemistry analysis, objective radar based analysis, satellite data evaluation, and numerical modelings are some of the recently developed methods to

evaluate effects of cloud seeding (NAIWMC, 2010). Snow trace-chemistry analysis confirms effective seeding based on concentration of chemicals, and silver to indium ratio in monitored snow samples over target area (Heggli et al, 2007). The Colorado White Paper has categorized the evaluation methods into three types: statistical, physical, and modeling (Griffith and Solak, 2006). A 'Target' group of seeded storms is compared with a 'Control' group of unseeded storms in the conventional statistical method or "time of origin analysis" (Terblanche et al, 2000).

Some studies used quartiles, 'p' values and confidence intervals (for seeded and control storms) to evaluate cloud seeding program (Terblanche et al, 2000). This same project compared routine rainfall measurements for the month of operational seeding (March 1995) and the rainy season (Oct 1995 to March 1996). Other studies have used regression models based on daily rainfall and 'Double Ratio (DR)' (ratio of rainfall in target area to control area) on seeded and unseeded days (Zvi and Fanar, 1997; Sharon et al, 2008; Morrison et al, 2009).

Strong physical evidences as well as highly significant statistical evidences are required to prove the effects of cloud seeding scientifically (Cotton, 2008). Although effectiveness and great successes (precipitation increase in the range of 20%) have been claimed for WM programs, the results are controversial due to lack of scientific evidence to demonstrate these claims (Silverman, 2001, 2003). Uncertainties due to downwind effects and natural variability of clouds, role of aerosols, identification of right cloud, wind effects e.t.c. are still inconclusive (Cotton, 2008). Difficulty still remains while selecting the region for cloud seeding, efficient targeting, and dispersing of seeding material (Breed, 2008). The Weather Modification Association (WMA) also supports

recommendations for randomized and statistical experiments (at least 10% of seeding events); a national program which includes exploratory and confirmatory field studies; and development of new statistical methods, to achieve statistically significant results and reduce uncertainties on effectiveness of WM programs (Ryan et al, 2005). Additionally, use of meso-scale models; high quality observational (radar based) dataset; more sophisticated targeting models to account for local variations in wind conditions; assignment of common time base and decision time; and other advanced technologies, are recommended for identification of highly seedable storms in target area and better evaluation of WM programs (Terblanche et al, 2000).

CHAPTER 3

MODELED STREAMFLOW RESPONSE UNDER WEATHER MODIFICATION IN THE NORTH PLATTE WATERSHED, WYOMING

3.1 Introduction

Snowpack augmentation and runoff enhancement are considered to be an integral part of regional water management in many arid and semi arid regions. Longer droughts in arid regions have necessitated weather modification (WM), or cloud seeding programs. The major goal of WM program is to prevent water shortage, reduce the impact of drought, and enhance reservoir storage, by utilizing clouds in the sky.

The wintertime cloud seeding is considered scientifically most efficient and credible for larger scale WM programs (Hunter, 2007). It has been reported that a properly designed and implemented WM programs could increase snowpack in the range of 5% to 15% (AMS, 1998; WMA, 2005). Studies have identified an increase of 6% in agricultural wheat production and a decrease in crop hail loss of 45% in North Dakota (Smith et al, 1992b, 1997; Pandil, 2009). An increase in snowpack of about 7 % and a higher reservoir level has been observed in the operational cloud seeding project in the Upper Snake River Basin, Idaho (Barker, 2009). The amount of rainfall was more than doubled in a silver iodide based cloud seeding project in Texas (Rosenfeld and Woodley, 1989). WM programs that were implemented in different regions and evaluated for rainfall enhancement have shown increases in rainfall in most cases (Kethley, 1970; Kahan, 1972; Osborn, 1972; Seely and DeCoursey, 1975; Zovne and Koelliker, 1979; Johnson, 1985; Rosenfeld and Woodley, 1989,1993; Holroyd et al, 1995; Mather et al, 1997; Bruintjes, 1999; Medina, 2000; Murty et al, 2000; Silverman and Sukarnjanaset,

2000; Terblanche et al, 2000; Fowler et al, 2001; Stauffer, 2001; Griffith et al, 2005a,2005b; Hunter et al, 2005; Ryan et al, 2005; Super and Heimbach, 2005; Curie et al, 2007; Heggli et al, 2007; Huggins, 2007; Hunter, 2007; Kang and Ramirez, 2007; Huggins et al., 2008; Woodley and Rosenfeld, 2008; Griffith et al, 2009; Levin, 2009; Chen and Xiao, 2010). WM programs are considered to be 'cost effective and environmental friendly' technology (WWDC, 2005; Kauser et al, 2008). The production of additional water supply through cloud seeding is considered inexpensive compared to building new infrastructure (Grant, 1983; Breed, 2008). KWO (2001) estimated the cost in the range of $1 to $15 per AF of additional runoff from snowpack in Kansas. Utah Department of Natural Resources (2005) has estimated the cost to be approximately $2.0 per AF of additional runoff for the combined projects in Utah.

WM programs are claimed effective with an increase in precipitation in the range of 5% to 20%. Verifying the seeding effects is difficult; however, WM programs are justified based on cost versus probabilistic benefit analysis (NRC, 2003). The recorded benefit cost ratio, which also includes the applications of increased runoff from the WM projects, ranges from 20 to 40 for most of the WM projects (Sell and Leistritz, 1998; Griffith and Solak, 1999; Stauffer and Williams, 2000; ASCE, 2006; Kauser et al, 2008). With increasing water demand, WM projects are expected to increase in different parts of the world.

WM programs have been operating in most of the western U.S. since the 1950s to fulfill the increasing water demand in these regions. Reconstructed climate data has indicated the occurrence of very lengthy and severe droughts in the arid western U.S. in the past (USGS, 2004). The Colorado River Basin, a major source of water supply for the

western U.S., has been in a drought since 1999 (BOR, 2006). Snowmelt runoff is the major source of water supply in the western U.S. but a significant decrease in the mountain snowpack is noticed in the last century in these regions (Mote et al., 2005). In California, there is a need of at least two million AF of additional water to sustain the urban growth by 2030 (Shaw, 2006). The United States Department of Interior (U.S. DoI, 2003) has also reported the continuous increase in the consumptive use of water in the West to sustain urban growth. It could create serious water conflicts in the future while meeting the higher water demand. In addition, decreased snowpack runoff could impact production of hydroelectric power, thus creating adverse impacts on the power demand of California and other western States (Griffith and Solak, 2006; Hunter, 2007). The trend of increasing water demand and declining snowpack could worsen the situation even more if no significant action is taken (U.S. DoI, 2003). WM programs have been considered the most attractive option for increasing water availability.

Since 1972, the glaciogenic seeding of winter orographic clouds has been ongoing in the headwater watersheds of the Colorado River Basin (Cotton, 2007). Cloud seeding is supposed to contribute from 0.8 to 1.8 million acre-feet (MAF) of water for the Colorado River Basin, which could result in a favorable benefit cost ratio for the program (Ryan et al, 2005; WMA, 2005; Griffith and Solak, 2006). The feasibility study of operational cloud seeding program in the Salt River and the mountains of Wyoming have shown an average increase of 10% in the November through March precipitation (Griffith et al, 2007). The Wyoming Water Development Commission (WWDC) through the Wyoming Weather Modification Pilot Project (WYMPP) has conducted silver iodide based cloud seeding during the winter period (60-80 days) for the months of November

through March (WWDC, 2005). Most of the cloud seeding for the WYMPP is done in the North Platte watershed (Sierra Madre and Medicine Bow ranges) in south central Wyoming and Wind Range River in west central Wyoming. WWDC initiated the program in spring 2005, and full scale cloud seeding operations started in 2007-2008. The present available water resources in the Platte River basin in Wyoming are fully allocated (WWDC, online accessed 2010). Under a moderate population growth, the water demand in the Green River Basin is expected to increase from 73 to 82 percent of its allocation given in the Colorado River and up to 88 percent in the Wind River (Big Horn) Basin. WWDC (2010) has estimated an additional 130,000 to 260,000 AF of water each spring from a 10% increase in precipitation from the proposed pilot projects. However there is a need to further evaluate this and quantify the impacts.

Most WM programs consider only the rainfall augmentation and do not quantitatively evaluate the significant hydrological impacts. Some past studies have utilized observed data to evaluate the hydrological impacts of WM, but they are limited and insufficient to account for uncertainties (natural variability of rainfall and runoff) in WM programs. Modeling is considered appropriate since various WM scenarios can be forced into the model that could consider uncertainties about the effects of these programs (Seely and DeCoursey, 1975). A physically based hydrologic model that operates at a higher resolution could provide more realistic simulations and account for complex topography and diverse climate of the western United States. This paper aims to evaluate the possible impacts of weather modification on water supply by utilizing a process based hydrologic model. The WM programs are expected to augment precipitation by 10% in the North Platte watershed. Through modeling and WM scenario

analysis, this paper provides a quantitative assessment of change in water supply (streamflow) as a result of transformation of increased precipitation in the watershed. Since no studies related to hydrologic impact evaluation are yet done in the watershed, the impact on streamflow due to operational WM programs can be utilized for future water supply and demand management study.

The rest of the paper is outlined as follows. The description of the study area, data needs and the hydrologic model used in this analysis are discussed in Section 3.2; model calibration along with the simulated results under forced WM conditions are discussed in Section 3.3; and the concluding remarks are provided in Section 3.4.

3.2 Methodology

3.2.1 Study Area

The study area is the North Platte Watershed, the boundary of which lies in the states of Wyoming and Colorado at latitude 40.3125° to 41.9375° N, and longitude 105.9375° to 107.0625° W (Figure 3.1). The annual precipitation varies from 25 to 60 inches with 40 to 70 percent as winter snow (> 250 inches of snow). The watershed contains six streamflow gauges and eight SNOTEL stations, which are operated by United States Geological Survey (USGS) and National Resource Conservation Service (NRCS) respectively. The North Platte River, which is a tributary of the Platte River and starts at the high basin of North Park in north-central Colorado, flows northward into Wyoming along the Westside of Medicine Bow ranges and finally meets the Medicine Bow River and Seminoe Reservoir. The Platte River is a tributary of the Missouri River which is a tributary of Mississippi River. The major sites of cloud seeding include the

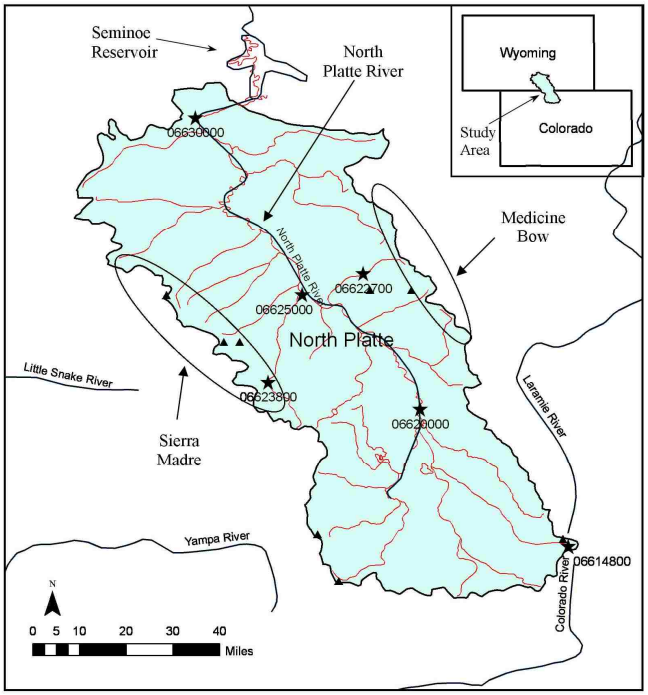

Figure 3.1 Location of the North Platte Watershed, major areas for cloud seeding operations, and rivers, streamflow gauges (indicated by stars) and SNOTEL stations (indicated by triangles) located inside the watershed.

Sierra Madre and Medicine Bow ranges in south central Wyoming. Around 250 storm events are estimated in the target areas to attain a 10 to 15% increase in precipitation due to cloud seeding operations (Breed, 2008). These operations are conducted only in the Wyoming ranges of the North Platte watershed; the operations in the Colorado ranges of the watershed are of future interest.

3.2.2 Hydrologic Model

The hydrologic model used in this analysis is the Variable Infiltration Capacity (VIC) model (Liang et al, 1994; Cherkauer and Lettenmaier 2003). VIC is a macro-scale land surface semi-distributed hydrologic model which has been used in a variety of water resource applications and climate change studies (e.g. Hamlet et al, 2005; Mote et al, 2005; Pierce et al, 2008; Hidalgo et al, 2009; Wang et al, 2009). The model uses 1/8

degree gridded, meteorological forcing data (precipitation, maximum and minimum temperature, wind speed), land cover, soil, elevation bands and other watershed characteristics. Simulations are carried out for each grid cell and the time series of output variables (e.g. runoff, soil moisture, snow water equivalent) are also stored separately for each specific grid. Simulations are carried out at a daily or sub-daily time step based on the two modes of operation- water balance and energy balance. Water balance mode considers equal temperature for soil surface and air, and it does not solve the surface energy balance. Energy balance mode solves the total water balance and simulates surface energy fluxes to compensate incoming total radiation fluxes. The surface fluxes include sensible heat, latent heat, ground heat, ground heat storage, and outgoing long wave.

The VIC model uses a separate river routing model of Lohmann et al. (1996) for the routing of streamflow. Various options exist during the VIC simulation, most of which are set in a 'global parameter file'. Newer versions of the VIC model include snow algorithm that solves the surface energy balance and incorporates spatially distributed snow coverage and snow sublimation. This snow model handles the snow interception and canopy processes at the macro-scale and considers two layer formulation- surface layer and pack layer. Energy exchange takes place from the thin surface layer; pack layer acts as a reservoir that stores excess snow in the surface layer. All important heat and energy fluxes such as sensible and latent heat, convective energy, and internal energy of the snowpack are considered in snow model.

3.2.3 Data Description

The SNOTEL station data are obtained from the National Water and Climate Center of National Resource Conservation Service (NRCS). The historical data available in the site are daily accumulated precipitation, snow depth, snow water equivalent, and temperature (maximum, minimum, average). These data are available from early 1980's for earlier established stations, and from early 1990's for other stations. The monthly and annual streamflow data, for a period of 1940-2009, are obtained from the United States Geological Survey (USGS). The retrospective meteorological forcing data (precipitation in mm, max and min temperature in degree Celcius, wind speed in m/s), vegetation, soil, and snow band data are obtained from Soil and Water Modeling Group, University of Washington (Maurer et al, 2002; access http://www.hydro.washington.edu/SurfaceWaterGroup/data.php). All of these data are available for 1/8-degree grid cell for the conterminous United States. The gridded data was prepared through estimation using spatial and temporal interpolation of observed data sources. The meteorological forcing data are in a binary format and daily time steps, for a period of 1949-2000, and are derived from the hydrologic simulation (at a 3 hourly time step) of land surface energy and water variables over the continental United States. The daily wind speed (m/s) represents wind speed measured at an average height of two meters above the surface.

The soil parameter file contains geographical information for each grid cell, and grid cell soil parameters including initial soil moisture conditions. The vegetation parameter file defines different landcover types that are used during simulation, number of vegetations and their coverage in each grid cell, and other vegetation parameters (e.g. LAI-leaf area index, root depth). The snow band file contains information on each

elevation band that is used by the snow model. The land cover data obtained from the Department of Geography, University of Maryland (www.geog.umd.edu/landcover) also contains different landcover types and their coverage at a higher (1km) resolution.

3.2.4 Model Simulations

All simulations are performed using the VIC model (version 4.1.1.) and its energy balance mode of operation. The VIC model is first calibrated and validated by forcing the historical meteorological data that reproduce the historical trend in streamflow. The most common parameters for calibration include soil parameters such as infiltration, soil depth, base flow velocity, and soil moisture (http://www.hydro.washington.edu/Lettenmaier /Models /VIC). Six snow elevation bands are selected to better represent snow processes for each grid cell. The routing model is not used for this analysis since the basin is small (only 97 grid cells) and the analysis is mainly focused on monthly, seasonal or annual changes in streamflow. The total simulated streamflow for the watershed is the sum of VIC simulated streamflow for each grid cell. A univariate calibration method is followed where most sensitive soil parameters are selected and sensitivity analysis is carried out to finalize each parameter. The sensitivity analysis for each parameter is based on model performance indicators. The commonly used indicators such as Pearson Correlation Coefficient (r), Root Mean Square Error (RMSE), Bias percentage, and Nash-Sutcliffe Efficiency (E) are calculated to evaluate the model performance in simulating the observed streamflow. They are calculated as follows (Krause et al, 2005; Wang et al, 2009):

$$r = \frac{\sum_{i=1}^{n}(Oi - \overline{O})(Pi - \overline{P})}{(n-1)SoSp} \qquad (3.1)$$

$$NSCE = 1 - \frac{\sum_{i=1}^{n}(Oi - Pi)^2}{\sum_{i=1}^{n}(Oi - \overline{O})^2} \quad (3.2)$$

$$Bias = \frac{\sum_{i=1}^{n}(Pi - Oi)}{\sum_{i=1}^{n} Oi} * 100\% \quad (3.3)$$

$$RMSE = \sqrt{\frac{1}{n}\sum_{i=1}^{n}(Oi - Pi)^2} \quad (3.4)$$

Where, O_i and P_i represent observed and predicted streamflows respectively; S_o and S_p are sample standard deviations for observed and predicted streamflows; and n is the number of observations.

A VIC model is developed for the watershed and the impacts of WM on streamflow are accessed quantitatively based on an anticipated increase in precipitation due to cloud seeding operations. Precipitation is increased only for the months of cloud seeding operations (Nov 15-April 15). No evaluations have been performed yet for the pilot project that could give an actual change of precipitation in the field. The cloud seeding operations in the North Platte watershed are expected to increase precipitation by 10%; this could be achieved only by seeding total storms during the months of cloud seeding operations. During this analysis, precipitation is increased by five (5) percent; a 5% increment represents at least half of the total storms are seeded during the months of cloud seeding. This is assumed realistic for this analysis since the operational WM project also aims to seed at most half of the total storms. The ground based generators for cloud seeding operations are mainly located at the central regions of the watershed. Therefore, only 12 grid cells (5 on Sierra Madre and 7 on Medicine Bow ranges) are

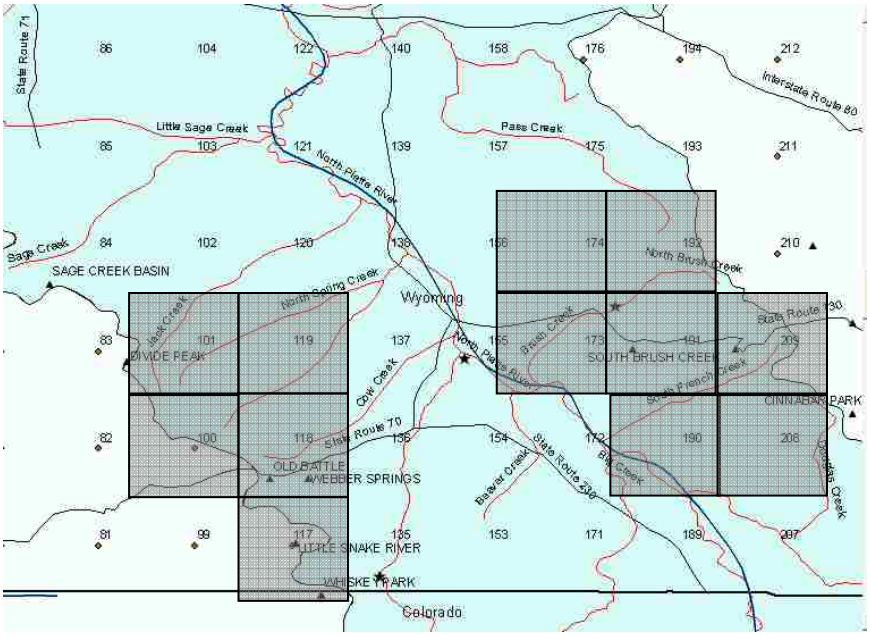

Figure 3.2 Central region of the North Platte watershed where most of the ground based generators are located for cloud seeding operations. The impact of cloud seeding is assumed higher for the highlighted region in this analysis.

selected from the central region where the impact of cloud seeding is assumed higher (Figure 3.2), and precipitations of half of the total storms during the months of cloud seeding, are increased by 5% (maximum). While developing the scenarios, precipitation is increased from 0.1% to 5%; this is done to quantify the variation in the runoff due to cloud seeding of different percentage of storms in the watershed. New sets of forcing data and various hypothetical scenarios are developed by changing precipitation in the retrospective meteorological data. These scenarios are forced into the calibrated VIC model to quantify additional streamflow due to increased precipitation.

Additional scenarios are simulated to observe the most likely impact of cloud seeding on different regions of the watershed and the type of landcover. These simulations are carried out by increasing precipitation (5%) of half of the total storms during the months of cloud seeding, but only on certain regions of the watershed, and

different types of landcover in the watershed. The grid cells within each specific region are selected for the first case, while the grid cells which contain about 30% of specific landcover type are selected for the later case. Simulations are then carried out for the whole watershed and the simulated streamflows from all of these forced WM scenarios are compared with the historical streamflows (1981-2000) for the watershed.

3.3 Results

3.3.1 Climate Observations

3.3.1.1 Precipitation

The average monthly observed precipitation (mm) is higher during the period of Nov-April and lower during June-August for the North Platte watershed (Figure 3.3). The cloud seeding operations are conducted during the Nov 15-April 15 period since this is the period of higher precipitation. Maximum monthly precipitation is observed at the Tower station that is located at the southwest border in the Colorado range; minimum monthly precipitation is observed at the SouthBrush Creek station which is located at the Medicine Bow range.

Figure 3.4 shows the spatial distribution of 10 years (1990-1999) average precipitation (mm/year) for the North Platte Watershed. Higher precipitation is observed in the Colorado ranges than the Wyoming ranges of the watershed. The average annual observed precipitation varies from 230mm to 1385mm throughout the watershed, with lower precipitation at the Northern regions of the watershed.

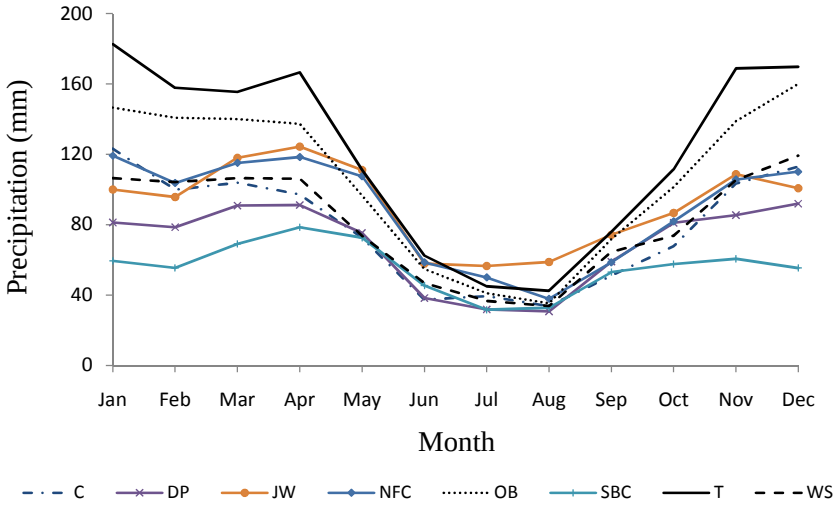

Figure 3.3 Average monthly precipitation (1980-2008) for the eight SNOTEL stations in the North Platte Watershed. (C: Columbine; DP: Divide Peak; JW: Joe Write; NFC: North Fork French Creek; OB: Old Battle; SBC: South Brush Creek; T: Tower; WS: Webber Springs).

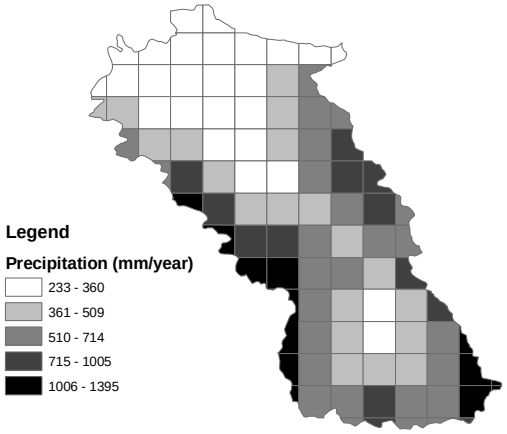

Figure 3.4 Spatial distribution of average annual precipitation (mm/year) during the period of 1990-1999 for the North Platte watershed.

3.3.1.2 Streamflow

Figure 3.5a shows the annual streamflow pattern (1940-2008) for the North Platte watershed; the annual observed streamflow from the Wyoming ranges is higher than the Colorado ranges (represented by USGS gauge '06620000') of the North Platte watershed.

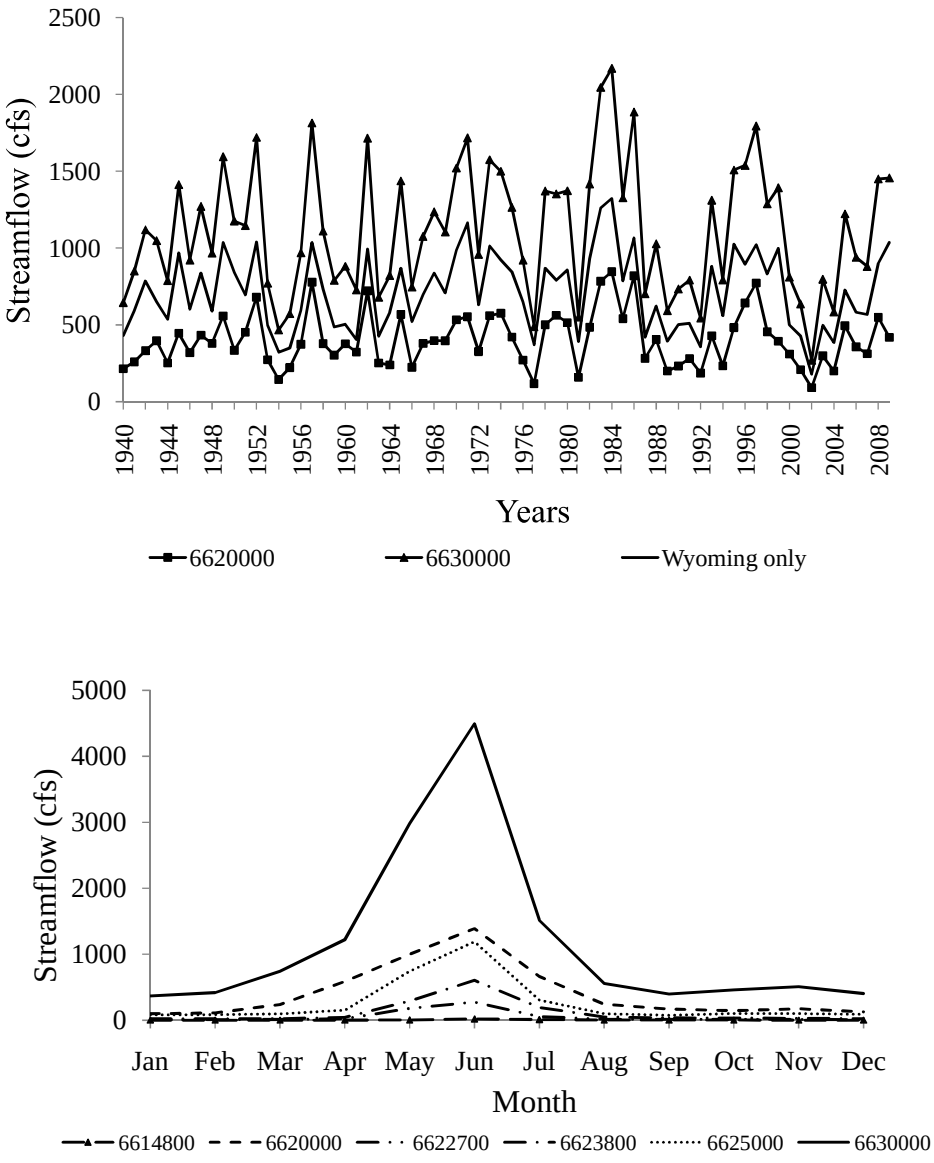

Figure 3.5 a) Annual streamflow pattern for the North Platte watershed; b) Average monthly streamflow (cfs) during the period of 1990-1999 for six USGS gauge stations in the watershed.

The annual observed streamflow for USGS gauge‘06630000’ is higher since it represents the total flow from the watershed and is located at the most downstream of the watershed. Both higher and lower annual streamflows are observed at different time periods;

maximum annual streamflows are observed during 1980-85. Figure 3.5b shows the 10-year (1990-1999) average monthly streamflows for six USGS gauge stations located within the watershed. Higher streamflows are observed during May-July; minimum streamflows are observed during August-February; maximum streamflows are observed during June with values more than 4000 cubic feet per seconds (cfs) for the entire watershed.

3.3.2 Model Calibration

The model is calibrated and validated with respect to historical monthly observed streamflow data, for the period of 1950-1980 and 1980-2000, respectively (Figure 3.6). The monthly data for USGS gauge 6630000, which is located at most downstream of the watershed and upstream of Seminoe Reservoir, is used for this purpose. For the calibration period, a RMSE (43000 ac ft.), Bias (0.26 %), r (0.90) and NSCE (0.79) are obtained, with slight under-estimation of higher peaks and over estimation of lower peaks. For the validation period, a RMSE (47000 ac ft.), Bias (-2.7 %), r (0.87) and NSCE (0.76) are obtained, with under-estimation and over-estimation similar to calibration. A negative bias means the observed streamflows are higher than the simulated streamflows. The infiltration parameter "b_{inf}" and soil depth "d2" are found more sensitive in compared to other parameters during model calibration. The scatter plots in Figure 3.6 show a good correlation between the modeled and observed streamflows at lower magnitude while more scatter if found at higher magnitudes. The computed NSCE was slightly higher when calibrated in the water balance mode of operation (not shown here). The energy balance mode of operation involves a larger number of parameters and various other processes that might have lowered NSCE during

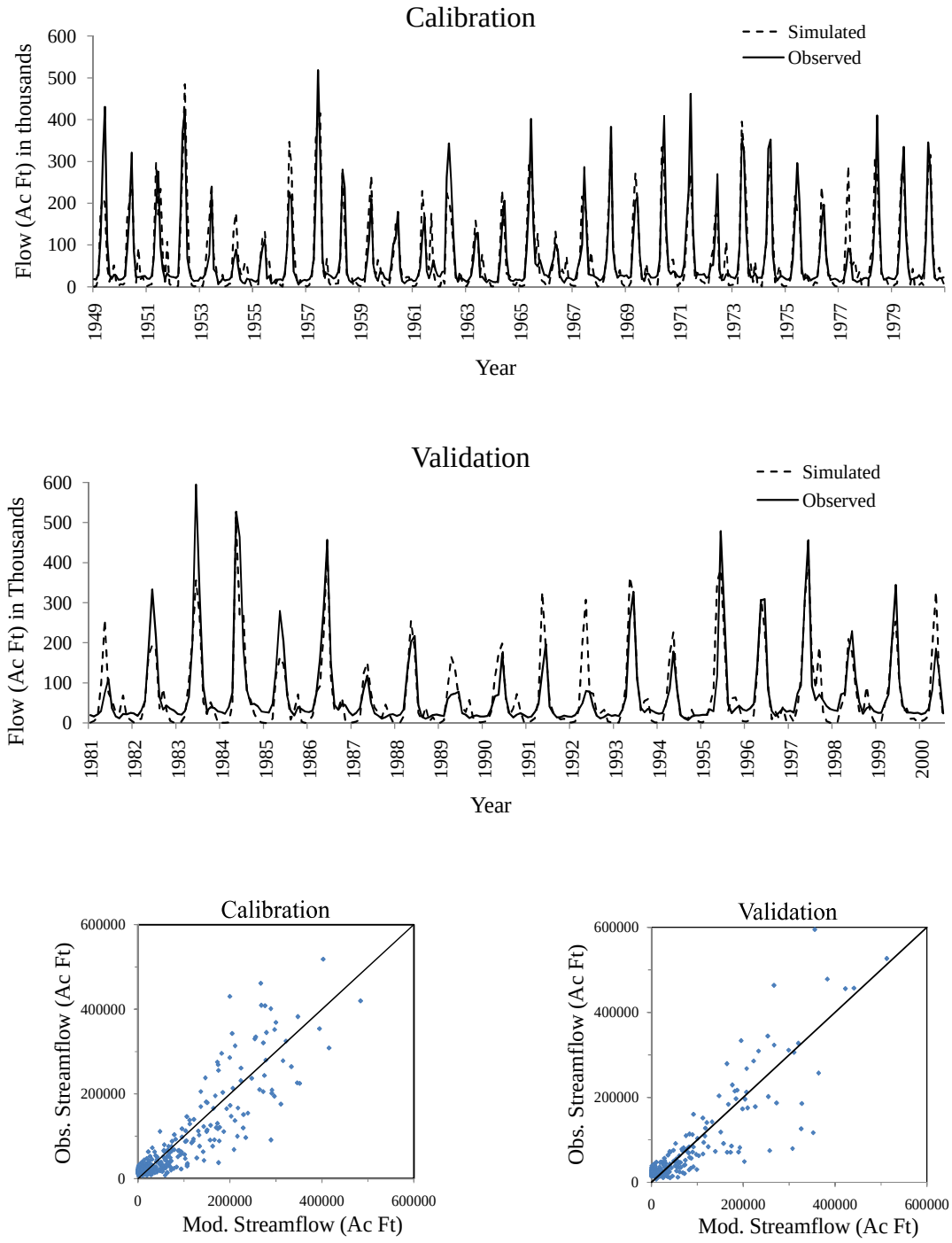

Figure 3.6 Variable infiltration capacity model calibration for 1950-1980 and validation for 1981-2000. Comparison of observed vs. modeled monthly streamflow.

model calibration. However, it is considered appropriate for this analysis since the peak and total runoff is simulated well with a very low bias and higher correlation coefficient. The finalized model calibrated parameters are: infiltration parameter (b_{inf} = 0.19); maximum baseflow (Ds_{max} = 11 mm/day); fraction of Ds_{max} (Ds = 0.04); fraction of maximum soil moisture (Ws = 0.15 mm/day); and soil depth (d2= 0.3 m).

3.3.3 Weather Modification Scenario Analysis

3.3.3.1 Change in Streamflow: Annual Pattern

Simulations are carried out to observe the changes in annual streamflow with respect to an anticipated increase in precipitation for the North Platte Watershed. As discussed earlier, precipitation for half of the total storms of selected grid cells (12) is increased by a maximum of 5%, ranging from 0.1% to 5%; this quantifies additional streamflow from certain regions of the watershed where the impacts of cloud seeding operations are assumed higher for this analysis. Figure 3.7 displays the changes in annual streamflow for the Wyoming ranges of the North Platte watershed for an increased precipitation (0.1% to 5%) during the months of cloud seeding operations. Annual streamflow shows an increasing pattern with increase in precipitation, with wet years showing higher increase than dry years. The simulated increase in annual streamflow varies from 0.02% to 2% for a 0.1% to 5% increase in precipitation.

The maximum, minimum and average changes in annual streamflow with respect to anticipated change in precipitation are summarized in Table 3.1. For an increased precipitation from 1% to 5%, the annual streamflow from the Wyoming area has increased from 0.3% to 1.4% (in average). This additional streamflow due to cloud seeding operations only in certain regions of the Wyoming corresponds to an average

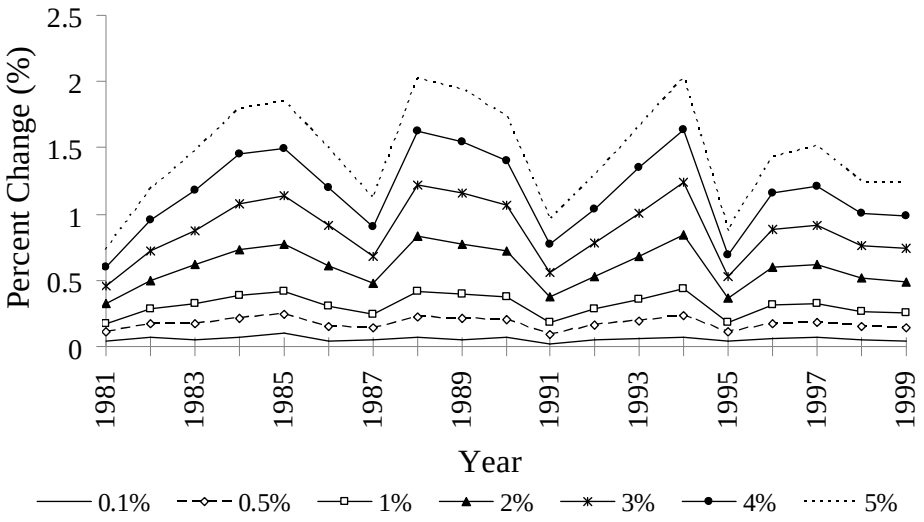

Figure 3.7 Percent change of annual streamflow with respect to an increase in precipitation from 0.1% to 5% for Wyoming area of the North Platte watershed.

Table 3.1 Change in annual streamflow for the Wyoming ranges and the whole North Platte watershed (which includes the Colorado ranges also).

Change in Precipitation (%)	Change in Annual Streamflow (%)					
	For Wyoming Area			For Full North Platte		
	Minimum	Maximum	Average	Minimum	Maximum	Average
0.1	0.02	0.10	0.06	0.02	0.06	0.04
0.5	0.10	0.24	0.17	0.06	0.16	0.10
1.0	0.17	0.44	0.32	0.11	0.29	0.17
2.0	0.32	0.85	0.61	0.20	0.54	0.32
3.0	0.46	1.24	0.89	0.28	0.78	0.46
4.0	0.60	1.64	1.19	0.36	1.03	0.61
5.0	0.73	2.03	1.48	0.45	1.27	0.75

increase of 0.1% to 0.7% of the total streamflow from the entire North Platte watershed. The cloud seeding operations are also performed by using an aircraft in the watershed and the Colorado ranges are considered a future option for these operations. As discussed in section 3.1.1, the Colorado ranges also possess higher precipitation as compared to other regions. Therefore, an increase in total streamflow (than summarized in Table 3.1) is

expected if these regions show a favorable condition for the extension of cloud seeding operations.

3.3.3.2 Change in Streamflow: Seasonal Pattern

The impacts of increased precipitation on seasonal streamflows are also examined. Figure 3.8 shows the change in streamflow pattern during May-June for an increased precipitation due to cloud seeding operations. During this period, the simulated increase in streamflow varies from 0.1% to 5% for a 1% to 5% increase in precipitation. The range of change of streamflows (min., max., average) during the period of May-August (May-June; May-July; June-August) is summarized in Table 3.2. The period of May-July is considered to contribute almost 70% of annual streamflow for the watershed (Figure 3.5a). As indicated in the Table 3.2, the average increase in streamflow is also comparatively higher for May-July in compared to other seasons; an average increase from 0.5% to 2.5% is observed for a 1% to 5% increase in precipitation. An average increase from 0.4% to 2% is observed during the summer period (June-Aug) for the same range of increased precipitation.

The higher snowpack accumulation due to wintertime (glaciogenic) cloud seeding operations increases snow cover during the late winter period. The higher snow cover during the winter period gradually melts in a warmer temperature at later periods that contributes to an increased soil moisture and streamflow. A successful implementation of WM programs in this watershed could serve as a viable option to augment precipitation and reduce impacts of declining streamflow during dry periods. However, an additional analysis, which also incorporates the impacts of climate change and water demands, is necessary to fully evaluate the impacts of the WM programs during dry periods.

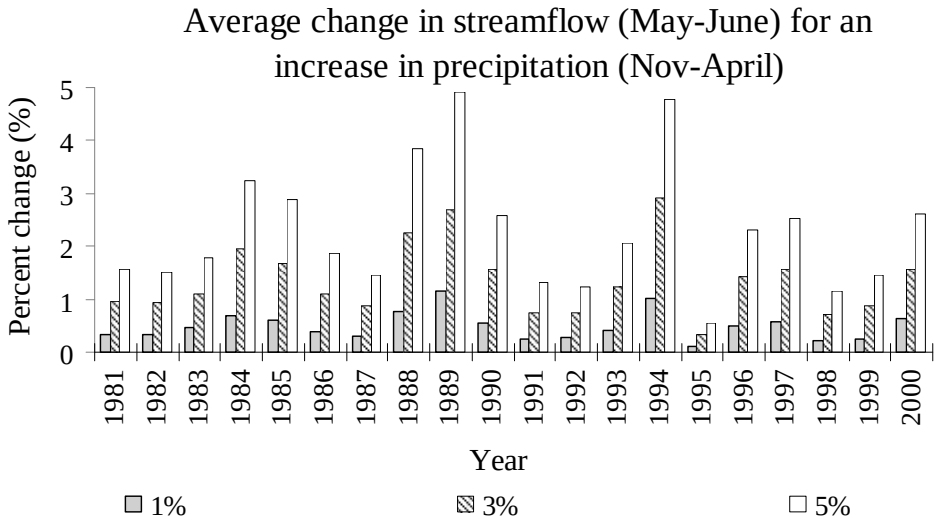

Figure 3.8 Seasonal change of streamflow with respect to an increase in precipitation (Nov 15 – April 15) from 1% to 5% for Wyoming ranges of the North Platte watershed. (MJJ: May-July).

Table 3.2 Change in seasonal streamflow for the cloud seeding operations on the Wyoming ranges of the North Platte watershed.

Change in Precipitation (%)	Change in Seasonal Streamflow (%)								
	May-June (MJ)			May-June-July (MJJ)			June-July-Aug (JJA)		
	Min	Max	Mean	Min	Max	Mean	Min	Max	Mean
0.1	0.01	0.21	0.07	0.01	0.15	0.07	0.03	0.15	0.08
0.5	0.08	0.64	0.26	0.11	0.66	0.27	0.07	0.60	0.26
1.0	0.09	1.16	0.49	0.20	1.33	0.53	0.12	1.19	0.48
2.0	0.21	1.94	0.91	0.34	2.62	1.02	0.18	2.33	0.90
3.0	0.32	2.90	1.36	0.51	3.88	1.51	0.26	3.44	1.35
4.0	0.43	3.87	1.83	0.66	5.18	2.03	0.33	4.58	1.81
5.0	0.56	4.91	2.28	0.83	6.45	2.54	0.41	5.69	2.2

3.3.3.3 Region Specific Change of Precipitation

This analysis could be helpful in identifying the most effective regions for cloud seeding operations, in terms of runoff augmentation in the watershed. For this purpose, the entire watershed is divided into six regions (Figure 3.9): southeast (SE), southwest

(SW), centraleast (CE), centralwest (CW), northeast (NE) and northwest (NW). Precipitations of the grid cells located within each specific region are increased by 5% and the simulations are carried out for the whole watershed; the simulations are continued for all regions, one region at a time, that considers increased precipitation for the specific region only. The simulated increases in annual streamflows for the Colorado range of the watershed, which is located on the Southern region (SE, SW), vary from 2% to 4% of the annual streamflows for that region (Figure 3.10); the median increase is calculated as 2.5% and 3.2% for SE and SW respectively.

The simulated increases in total annual streamflows (measured at USGS gauge 06630000) from the entire watershed vary depending on regions where precipitation is increased. An increase in streamflow from 0.2% to 3% is simulated for different regions, where a median increase of 1.50% and 1.62% is simulated for CW and SW regions respectively. A maximum increase in annual streamflows in CW and SW regions indicates that the cloud seeding operations can be considered most effective in these regions. SW is more favorable if the median increase in streamflow is considered, while CW is favorable if the maximum increments are considered. A comparatively higher streamflow from the western area of Southern and Central regions could also be attributed to higher precipitation in these regions than other areas in the watershed (Figure 3.4). CE and CW regions are found to have slightly higher median increase in streamflow than SE region. The operational cloud seeding programs are conducted over the Medicine Bow and Sierra Madre ranges of the North Platte watershed which are located at the central (CE and CW) regions. The Southern regions have shown higher contribution for increased streamflow for the Colorado ranges as well as the entire

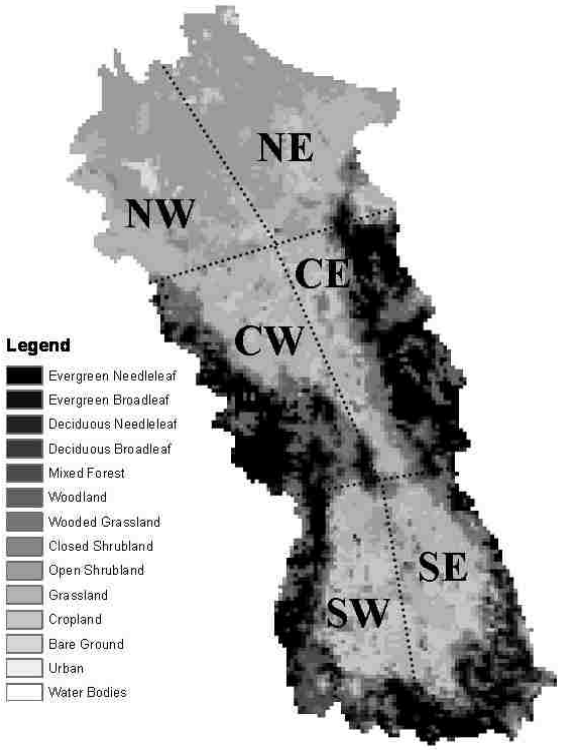

Figure 3.9 North Platte Watershed showing different types of land cover and regions for cloud seeding operations considered for this analysis.

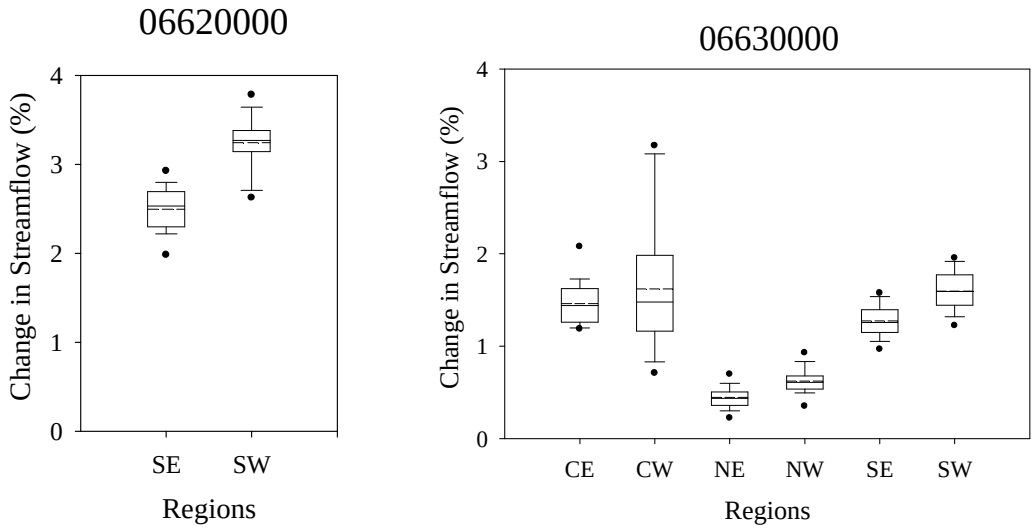

Figure 3.10 Boxplots of percentage change of annual streamflow for USGS gauge 06620000 and 0663000, when precipitation is increased for specific regions (Figure 3.8) only.

watershed; therefore, these regions can be considered favorable for the extension of cloud seeding operations. The minimal increase in simulated streamflow in northern (NW and NE) regions indicate that these regions can be considered less effective for cloud seeding operations.

3.3.3.4 Change of Precipitation for Different Landcover

This analysis determines the dominant landcover that simulates higher streamflow during the cloud seeding operations in the watershed. As shown in Figure 3.9, the landcover in the watershed has been classified into nine major classes**:** Evergreen Needleleaf Forest (EG), Open Shrublands (OS), Grasslands (GL), Woodland (WL), Wooded Grasslands (WGL), Deciduous Broadleaf Forest (DF), Mixed Forest (MF), Closed Shrub lands (CS) and Crop lands (CL). The grid cells with approximately 30% coverage of specific landcover are selected and precipitations of the selected grid cells are increased by 5%. Simulations are carried out for the whole watershed with increased precipitation for each landcover; the simulations are performed for all landcover types separately. The impacts of DF and MF are not considered in this analysis, since no grid cells are found to occupy more than 15% of this type of landcover. As shown in Figure 3.11, EG and WL show higher increase in annual streamflow for the watershed; the annual streamflow has increased from 1% to 4.5%, with EG showing higher increase than WL. The median increase in annual streamflow is calculated between 1.8% to 2% for WL and 3.1% to 3.3% for EG, when comparisons are made for annual streamflows from the whole watershed and the southern ranges only. A median increase of less than 1% is

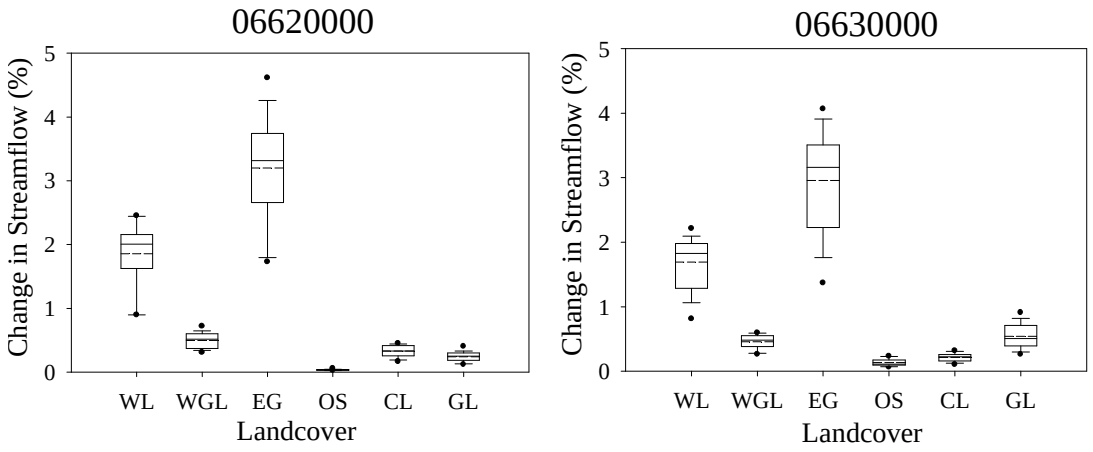

Figure 3.11 Boxplots of percentage change of annual runoff for an increase in precipitation (10%) for different landcover. a) USGS gauge 06620000; b) USGS gauge 06630000.

calculated for other landcover types (WGL, OS, CL, GL), with OS showing the minimal changes on streamflow.

As discussed earlier, the cloud seeding operations are found more effective on CW and SW regions of the watershed. CW regions have higher coverage of WL, EG and GL; SW regions have higher coverage of EG and MF, and lower coverage of a combination of WL, WGL, CL and GL. Both regions, which are considered more favorable for cloud seeding operations, have higher coverage of EG land cover. NE and NW regions, which are found to contribute less for cloud seeding operations, have higher coverage of OS and GL. Under similar conditions of increased precipitation and watershed characteristics, the difference in simulated annual streamflows could be due to the properties of landcover and soil present in different regions of the watershed. The saturated hydraulic conductivity of soil is similar for all regions. But the initial layer moisture content is approximately three times higher for the central and southern part as

compared to the northern part; this may contribute to the higher and earlier peak runoff from these regions. The minimal change in streamflow for OS may be attributed to higher evaporation and lower initial soil moisture. The thickness of soil moisture layer and average soil temperature that are used as the bottom boundary for soil heat flux solution in the VIC are also higher for the northern region. This may influence the water budget and energy balance and increase evaporation (evapo-transpiration) which further reduces total runoff, and slows down the time for seasonal peak flows from this region.

This analysis can identify the dominant landcover types in the areas that receive higher precipitation and produce higher streamflow. Additional analysis may be required to determine the most favorable landcover for cloud seeding operations in the watershed.

3.3.4 Accuracy of the Results

This analysis has developed a hydrologic model for the North Platte watershed and tried to evaluate the impacts of weather modification on streamflow. However, there are various uncertainties associated with this analysis. Although the operational cloud seeding projects are estimated to attain a 10% to 20% increase in precipitation, evaluations are yet to be done for the project to ascertain this claim. Other sources of uncertainties in the simulated results are associated with the capability of the hydrologic model, data needs, topography, and natural continuous climate variability.

Uncertainty in the selection of hydrologic model is addressed by selecting the VIC model. VIC is considered suitable because this model accounts for the physical processes in between soil, land and atmosphere, and considers the sub-grid variability in soil moisture storage capacity, precipitation, land surface vegetation classes, and topography. More realistic simulations of water budget and energy balance processes can

be carried out at higher spatial and temporal resolution. Higher resolution simulation is considered important due to the complex terrain and diverse climate regimes of the western United States (Leung et al, 2004). Although the hydrologic model is physically based and doing a good job in simulating changes at higher resolution, the performance of the model is restricted by the data used during simulation. The measured station data (e.g. meteorological, streamflow) that are used during calibration, validation, and all other simulations are likely affected by many microclimatological effects (Osborn and Hulme 1997).

Other data used in this analysis (such as soil and land use) may have some discrepancy with respect to the accurate field measurements and may need an update. Surface and atmospheric processes differ with the change in temperature, precipitation, and land use. Although the soil parameters chosen for calibration retain their properties for a longer time period, the use of same optimized parameters for all scenarios ignores the potential feedback in between these processes (Chiew et al, 1995). These uncertainties could lower our confidence to some extent while concluding the reliability of the simulated results in this research.

3.4 Conclusions

This paper has developed a hydrologic model (within VIC) to evaluate the impacts of WM programs on water supply. The impacts have been evaluated in terms of change in streamflow. This paper has also provided a proof of concept of development and application of WM scenarios for hydrologic impact evaluation. The concept of

modeling and WM scenario analysis as presented here can be implemented to any WM projects to observe their impacts on water supply.

The corresponding changes in streamflow are quantified as a result of cloud seeding operations in the North Platte watershed. With effective WM programs, the increased precipitation could augment annual and seasonal streamflow and reduce the impact of declining streamflow during dry periods. The present cloud seeding operations are conducted on the central regions of the watershed. This research has found the centralwest and southwest regions of the watershed, which consist of higher percentage of woodland and evergreen needleleaf land cover, to be more favorable for runoff augmentation through cloud seeding operations. These operations are found to be less effective in northern regions that consist of a higher percentage of open shrublands and grasslands.

In both cases- the operational WM programs are claimed effective based on precipitation augmentation or the WM programs are proposed as future options, the impacts of these programs on water supply can be evaluated based on this analysis. The results presented here can also be utilized directly by the WM projects operating at representative watersheds. This study calls for a further work that estimates the impacts of WM on other hydrologic parameters-for example, soil moisture, reservoir level, evapo-transpiration, snow water equivalent, e.t.c. Building upon this research, future research projects can be carried out to consider climate, water demand, and land use changes and assess the effectiveness of the WM programs. Chapter 4 has utilized this hydrologic model to evaluate the impacts of climate change on water availability over the North Platte watershed.

CHAPTER 4

QUANTITATIVE ASSESSMENT OF LONG TERM HYDROLOGIC IMPACTS OF CLIMATE CHANGE OVER NORTH PLATTE WATERSHED, WYOMING

4.1 Introduction

The impact of climate change on water resources is a major issue for the world. The likely impacts of climate change have been documented by various studies in different parts of the world (Bates et al, 1994; Aizen et al, 1997; Arnell, 1999; Bronstert et al, 1999; Hamlet and Lettenmaier, 1999; Miller et al, 1999; Braun et al, 2000; Arora and Boer, 2001; Bergstrom et al., 2001; Loukas et al, 2002; Jian and Shuo, 2006; Kay et al, 2006; Hayhoe et al, 2007; Liu et al, 2007; Minville et al, 2008; Barontini et al 2009; Gerbaux et al, 2009). The major impacts are observed on the hydrological cycle and regional water availability for industry, domestic use, flood control, irrigation and agriculture, aquatic life survival, reservoir operation and navigation. The hydrologic response due to climate change further affects the strategies and polices of water resources management (Liu et al 2007; Barontini et al 2009). It has been identified that almost 90% of the observed changes on physical and biological systems on a global scale are much more likely due to increased warming (NASA, 2008). The increasing temperature trends are attributed to increasing anthropogenic activities (IPCC, 2007a) and IPCC (2007b) suggest a general trend of increasing temperature (and drier conditions) in mid latitudes.

Snowmelt runoff is a major source of water supply in the western United States. A significant decrease in mountain snowpack was noticed in the last century in these regions, which was primarily driven by increase in temperature rather than the change in

precipitation (Mote et al., 2005; Hamlet et al, 2005; Mote, 2006; Maurer et al, 2007; Miller and Piechota, 2008). The increase in temperature is attributed to higher anthropogenic input of GHGs, ozone and aerosols (Barnett et al, 2008; Bonfils et al., 2008; Hidalgo et al, 2009; Pierce et al, 2009). Several earlier studies have showed the continuous climate disruption and hydroclimatic changes in the western U.S., in terms of declining snowpack, lower snow water content, earlier snowmelt, and shift in spring runoff timing (Roos 1987, 1991; Wahl 1992; Aguado et al. 1992; Pupacko, 1993; Dettinger and Cayan 1995; Groisman et al., 2004; Leung et al, 2004; Vanrheenen et al, 2004; Regonda et al, 2005; Stewart et al, 2005; Knowles et al., 2006; Hunter 2007).

Reconstructed climate data has also indicated the occurrence of very lengthy and severe droughts in the arid western U.S. in the past (USGS, 2004). The Colorado River Basin, a major source of water supply for the western U.S., has been in a drought since 1999 (BOR, 2006). The U.S. DoI (2003) has reported a continuous increase in the consumptive use of water in the West to sustain urban growth. In California, there is a need of at least two million more acre feet (AF) of water to sustain the urban growth by 2030 (Shaw, 2006). It could create serious water conflicts in the future while meeting the higher water demand. In addition, decreased snowpack runoff could impact production of hydroelectric power, thus creating adverse impacts on the power demand of California and other western States (Griffith and Solak, 2006; Hunter, 2007). The trend of increasing water demand and declining snowpack could worsen the situation even more if the dominant affect of anthropogenic climate change is continued into the future.

Model simulations applying a number of Global Climate Models (GCMs), Regional Climate Models (RCMs), and multiple projections over the western U.S. have

shown increasing temperatures for all future scenarios and regions; but it was difficult to predict precipitation response for these regions (Giorgi et al, 1994; Leung and Ghan, 1999; Kim et al., 2002; Snyder et al., 2002; Coquard et al., 2004; Hamlet et al, 2005). It is documented that the dry subtropics are likely to dry further while the wet higher latitude regions are likely to get wetter in the future (Held and Sodden, 2006). The U.S. Global Change Research Program (2009) has also reported a strong seasonal climatic variation in the arid western regions of U.S. in the past. The greatest seasonal change was observed during the winter months. The projected changes in temperature over this century have shown the summer changes larger than winter. An observed temperature rise of about 2.0 ºF at present with respect to baseline periods (1960-1979) is expected to increase from 2.5 ºF to 13 ºF under increased greenhouse gas conditions.

The North Platte watershed in Wyoming is a region in the western U.S. and the temperature and precipitation are projected to change in the future. The North Platte River is a tributary of Platte River and the present available water resources in the Platte River basin in Wyoming are fully allocated (WWDC, online accessed 2010). The water demand in nearby River Basins- Green River Basin is expected to increase from 73 to 82 percent of its allocation given in the Colorado River and up to 88 percent in the Wind River (Big Horn) Basin under a moderate population growth. Under changing future climatic conditions, it is expected to further stress future water availability over the North Platte watershed.

A number of GCMs and scenarios have been used by several studies to address uncertainty in the climate change related studies (McGuffie et al, 1999; Durman et al, 2001; Jones and Reid, 2001; Ra¨isa¨nen and Joelsson, 2001**;** Prudhomme et al, 2002;

Covey et al, 2003; Huntingford et al., 2003; Watterson and Dix, 2003; Leung et al, 2004; Ekstro¨m et al, 2005; Fowler et al, 2005; Milly et al, 2005; Frei et al, 2006; Merritt et al, 2006; Tebaldi et al, 2006; Beniston et al, 2007; Buonomo et al, 2007; Fowler et al, 2007; Maurer, 2007; Seager et al, 2007; Vicuna et al, 2007; Dankers and Feyen, 2009; Dankers et al, 2009; Fowler and Ekstro¨m, 2009). Various climate scenarios and GCMs for regional analysis have simulated different results. The use of a single GCM output is not usually the best approach since the observed changes are very likely prone to uncertainty (McGuffie, 1999). The mean model result, which is obtained by averaging all the ensemble model simulations, is considered to provide the best comparison with observations for climatological mean fields (Lambert and Boer, 2001; Coquard et al, 2004).

Most regional hydroclimatic studies have utilized the regional climate change scenarios from GCM output and hydrologic models to study the potential impacts of climate change on existing water resources. Major uncertainties are associated with the scales (spatial and temporal) and development of scenarios used in hydroclimatic modeling. Higher spatial resolution better represents the complex terrain and diverse climate regimes of the western United States (Leung et al, 2004). The process-based models such as variable infiltration capacity (VIC) have been utilized previously to study the hydroclimatic impacts on water resources in these regions (Liang et al, 1994). Therefore, hydrological simulations using process based models and downscaled regional climate change scenarios may be helpful in producing more realistic simulations of hydrological changes at a regional scale. The use of a number of GCMs and scenarios are recommended to address uncertainty in the simulated results. This paper utilizes a

process based model and higher resolution climate data for long term forecasting. This paper aims to develop an improved methodology that incorporates downscaled climate data into a process based hydrological model and derive streamflow projections to evaluate the potential impacts of climate change on water availability. The climate parameters such as temperature and precipitation are expected to change in future that may significantly impact available water resources.

This paper quantitatively assesses the long term response of streamflow under changing climate scenarios over the North Platte watershed. Since no studies related to streamflow forecasting under anthropogenic climate change conditions are yet done in the watershed, this study can be utilized in future water availability assessment and demand management study. In order to achieve this goal, this paper utilizes the VIC model and climate inputs from the ensemble multi-model, multi-scenario, multi-projection data from the World Climate Research Programme's (WCRP's) Coupled Model Inter-comparison Project Phase 3 (CMIP3), hosted by Lawrence Livermore National Laboratory (LLNL) Program for Climate Model Diagnosis and Inter-comparison (PCMDI) (Maurer et al, 2007). With both VIC model and downscaled WCRP CMIP3 data at same scale (12 km squared, daily), the hydrologic simulations can be performed at same spatial and temporal resolution. The monthly temperature and precipitation data from WCRP CMIP3 are already statistically downscaled using the bias correction and spatial downscaling (BCSD) technique. BCSD is considered to have the capabilities comparable to other statistical and dynamical downscaling approaches (Wood et al., 2004).

The rest of the paper is outlined as follows. The description of the study area, data needs and the hydrologic model used in this analysis are provided in Section 4.2; simulated results and discussions in Section 4.3 and 4.4; and conclusion in Section 4.5.

4.2 Methodology

4.2.1 Study Area

The study area is the North Platte Watershed which lies in the states of Wyoming and Colorado at latitude 40.3125° to 41.9375° N, and longitude 105.9375° to 107.0625° W (Figure 4.1). The watershed contains six streamflow gauges and eight SNOTEL stations that are operated by the United States Geological Survey (USGS) and the National Resource Conservation Service (NRCS) respectively. The annual precipitation varies from 25 to 60 inches with 40 to 70 percent falling as winter snow (> 250 inches of snow) (WWDC, online accessed 2010). The North Platte River, which is a tributary of Platte River and starts at the high basin of the North Park in north-central Colorado, flows northward into Wyoming along the Westside of Medicine Bow ranges and finally meets the Medicine Bow River and Seminoe Reservoir. The Platte River is a tributary of the Missouri River, which is a tributary of the Mississippi River.

4.2.2 Hydrologic Model

The hydrologic model used in this analysis is known as the Variable Infiltration Capacity (VIC) (Liang et al, 1994; Cherkauer and Lettenmaier 2003), which is a macro-scale, physically based, semi-distributed, land surface hydrologic model. The VIC model has been used in a variety of water resource applications and climate change studies (e.g. Hamlet et al, 2005; Mote et al, 2005; Pierce et al, 2008; Hidalgo et al, 2009; Wang et al,

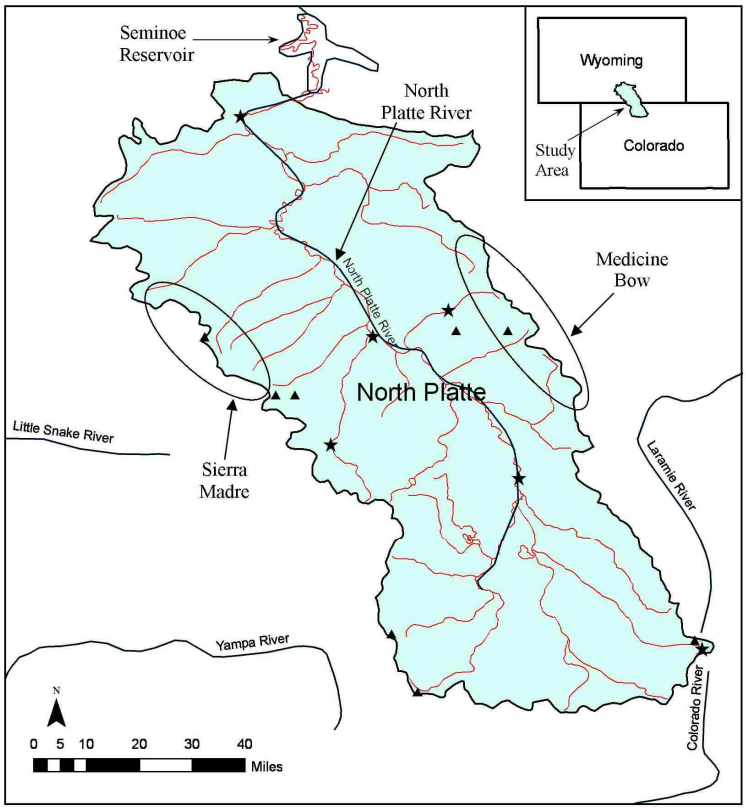

Figure 4.1 Location of the North Platte River, streamflow gauges (indicated by filled stars) and SNOTEL stations (indicated by filled triangles) inside the North Platte watershed.

2009). The major input data such as meteorological forcing data (in essences precipitation, maximum and minimum temperature, and wind speed), land cover, soil, elevation bands, and other watershed characteristics are 1/8 degree gridded data. The VIC model operates in two modes- water balance and energy balance; simulations are carried out at a daily or sub-daily time steps based on these two modes of operation. The water balance mode does not solve the surface energy balance, while the energy balance mode solves the total water balance and simulates surface energy fluxes to compensate for incoming total radiation fluxes. Simulations are carried out for each grid cell and the time series of output variables (e.g. runoff, soil moisture, evapo-transpiration) are also stored

separately for each specific grid. The energy fluxes such as sensible heat, latent heat, ground heat, ground heat storage, and outgoing long wave are incorporated in the energy balance mode.

The VIC model uses a separate river routing model (Lohmann et al., 1996) and snow model. The routing model is not used in this analysis since this analysis is focused on monthly, seasonal, or annual streamflows. The snow algorithm incorporated in the VIC model solves the surface energy balance and also includes spatially distributed snow coverage and snow sublimation. All important heat and energy fluxes (e.g. sensible and latent heat, convective energy, and internal energy), snow interception, and canopy processes are incorporated in the snow model. Two layer formulations are considered- surface layer and pack layer. The thin surface layer acts as an energy exchange layer and the pack layer acts as a reservoir to store excess snow in the surface layer. The various simulation options inside the VIC model are set in a 'global parameter file'.

4.2.3 Data Description

The retrospective meteorological forcing data (precipitation in mm, maximum and minimum temperature in degree Celcius, and wind speed in m/s), vegetation, soil, and snow band data are obtained from the Soil and Water Modeling Group, University of Washington (http://www.hydro.washington.edu/SurfaceWater Group/data.php; Maurer et al, 2002). All of these data are available for 1/8-degree grid cell for the conterminous United States. The meteorological forcing data are in a binary format and daily time steps, for a period of 1949-2000, which were derived from the hydrologic simulation (at a 3 hourly time step) of land surface energy and water variables over the continental United States. The gridded data was prepared through estimation using spatial and temporal

interpolation of observed data sources. The daily wind speed (m/s) represents wind speed measured at 2m above the ground surface. The soil parameter file contains geographical information for each grid cell, and grid cell soil parameters including initial soil moisture conditions. The vegetation parameter file defines different landcover types that are used during simulation, number of vegetations and their coverage in each grid cell, and other vegetation parameters (e.g. LAI-leaf area index, root depth). The snow band file contains information on each elevation band that is used by snow model.

The SNOTEL stations located within the North Platte watershed contains historical data for daily accumulated precipitation, snow depth, snow water equivalent, and temperature (max, min, average). These station data are obtained from the National Water and Climate Center of National Resource Conservation Service (NRCS). These data are available from early 1980's for earlier established stations, and from early 1990's for other stations.

The WCRP's CMIP3 multi-model dataset used in this analysis contains the fine spatial resolution (1/8-degree) translations of 112 contemporary climate projections for three major climate emission scenarios (A1B, A2 and B1) from IPCC and 16 robust GCMs, for the whole contiguous United States (http://gdo-dcp.ucllnl.org). These GCMs are developed from different parts of the world. The three emission scenarios are categorized as higher (A2, CO_2 concentration ~ 820 ppm by 2100), medium (A1B, CO_2 concentration ~ 700 ppm by 2100), and lower forcing (B1, CO_2 concentration ~ 550 ppm by 2100) for the multi-model runs. A more detailed description of the type of GCMs and scenarios can be obtained through the above link. The multi-model dataset consists of

statistically downscaled average monthly temperature and precipitation data from 1950-2100.

There is a need to further temporal downscale the BCSD monthly data based on the VIC model daily input requirement. The BCSD monthly data for each grid are downscaled to daily data via random sampling and temporal downscaling (Wood et al, 2002, 2004). During random sampling, a random month is selected from historical observations that represent the same month that needs downscaling. Anomaly fields (multiplicative for precipitation and additive for temperature) are constructed with respect to observed and modeled data, which are different for each calendar month and are applied to data series to downscale it from monthly to daily time intervals. The daily wind speed (m/s) data required for the VIC model for future climate simulations are developed by generating random samples from historical wind observations.

4.2.4 Model Simulations

The VIC model used in this analysis is calibrated as described in Section 3.3.2 for the North Platte Watershed. Calibration and validation of the VIC model was done in energy balance mode of operation based on historical monthly streamflow. The downscaled daily forcing data for each grid located on the North Platte Watershed and climate projection (scenario) are forced into the calibrated VIC model. A continuous simulation is carried out from 1950-2100 to observe the long-term streamflow projections under anthropogenic climate conditions. Model simulations are carried out for multiple projections from 16 GCMs and multiple scenarios (39 for A1B, 36 for A2, and 37 for B1). All comparisons in this analysis are based on simulated streamflows (for future and historical period) derived by using GCM output data. The model simulated streamflows

are compared between different time frames (2011-2040, 2041-2070, and 2071-2100) and time scales (monthly and annual) with respect to the baseline period (1971-2000). The simulated streamflow are compared to USGS gauge 06630000 which is located at the most downstream point of the North Platte watershed, but upstream of the Seminoe Reservoir.

The variation and the distribution of simulated changes in streamflow for multi-model projections from each emission scenario are compared using box plots and projections probability density function (pdf) plots. Box plots provide a quantitative comparison of location (median) and scale (inter-quartile range). For this research, a box plot is used to show the variability in terms of mean, median and quartiles of changes in streamflow. A pdf provides the relative likelihood of occurrence of a random variable. The Kernel density function is used in this analysis as a non- parametric way of estimating probability density function for continuous random variables.

4.2.5 Goodness of Fit Test

A goodness of fit test provides a statistical measure of the existence of any significant difference in streamflow distributions between emission scenarios at different time periods. A two-sample Kolmogorov-Smirnov (KS) non-parametric test is used in this analysis to test the streamflow distributions of two data vectors. The KS-Test measures absolute maximum cumulative difference between the two distribution functions (Stephens, 1970; Kharin and Zwiers, 2000).

$$D = \max |Z1 - Z2| \tag{4.1}$$

Where, Z1 and Z2 represent data vectors for each distribution. While performing this test, the null hypothesis assumes that the two data vectors (Z1 and Z2) are from the

same continuous distribution; the alternative hypothesis is that they are from different distributions. The hypothesis is rejected if the test value, which is based on maximum cumulative distance, exceeds a critical value based on sample size.

The KS-Test is generally applied for independent samples; however streamflow distribution may show temporal dependency in the data series. A random permutation test is also applied to verify the results from the general KS-Test for streamflow distributions that show autocorrelation. This test is performed by randomly permuting each pair of streamflow data from two distributions that are holding a same time frame. The random permutation is carried out for 1000 times and the final test value (in this case critical 'p' value) is calculated based on the distribution of test statistics obtained from each permutation. Each test statistic represents the maximum cumulative difference in between the two streamflow distributions for each random permutation.

4.3 Results

4.3.1 Precipitation and Temperature Pattern

Based on the ensemble climate projections for each scenario, the average annual temperature shows a linear increasing trend for future periods when compared with the average annual temperature for the baseline period (Figure 4.2a). Higher temperatures are observed for the medium emission scenario (A1B) during 2041-70, while maximum temperatures are observed for the higher emission scenario (A2) during 2071-2100. An increase of about 2°C is observed for all scenarios until 2040, which reaches maximum at the end of this century (4°C for A1B, 5°C for A2, and 2.5°C for B1).

As shown is Figure 4.2b, the percent change of annual precipitation with respect to the average annual precipitation from the baseline period shows both increasing and decreasing patterns with changes in magnitude for each scenario and time periods. No specific trends are observed for changing precipitation until 2035; an increasing trend is observed for scenarios at later periods-A1B after 2035, and B1 and A2 after 2050. Up to the year 2100, the calculated change in annual precipitation is between -6% to 8% for B1, -3% to 9% for A2, and -2% to 12% for A1B; the average increase in annual precipitation is calculated to be 3.2% for A2 and B1, and 4.2% for A1B.

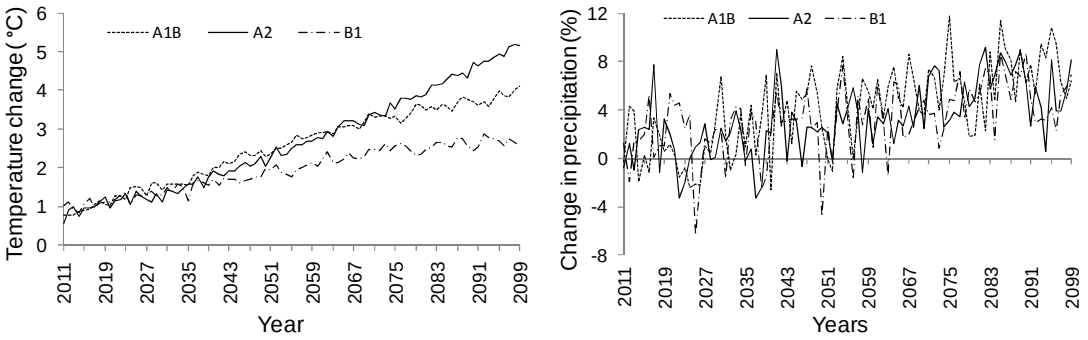

Figure 4.2 Observed climate pattern for each emission scenario, averaged over multi-model climate projections from WCRP CMIP3 dataset. a) Change in temperature and b)Change in precipitation, with respect to average annual temperature and precipitation for the baseline period (1971-2000).

The spatial distribution of modeled and observed average annual precipitation (mm/year) during the period of 1990-1999 shows similar distribution at most regions of the watershed (Figure 4.3a). Modeled precipitation from a single GCM (BCCR BCM 2.0) based on the A1B scenario is taken here as an example for comparison. The average annual precipitation varies from 200 to 1400 mm per year throughout the watershed, with

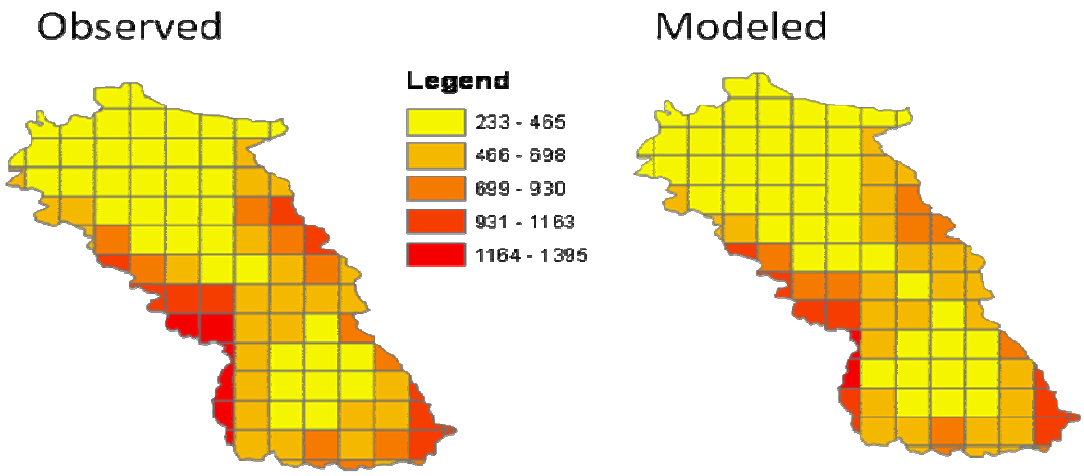

Figure 4.3 a) Spatial distribution of observed and modeled average annual precipitation (mm/yr) for the North Platte watershed during the period of 1990-1999.

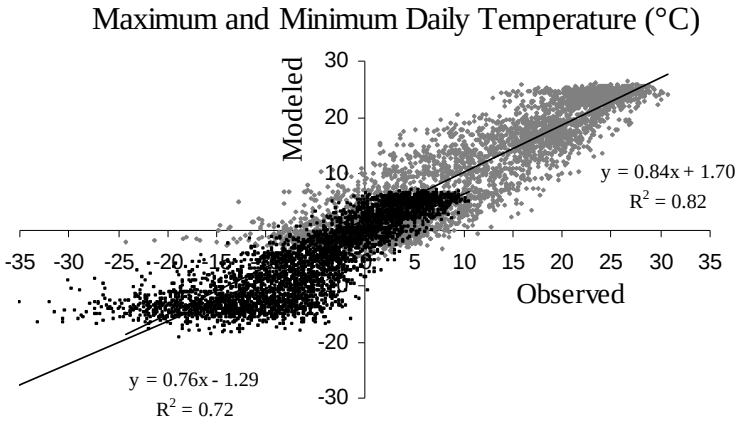

Figure 4.3 (b) Modeled vs. observed maximum and minimum daily temperatures (°C) for the North Platte watershed during 1990-1999. Modeled temperature represents an average temperature from 112 climate projections. The light and dark grey symbols represent maximum and minimum temperatures respectively.

comparatively higher precipitation towards the Colorado regions of the watershed. A good correlation is observed between the modeled and observed min and max daily temperatures for the watershed during the same period; a higher correlation is observed for the maximum temperature than the minimum temperature (Figure 4.3b). Modeled

temperature represents the gridded average of temperature from 112 climate projections for three emission scenarios for the watershed.

4.3.2 Streamflow Projections

The simulated annual streamflows during the period of 1971-2100 for 112 climate projections from emission scenarios A1B, A2, and B1 are shown in Figure 4.4. Maximum and minimum annual streamflows are observed at different future time periods for different climate projections. Some of the GCMs have simulated very high streamflows; the maximum annual streamflow is simulated by CCCMA CGCM 3.1.2 in the year 2030 for A1B. For probable maximum and minimum streamflows (in this case 90^{th} and 10^{th} percentile) over this century, the simulated streamflows show the same range of variation between the scenarios. Both increasing and decreasing streamflow patterns are observed until the end of this century. The simulated streamflows are different between the climate projections; during certain time periods they are opposite to each other. The observed annual streamflow also shows both increasing and decreasing pattern and varies within the probable max and min range for most years (except some wet and dry years). A 10-year moving average of annual streamflow show smaller variation in compared to variation from multiple projections for each emission scenario.

4.3.2.1 Inter-Scenario Comparison

The simulated annual streamflows are compared between the scenarios. Annual streamflow represents an average of annual streamflows from all climate projections for each scenario. As shown in Figure 4.5, the simulated streamflows are comparatively higher for A2 and B1 until 2020, while it's higher for A1B towards the end of this century. The calculated 10-year moving average shows an increasing pattern for future

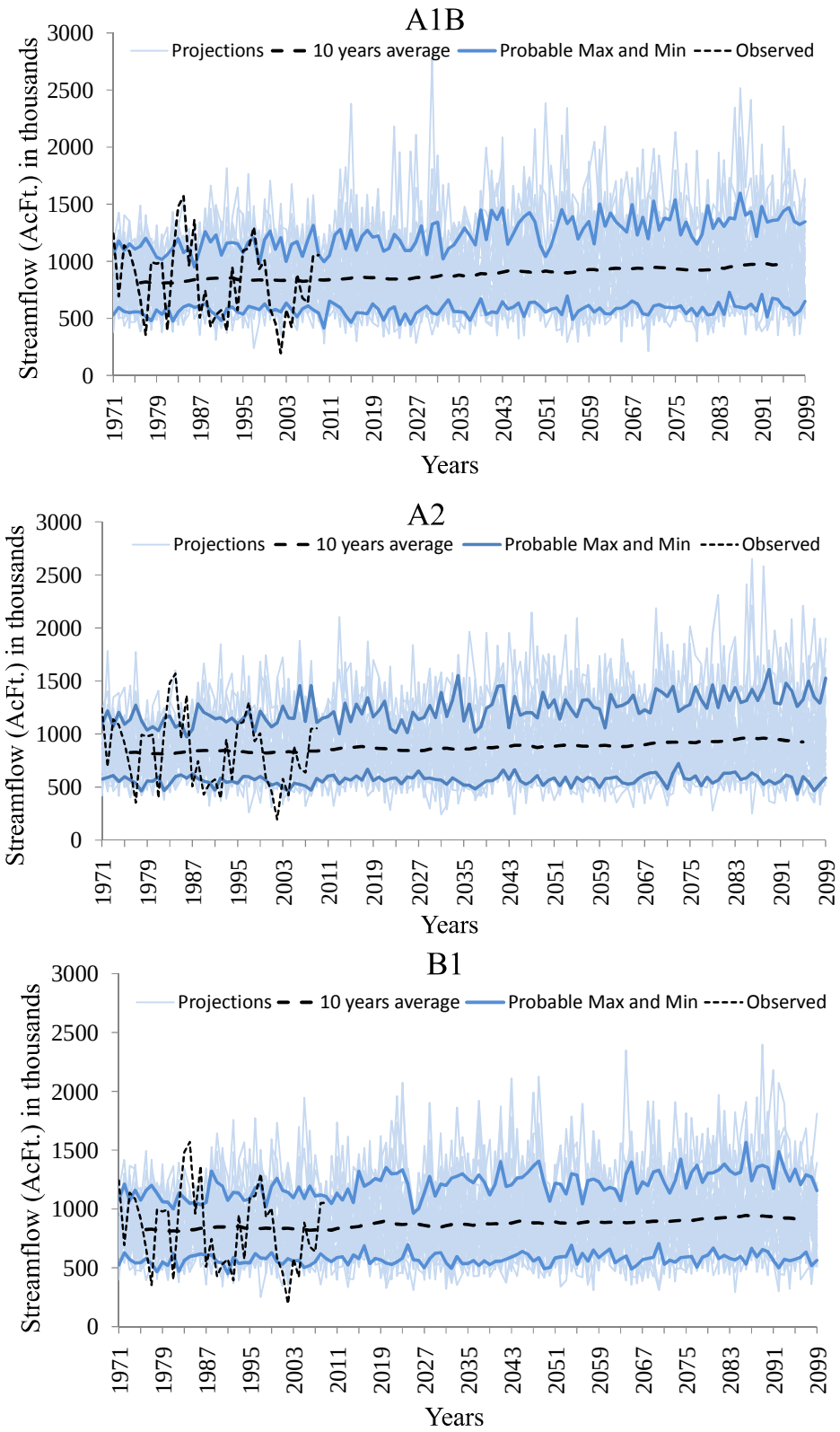

Figure 4.4 Observed and model simulated long term streamflow for multi-model climate projections from emission scenarios A1B, A2 and B1 respectively. Total number of climate projections: 39 for A1B, 36 for A2, and 37 for B1.

periods that is visible after 2020. The calculated average annual streamflows are higher during the period of 2085-90 and maximum in 2087 and 2089; A1B has also shown the maximum annual streamflow in 2087.

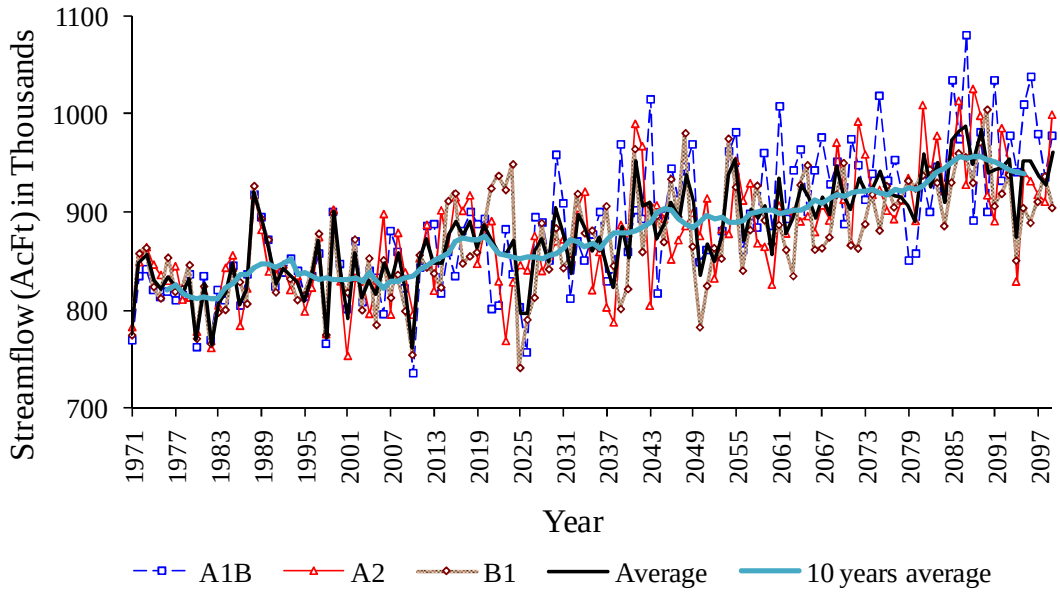

Figure 4.5 Streamflow projections for emission scenarios A1B, A2 and B1 during 1971-2100. Average streamflow represents the average of annual streamflows for all scenarios.

The inter-scenario comparison of percent change of annual streamflow with respect to average annual streamflow for the baseline period (1971-2000) is also performed. Although lower streamflows are observed for some years, the average change in streamflow indicates an increase until 2100. An average increase of about 7.2%, 4.8% and 5.3% is calculated for A1B, A2, and B1 respectively during 2011- 2100. The calculation of percentiles, mean, minimum and maximum change in streamflow for all scenarios are summarized in Table 4.1. The mean results obtained from the ensemble

Table 4.1 Calculation of minimum, maximum, mean and percentiles of change in annual streamflow (%) for emission scenarios A1B, A2 and B1, during the period of 2011-2100 with respect to baseline period (1971-2000).

Emission Scenarios	Percent Change (%)					
	1st Quartile	Median	3rd Quartile	Min	Max	Mean
A1B	0.7	6.9	12.4	-12.8	27.4	7.2
A2	0.3	4.7	9.0	-10.5	23.0	4.8
B1	1.2	5.5	9.5	-13.6	22.0	5.3
Average	0.7	5.7	10.3	-12.3	24.2	5.8

multi-model climate projections are considered to address the uncertainties in the scenarios of change. While considering all scenarios, an average increase of 5.8% is calculated in annual streamflow for the projected climate change conditions.

Figure 4.6 shows the average annual streamflows derived from multiple projections during 1971-2100 for 90th. percentile (upper solid line) and average annual streamflow (lower dotted line) for the baseline period. The number of years that exceed the 90th. percentile streamflow for the baseline period increases while moving towards 2011-2040, 2041-2070, 2071-2100; all years during 2071-2100 show higher streamflows. Except some years (2025-26, 2038), all future years during 2011-2100 show streamflows higher than the average annual streamflow for the baseline period; a maximum decrease of 4% is calculated in annual streamflow in the years 2025/26; a maximum increase of 19% is calculated in the year 2087.

The lower annual streamflows for some years may be due to a decrease of precipitation and a continuous increase of temperature during these periods. This causes an increase in evapo-transpiration and reduction in soil moisture and streamflow. The overall increase in streamflow may be due to the projected increase in average annual

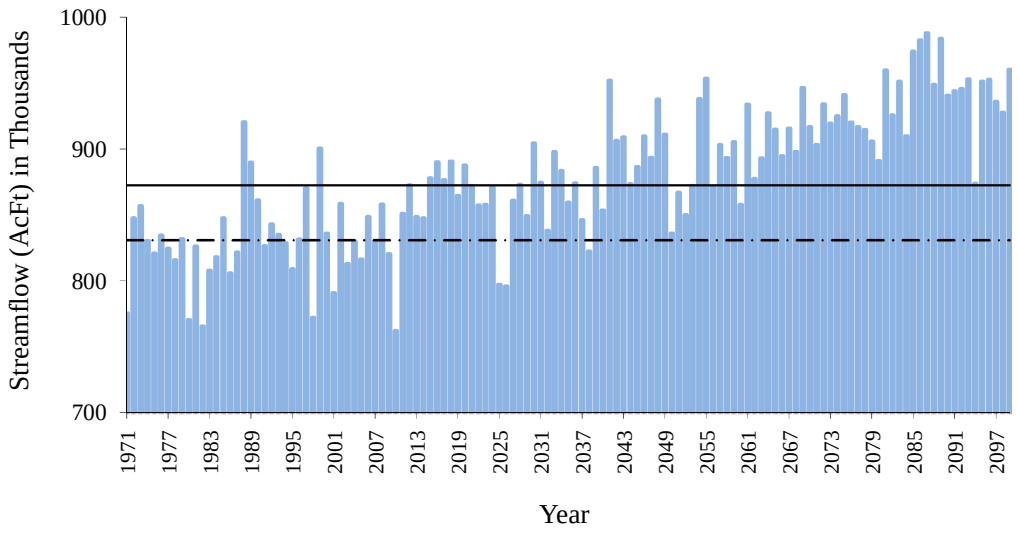

Figure 4.6 Average of annual streamflows from three emission scenarios A1B, A2 and B1 during 1971-2100. The upper solid and lower dotted line represent 90th. percentile and average annual streamflow for the baseline period (1971-2000).

precipitation and higher snow melt in a warmer future climate; an overall increase in annual precipitation with respect to average annual precipitation for the baseline period is calculated 3.5% during 2011-2100; an average increase of 5.5% is calculated during 2071-2100. This increasing streamflow pattern is similar to upward trend in runoff observed for the far Northwestern U.S. by Milly et al (2004).

4.3.2.1.1 Periodical Variation

The annual streamflow for each emission scenario during 2011-40, 2041-70, and 2071-2100 (represented as 2030's, 2060's and 2090's) are compared with average annual streamflow for the baseline period. Maurer et al, 2007 have suggested that the results and statements can be supported more confidently if the comparisons are made with respect to some range of time rather than a specific month or day within that time period. As shown in Figure 4.7, the change in streamflow varies from -20% to 62% depending on the emission scenarios and future time periods. The highest and lowest range of

variations is shown by A1B and B1 respectively. For multi-decadal period, similar increasing and decreasing streamflow patterns are observed for all scenarios; the median change in streamflow is higher during 2071-2100 and lower during 2011-40. As noted earlier, the average annual precipitation and temperature both show a maximum increase during 2071-2100 with respect to baseline period. An increase in precipitation and an additional runoff from snowmelt due to higher temperature may be contributing for an increased streamflow during this period. The calculated range of median change in streamflow during 2011-2100 is higher for scenarios in the order of A1B, A2 and B1; it varies from 2% to 12%, 1% to 7%, and 4.5% to 7.5% for A1B, A2 and B1 respectively.

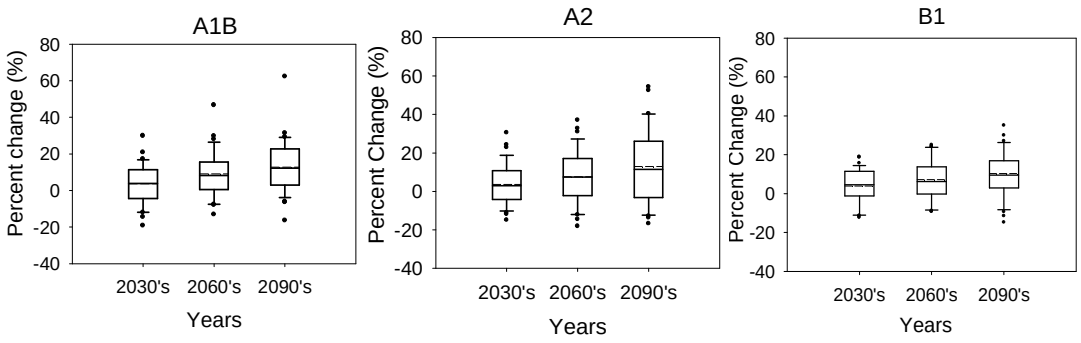

Figure 4.7 Boxplots of percent change of annual streamflow for each climate emission scenario during 2011-2040, 2041-2070 and 2071-2100 (represented here as 2030's, 2060's and 2090's), with respect to average annual streamflow for the baseline period (1971-2000).

4.3.2.1.2 Non Parametric Test

The KS–Test is applied for monthly streamflow projections derived by using 112 climate projections for different emission scenarios. Since all scenarios are holding the same time frame for multi-model projections, the KS-Test is suitable to identify if there exists any significant difference in streamflow distributions between the scenarios. Using

MATLAB software to perform a KS-Test, the result ‘h’ is 1 and ‘p’ value is less than 0.05, if the test rejects the null hypothesis at 5% significance level. The test statistic ‘k’ represents the maximum difference observed between the two cumulative distribution functions (cdfs). The test statistics for all performed tests for this analysis are summarized in Table 4.2.

The test is first applied for streamflow projections over the period of 2011-2100 with respect to the baseline period (1971-2000) separated by emission scenarios. The calculated test statistic is lower than the critical test value. Therefore the null hypothesis that the data are coming from same continuous distribution is rejected. The test is then applied for streamflow projections over the period of 2011-2100 with respect to the baseline period separated by emission scenarios and multi-decadal period (2011-2040, 2041-2070, 2071-2100). As expected, the null hypothesis is rejected for all cases. These tests demonstrate the non-stationarity nature of the future climate. Higher ‘k’ value towards the end of this century indicates that the maximum streamflows are simulated during 2071-2100 in compared to the earlier periods.

The test is then applied for streamflow projections between the scenarios over the period of 2011-2100 and for multi-decadal period. The null hypothesis is rejected only during 2071-2100 in between A1B and B1, and A2 and B1. This indicates a significant difference in streamflow distributions in between these scenarios. A significant increase in monthly streamflows for A1B and A2 may be due to higher temperature and precipitation for these scenarios when compared with B1 during this period.

The streamflow distributions for each emission scenario showed temporal dependency in the data series with an oscillation pattern and higher autocorrelation

Table 4.2 Summary of the results from KS-Test

Streamflow Projections	Test Statistic (k)	'p'-Value (KS Test)	h	'p'-Value (Permutation Test)	Null Hypothesis
A1B 2011-2100	0.18	<0.05	1	<0.05	Rejected
A1B 2011-2040	0.14	<0.05	1	<0.05	Rejected
A1B 2041-2070	0.22	<0.05	1	<0.05	Rejected
A1B 2071-2100	0.25	<0.05	1	<0.05	Rejected
A2 2011-2100	0.19	<0.05	1	<0.05	Rejected
A2 2011-2040	0.15	<0.05	1	<0.05	Rejected
A2 2041-2070	0.22	<0.05	1	<0.05	Rejected
A2 2071-2100	0.28	<0.05		<0.05	
B1 2011-2100	0.18	<0.05	1	<0.05	Rejected
B1 2011-2040	0.13	<0.05	1	<0.05	Rejected
B1 2041-2070	0.18	<0.05	1	<0.05	Rejected
B1 2071-2100	0.23	<0.05	1	<0.05	Rejected
A1B and A2 1971-2000	0.02	0.99	0	0.54	Accepted
A1B and A2 2011-2040	0.03	0.94	0	0.92	Accepted
A1B and A2 2041-2070	0.05	0.68	0	0.38	Accepted
A1B and A2 2071-2100	0.05	0.66	0	0.06	Accepted
A1B and A2 2011-2100	0.01	0.99	0	0.36	Accepted
A1B and B1 1971-2000	0.02	0.99	0	0.50	Accepted
A1B and B1 2011-2040	0.02	0.99	0	0.91	Accepted
A1B and B1 2041-2070	0.07	0.21	0	0.18	Accepted
A1B and B1 2071-2100	0.11	0.01	1	<0.05	Rejected
A1B and B1 2011-2100	0.04	0.08	0	0.06	Accepted
A2 and B1 1971-2000	0.03	0.99	0	0.25	Accepted
A2 and B1 2011-2040	0.03	0.99	0	0.62	Accepted
A2 and B1 2041-2070	0.05	0.62	0	0.16	Accepted
A2 and B1 2071-2100	0.16	0.01	1	<0.05	Rejected
A2 and B1 2011-2100	0.04	0.09	0	0.06	Accepted

(Figure 4.8a). The random permutation test is applied for all scenarios in Table 4.2 that resulted in a separate distribution of test statistic (k) for each test (Figure 4.8b). The bold line in Figure 4.8b represents the location of observed test statistic based on sample size. The critical 'p'values for each test are summarized in Table 4.2. The obtained results for

null hypothesis from random permutation test is similar to the normal KS-Test, however, the lower 'p' values from the permutation test demonstrates the temporal dependence of the streamflow distributions.

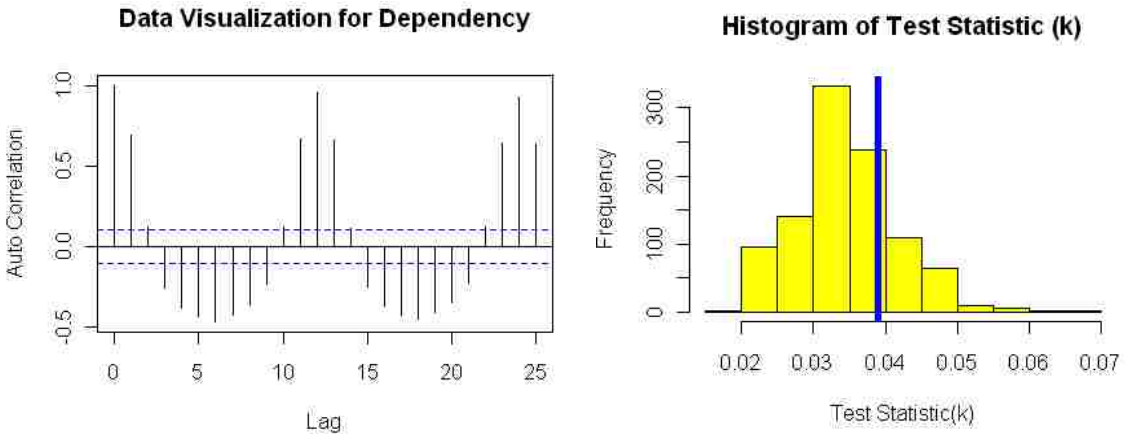

Figure 4.8 a) Autocorrelation plot of monthly streamflow from A1B scenario during 2011-2040; b) Histogram of test statistics (k) from random permutation test of monthly streamflows between A1B and A2 scenarios during 2011-2040. The middle bold line represents the 'k' value based on sample size.

4.3.2.2 Inter-Model Comparison

The inter-model comparison of simulated changes in streamflows for each emission scenario show a wide range of variation when the annual streamflows for future periods (2011-2100) are compared with average annual streamflows for the baseline period. The calculated change in streamflow varies from -74% and 162% for A1B, -72% and 154% for A2, and -65% and 181% for B1 (Figure 4.9). The GCM that simulates the maximum change (positive or negative) also varies based on the scenario. The highest variation in annual streamflow is simulated by IPSL CM 4.1 for all scenarios; the lowest variations are simulated by MIROC 3.2 MEDRES, MIUB ECHO-g, and NCAR CCSM 3 for A1B, A2, and B1 respectively. The calculated median change in streamflow is very

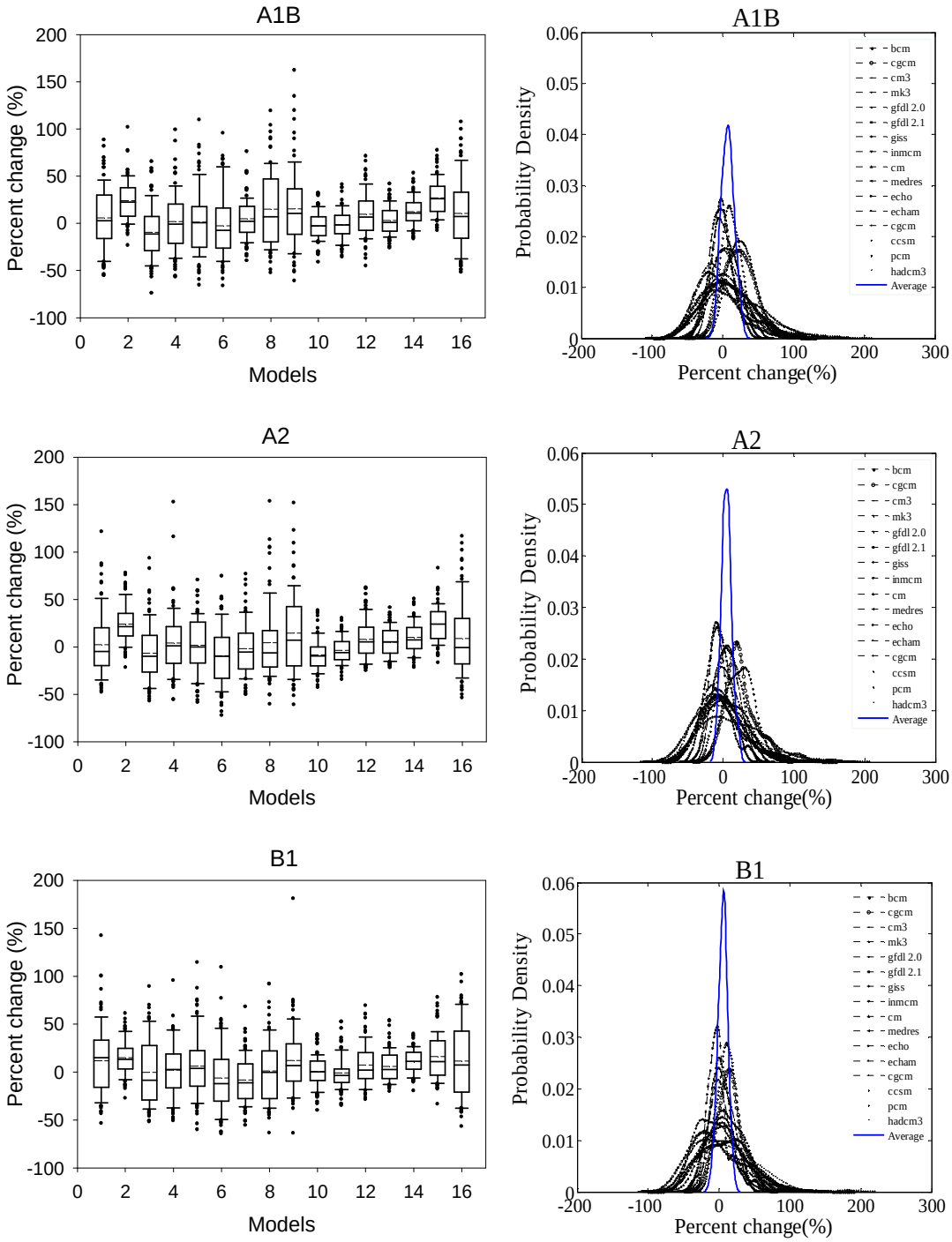

Figure 4.9 Boxplots and probability density function (pdf) plots for inter-model comparison of percent change of simulated streamflows, during 2011-2100 with respect to 1971-2000, for each emission scenario.Here, 1 to16 represents the 16 models used for simulation: 1-bccr bcm 2.0.1; 2-cccma cgcm 3; 3-cnrm cm 3.1 ; 4-csiro mk 3.0.1; 5-gfdl cm 2.0; 6-gfdl cm 2.1; 7-giss model e.r.1; 8-inmcm 3.0.1;9-ipslcm 4.1; 10-miroc 3.2 medres; 11-miub echo-g;12-mpi echam 5; 13-mri cgcm 2.3.2a;14-ncar ccsm 3; 15-ncar pcm 1;16-ukmo hadcm 3.1

small for some models although they are showing higher variation within the model. A higher median change in streamflow is calculated for CCCMA CGCM3 and NCAR PCM1 for all scenarios.

The distribution of percent changes in annual streamflow for multi-models and scenarios are also compared by using projection probability density function (pdf) plot. As displayed in Figure 4.9, the pdf plot for each model shows a slight difference in its distribution pattern for different emission scenarios. For the same emission scenario, some models show changes in annual streamflow for more years compared to others. The average distribution represents an average of change in annual streamflow from all model projections for each scenario. The calculated range of average distribution varies from -13% to 27% for A1B, -11% to 23% for A2, and -13% to 22% for B1. The higher concentration at zero percent change indicates that the lower emission scenario (B1) show changes in annual streamflow for fewer years as compared to A1B and A2; a wider distribution for A1B indicates changes in annual streamflow for more years during 2011-2100.

The diverse results in streamflow across models and scenarios, which is verified by the box plots and pdf plots of multi-model climate projections, is due to the various uncertainties resulting from climate models. These uncertainties are associated with the type of GCMs, emission scenarios, and climate projections. All climate projections possess different climate (meteorological) forcings for the hydrologic model simulation. The differences exist because each climate model differs in its origin, processes, physical parameterization of land surface processes, as well as in its spatial and temporal resolution (Milly et al, 2004). The model simulation capability differs based on

resolution. Each model projection also possesses different assumptions for the initial and boundary conditions, GHGs emissions, human induced changes, radiation and volcanic activity. Thus the processes such as water budget and energy balance differ for different warming conditions and causes change in the simulated streamflows.

4.3.2.3 Monthly Comparison

The monthly streamflows for each scenario during 2011-40, 2041-70, and 2071-2100 show larger changes in streamflow with respect to the baseline period. Monthly streamflow here represents an average of monthly streamflows from all climate projections for each scenario. As shown in Figure 4.10, all scenarios show a continuous increase in streamflow for future periods during the months from Oct-May; a maximum increase in streamflow is observed for January and February. Summer months (June-August) show a gradual decrease in streamflow for future periods. A maximum decrease in streamflow is observed for July. In general, the simulated change (increase/decrease) is maximum for all scenarios during 2071-2100. Almost equal changes are observed in monthly streamflows for all scenarios during 2011-40; however, the observed changes are higher for A1B and A2 during 2041-70 and 2071-2100 respectively. An exception to this is during August when a larger decrease is observed in 2041-70 than 2071-2100 for A1B and B1. The mean (in Figure 4.10) represents an average of percent change of monthly streamflows from all scenarios. The calculated maximum decrease in monthly streamflow between the scenarios is 36%, 49% to 54%, and 55% to 61% (mean 36%, 52%, 58%) during 2011-40, 2041-70 and 2071-2100 respectively. The calculated maximum increase in monthly streamflow between the scenarios varies from 74% to 77%, 148% to 195%, and 190% to 405% (mean 73%, 176%, 308%) for the same periods.

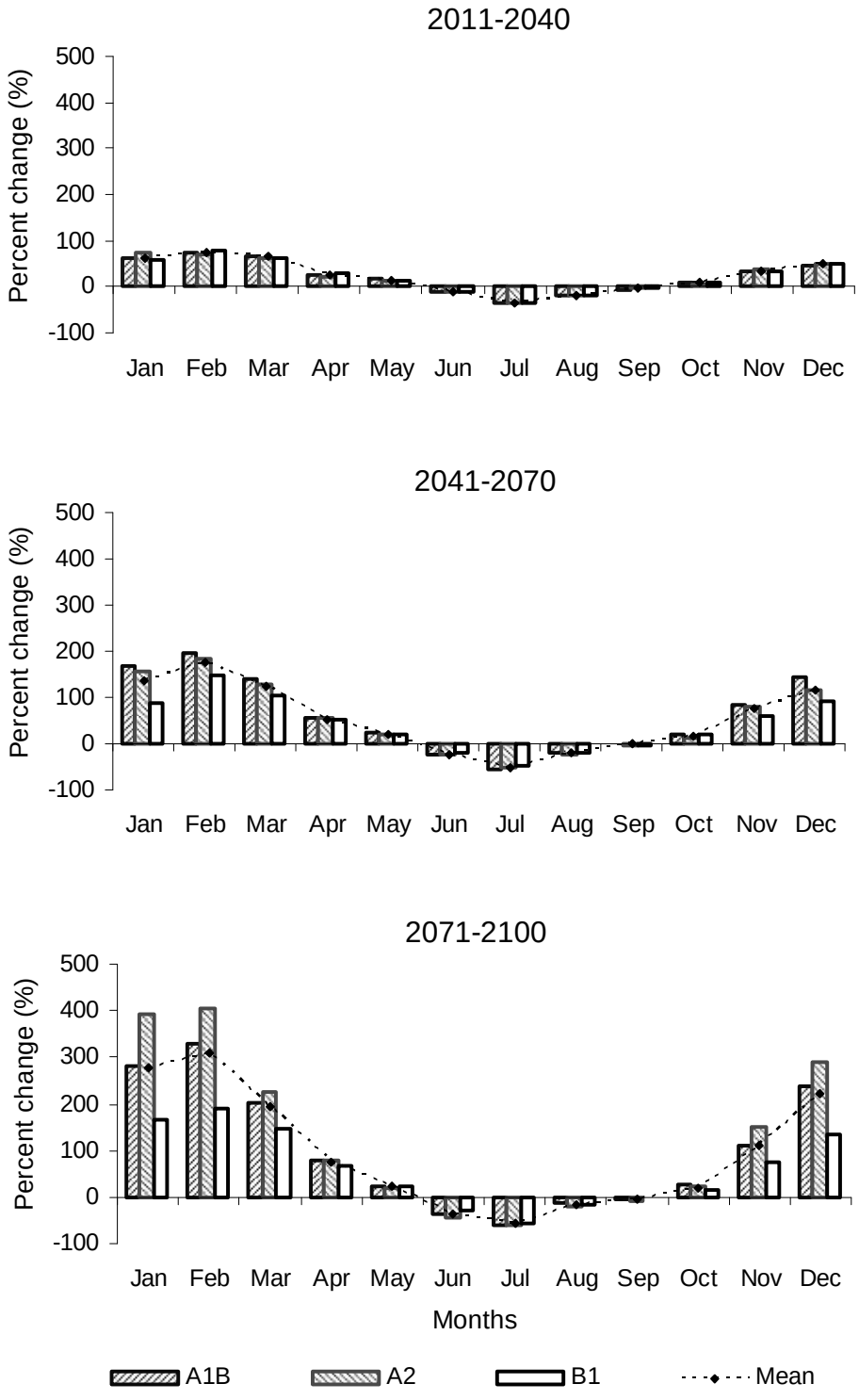

Figure 4.10 Percent change of monthly streamflows for emission scenarios A1B, A2 and B1, for each 30- year time period, with respect to baseline period (1971-2100). Mean in the plot represents an average of monthly changes observed for all scenarios.

September shows a decrease from 2% to 4% until the end of this century.

The temperature pattern shows a warmer future climate (Figure 4.2). The enhanced total precipitation with higher proportion of rainfall than snowfall, increasing soil moisture, and higher and earlier spring snowmelt due to warmer temperature may be contributing directly to a higher percentage of streamflow during what is typically the cold season. The increased warming causes a reduction in snowpack during the winter season; this reduction in mountain snowpack reduces surface albedo which causes further reduction in winter and late spring snow cover (Leung et al, 2004). The higher snowmelt and decline of snow accumulation, and more extreme warming during summer period increases sensible heat, which may cause higher evapo-transpiration, reduction of soil moisture, and lower streamflows. Summer months further dry making it difficult to meet increasing water demands. This indicates that the drier summer months will further dry and the wet months will be even wetter under anthropogenically driven climate change conditions. Similar results have been documented by Hamlet et al (2005) in a study conducted in the Pacific Northwest (PNW).

4.3.3 Sensitivity of Hydrologic Parameters

The major soil parameters used during the VIC model calibration are infiltration parameter (b_{inf} = 0.19), maximum baseflow (Ds_{max} = 11 mm/day), fraction of Ds_{max} (Ds = 0.04), fraction of maximum soil moisture (Ws = 0.15 mm/day), and soil depth (d2= 0.3 m) (refer to Chapter 3). The sensitivity of hydrologic parameter to streamflow projections is studied by selecting the most sensitive parameter during calibration, and developing streamflow projections by altering the parameter. The infiltration parameter ($b_{inf.}$) is found to be the most sensitive parameter during calibration (Figure 4.11).

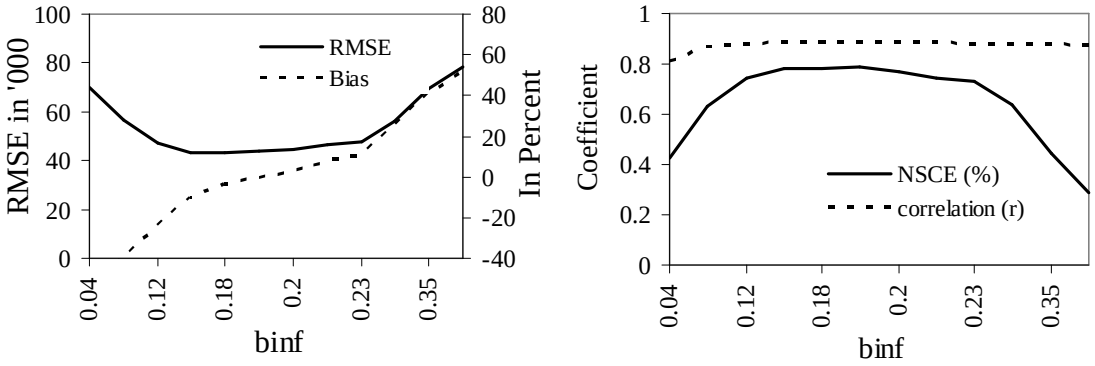

Figure 4.11 Sensitivity of infiltration parameter 'b_{inf}' during the VIC model calibration. This was determined by calculating the Pearson Correlation Coefficient (r), Root Mean Square Error (RMSE), Bias percentage and Nash-Sutcliffe Efficiency (E).

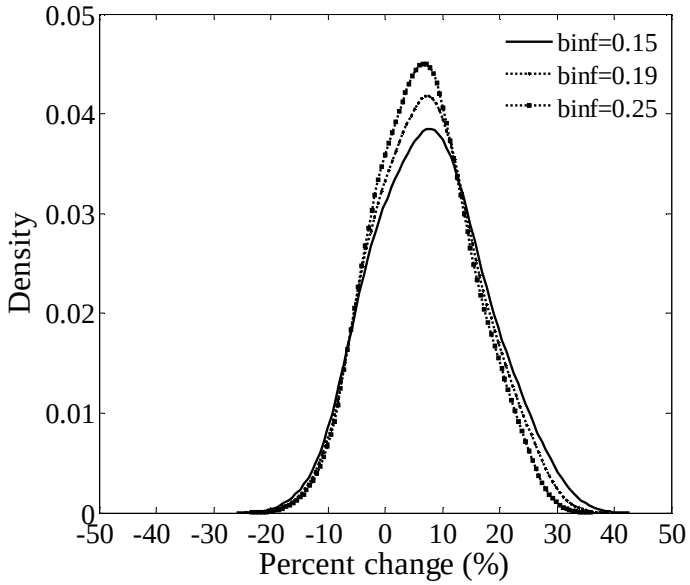

Figure 4.12 Pdf plot of percent change of annual streamflow during 2011-2100 when the infiltration parameter ('b_{inf}') is varied from 0.15 to 0.25 for A1B scenario.

In this analysis, all climate projections for A1B scenario are forced into the calibrated VIC model and the simulations are carried out by varying the calibrated '$b_{inf.}$' by ±20%. Figure 4.12 shows a pdf plot for an average change in annual streamflow (2011-2100) for A1B (similar to Figure 4.8) over different values of $b_{inf.}$-0.15, 0.19, and

0.25. With respect to these values, a small difference is observed in the distribution range of percent change of simulated streamflows. This indicates that the simulated results, which are based on multiple climate projections from GCMs, show uncertainty attributed to change in the hydrologic parameters for the future climate.

Uncertainty in a hydrologic model arises when using the same optimized parameters for present and future climatic conditions. This ignores the potential feedback between the surface and atmospheric processes (Chiew et al, 1995). The change of hydrologic parameters for future climate provides an additional uncertainty as observed in this analysis, given that the uncertainty attributed to the use of GCM outputs (results) is not known perfectly. However, from this analysis it can be assumed that the uncertainty attributed to the use of multiple GCM output is very high as compared to changes in hydrological parameters.

4.4 Conclusions

The hydroclimatic modeling approach as presented in this paper can successfully incorporate higher resolution climate data (projections) in a process based hydrological model for streamflow forecasting. Although previous studies on climate change have followed hydroclimatic modeling, the coupling of higher resolution BCSD climate data and process based model (VIC) as presented here is not performed. The BCSD climate data available from WCRP CMIP3 database can be utilized for similar regional hydroclimatic studies. Using this method, streamflow projections are developed based on forecasted multi-model multi-scenario climate projections for the North Platte watershed. Based on streamflow projections, there is a possibility of increased annual streamflow for

this region until 2100. An increase in streamflow is predicted for cold seasons while projecting a higher reduction during dry seasons. Managing water in this basin under anthropogenic climate conditions will be a challenging job when this reduction in streamflow during summer periods coincides with the increasing water demand.

The developed streamflow projections and the range of streamflows can be utilized by decision makers in water availability assessment and demand management under anthropogenic climate change conditions. The simulated streamflows have shown larger variation under changing climatic conditions. This analysis has tried to address some of the known uncertainties. However, improvements could be achieved in the simulated results if other associated uncertainties (such as perfect GCM, best scenario, method of downscaling) can be addressed in future. This research calls for a future work that can be performed at a regional scale to test the sensitivity of projected streamflow to change in landuse pattern.

CHAPTER 5

IMPACTS OF CLIMATE CHANGE ON EXTREME PRECIPITATION EVENTS OVER FLAMINGO TROPICANA WATERSHED, LAS VEGAS, NEVADA

5.1 Introduction

The occurrences of extreme storm events are one of the major aspects of climate. The increase in the frequency and intensity of extreme rainfall events may cause serious impacts on both environmental and human systems in terms of increased frequency and severity of floods. For many regions, the frequency and intensity of heavy precipitation events have increased in the past 50 years (Frich et al, 2002; IPCC, 2007). Easterling et al. (1999) have suggested the higher occurrence of various extremes in the United States (U.S.) since the 1970s. The increase in extreme precipitation events is contributing to increasing number of days of higher precipitation (>50 mm) and the frequency of occurrence of events in the United States (Karl et al., 1996; Karl and Knight 1998). An increase of at least 5% in mean summer precipitation is documented in the past century, and an increase of 20% of summer daily precipitation is suggested in the future for the northern countries (Canada, Norway, Russia, Poland) and mid latitude countries (U.S., Mexico, China, Australia) for the same increase in mean summer precipitation (Groisman et al, 1999). Under enhanced greenhouse gases (GHGs) conditions, the possibility of significant increase in frequency and magnitude of extreme daily precipitation- both at global and regional scale- is supported by various studies (Noda and Tokioka, 1989; Gordon et al., 1992; Fowler and Hennessey, 1995; Hennessey et al, 1997; Zwiers and Kharin, 1998; Groisman et al, 1999; McGuffie, 1999; Kharin and Zwiers, 2000; Cubasch et al, 2001; Frich et al, 2002; Milly et al, 2002; Palmer and Ra¨isa¨nen, 2002; Semenov

and Bengtsson, 2002; Voss et al, 2002; Fowler and Kilsby, 2003b; Watterson and Dix, 2003; Wehner, 2004; Meehl et al, 2005; Ra¨isa¨nen, 2005; Goswami et al, 2006). The extreme flows are predicted to increase more than the mean flows under different climate change conditions (Arnell et al, 2003).

The evaluation of extreme events requires either use of regional climate models (RCMs), high resolution Global Climate Models (GCMs), or downscaling of data to a smaller time scale to improve the analysis and accuracy of GCM results (Mearns et al. 1995; Kim et al, 2002). The use of coarser GCMs in the past century didn't simulate the extreme rainfall events well (Rind et al, 1989; Mearns et al, 1990; Gordon et al. 1992; Cubasch et al, 1995; Mearns et al, 1995; Jones et al, 1997; Hennessy et al, 1997; Zwiers and Kharin, 1998; McGuffie, 1999; Kharin and Zwiers, 2000). The use of fewer climate projections in model simulations also restricted the full range of possible scenarios and increased the uncertainty related to future climate change conditions. Some studies have utilized the multi-model approach, the multi-scenario approach, or both along with a high resolution simulation to address uncertainties of studies related to extreme precipitation events (McGuffie et al, 1999; Durman et al, 2001; Jones and Reid, 2001; Ra¨isa¨nen and Joelsson, 2001**;** Palmer and Ra¨isa¨nen, 2002; Prudhomme et al, 2002; Semenov and Bengtsson, 2002; Voss et al, 2002; Huntingford et al., 2003; Watterson and Dix, 2003; Ekstro¨m et al, 2005; Fowler et al, 2005; Frei et al, 2006; Tebaldi et al, 2006; Beniston et al, 2007; Buonomo et al, 2007; Fowler et al, 2007; Dankers and Feyen, 2009; Dankers et al, 2009; Fowler and Ekstro¨m, 2009; Kyselý and Beranová, 2009; Mailhot et al, 2010).

The changing intensity of extreme storm events, which are likely to occur as summer monsoon storms, are found disproportionately larger than changes in

precipitation during other seasons (Zwiers and Kharin, 1998; Groisman et al, 1999). Based on the results of climate models, the total summer precipitation is expected to less. But the increase in intensity and duration of extreme precipitation events is expected in most areas (Christensen and Christensen, 2003; Fowler and Kilsby, 2003a). For the few studies, the extreme precipitation projections have shown the greatest increase in the precipitation intensity for the most intense storms (i.e. extreme short duration storms) (Ra¨isa¨nen and Joelsson, 2001; Buonomo et al, 2007). These events could be more extreme in arid and semi-arid regions. The response of streamflow to changes in precipitation may range from a double in wet and temperate areas to more than 5 times in arid areas (Chiew et. al, 1995).

A proper understanding of the impacts of climate change at a regional scale is important for local impact analysis. This paper proposes to answer the following question: How would an urban basin respond to the most intense storm under projected climate change conditions? The intensity of extreme storms is expected to change under anthropogenic climate change conditions. This paper concentrates on the application of a hydrologic model, which incorporates downscaled climate information from multiple GCMs and multiple scenarios, and examines the potential impacts of climate change on extreme storm events. In order to achieve this goal, this study focuses on the semi arid watershed areas of southwestern Nevada (such as Las Vegas), where, short duration summer storms, which are mostly developed by convective processes and result in intense thunderstorms that have caused heavy damage to life and property in the past (CCRFCD, 2006). These intense thunderstorms during the summer months are localized. A change in intensity of extreme storms under anthropogenic climate conditions could

cause a significant hydrological impact (change in peak streamflow and total runoff volume) on this region. The direct changes in intense storms and its watershed level impact can be utilized to evaluate the performance capacity of existing flood control facilities.

This paper utilizes the Master Plan Update model developed for the Clark County Regional Flood Control District. The uncertainties in the climate data are addressed by utilizing the bias corrected and spatially downscaled (BCSD) multi-model, multi-scenario data from the World Climate Research Programme's (WCRP's) Coupled Model Inter-comparison Project Phase 3 (CMIP3), hosted by Lawrence Livermore National Laboratory (LLNL) Program for Climate Model Diagnosis and Intercomparison (PCMDI) (Maurer et al, 2007). The BCSD average monthly temperature and precipitation data also addresses the higher resolution data input requirement for the evaluation of extreme storm events. The BCSD technique uses statistical downscaling method which compares well with other statistical and dynamical downscaling approaches (Wood et al., 2004).

The outline for this paper is arranged as follows. The description of the study area, data needs, hydrologic model and major simulations for this analysis are provided in Section 5.2; the observed and simulated results are summarized in Section 5.3; a brief discussion on shortcomings of the results is provided in Section 5.4, and finally concluded in Section 5.5.

5.2 Methodology

5.2.1 Study Area

The study area is an urban watershed located in Las Vegas, Nevada (Figure 5.1). Flamingo-Tropicana (FT) watershed lies at latitude 35.95° to 36.22° N, and longitude 115.02° to 115.53° W. It has a boundary area of approximately 215 sq. miles and it is one of the major tributaries to the Las Vegas Wash which discharges into the Colorado River at Lake Mead. The watershed consists of the Flamingo and Tropicana washes, 32 weather stations, and two major detention basins. The average yearly rainfall in the Las Vegas Valley is 4.49 inches with the most damaging storms occuring between July and September due to short duration storms caused by convective processes (CCRFCD, 2006).

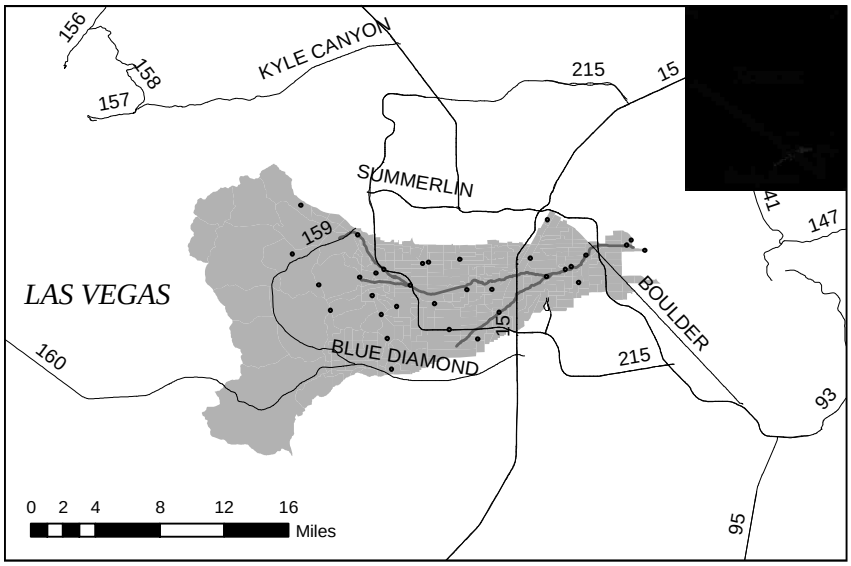

Figure 5.1 Location of the Flamingo Tropicana Watershed in the Las Vegas, Nevada, and major washes and weather stations (indicated by filled circles) located inside the watershed.

5.2.2 Hydrologic Model

The hydrologic model used in this analysis is the 2008 Flood Control Master Plan Update (MPU) model which is developed by the Clark County Regional Flood Control District (CCRFCD). The MPU model is utilized by CCRFCD as a major tool for various flood management purposes, flood plain regulation, drainage design, and watershed management for Clark County, Nevada. The MPU model uses the Hydrologic Modeling Software (HMS) developed by U.S. Army Corps of Engineers Hydrologic Engineering Center (HEC). It is a physically based quasi-distributed hydrological model that can simulate the rainfall runoff processes for an event based and continuous storm events in a watershed.

The major parts of the HMS model include the basin model, meteorological model and control specifications. The basin model represents physical characteristics of a watershed, stream network and various hydrological processes such as infiltration, runoff, base flow, routing and lakes. The meteorological model creates a boundary condition for each sub-basin. The major meteorological parameters include precipitation, evapo-transpiration and snowmelt. Both recording and non recording gauges are available in the watershed. Therefore, the gauge weighting method is selected in the meteorological model to spatially distribute precipitation data in the watershed. The control specification controls the run of a simulation and start the computation of a hydrograph after rainfall starts. The starting and ending date, storm duration, and simulation time steps are provided in control specification. In the MPU model, the entire Las Vegas valley is divided into nine major watersheds which are discharged into the Las Vegas Wash. All of these watersheds are analyzed by developing synthetic storm hydrographs and using

other consistent criteria during modeling. The MPU model uses an ultimate condition (fully developed), a 100 year design storm, and no base flow, thus contributing higher peak flow and volume for the design of flood control facilities.

5.2.3 Data Description

The WCRP's CMIP3 multi-model dataset used in this analysis consists of fine spatial resolution (1/8-degree) translations of 112 contemporary climate projections, for 3 major climate emission scenarios (from IPCC) and 16 robust GCMs for the whole contiguous United States. The 3 emission scenarios are categorized as higher (A2, CO_2 concentration ~ 820 parts per million (ppm) by 2100), medium (A1B, CO_2 concentration ~ 700 ppm by 2100), and lower forcing (B1, CO_2 concentration ~ 550 ppm by 2100) for the multi-model runs. The multi-model dataset consists of average monthly temperature and precipitation data for a period of 1950-2100 which are already statistically downscaled using BCSD technique (Wood et al, 2004). While using the BCSD method, the bias between the GCM monthly data and observed data is corrected using a quantile based mapping. The bias corrected temperature and precipitation are then interpolated into a finer grid by using additive anomalies for temperature and scaling factor for precipitation.

The historical real time rainfall and water depth data (from 1998-2009) are collected from the CCRFCD online database (http://ccrfcd.org/sensordata.htm); these data are collected for all 32 stations located inside the watershed. The three types of weather stations (precipitation, water level, full weather station) in the watershed measure daily precipitation, water level and other meteorological parameters. Based on the historical rainfall and water depth data, a number of flood events are identified and

compared in the study area. An extreme event (for the purpose of this chapter, is defined as the 100 year return period event) is selected which represents the most severe historical flood event for this area. Other physical characteristics (such as land use, soil e.t.c.) of the FT watershed are imported from the MPU model and remain similar during this analysis. Land use data is based on the zoning information obtained from the local entities in the valley which is categorized into several classes- undeveloped, roads and highways, commercial, industrial, residential, park/golf courses, and public land. The Soil Conservation Service method is used to classify soils that uses infiltration rates (High-Soil A, Low-Soil D) as a basis of classification. The mountainous regions of the watershed are covered with soil group D while the valley floor has soil type B and C.

5.2.4 Data Downscaling

No further spatial downscaling is performed for the average monthly precipitation data available in WCRP's CMIP3 dataset. The temporal downscaling technique as described in Wood et al. (2004) is extended to downscale the precipitation data from monthly to daily and daily to hourly or real time storm event. Since the analysis is event based, the temporal downscaling is performed with respect to the selected storm event. Bias in the mean is identified and corrected for monthly simulations. An hourly based simulation is performed in this analysis, thus the bias in monthly total precipitation is identified and corrected. The scaling factor between the modeled and observed monthly total precipitation is applied to observed daily precipitation to obtain modeled daily values. A similar procedure is followed to downscale the daily precipitation to real time storm event. The scaling factor between the modeled and observed daily precipitation is applied to the actual storm to transform it to future climatic conditions.

5.2.5 Model Simulations and Analysis

The hydroclimatic modeling follows three major steps initiated by Bultot et al. (1988) and further adopted by most of the climate change studies: selection of a hydrologic model; selection of a storm event and scenarios construction; and application of constructed scenarios to the hydrologic model. An extreme storm event is selected in this research which is different from the synthetic storms used by the MPU model. Only the basin components of the MPU model are imported thus creating a custom meteorological model and control specifications. The stream networks for the FT watershed are the same as the MPU model. Rainfall is considered as a major meteorological parameter. The effects of temperature are neglected because its impact on runoff is negligible for short duration extreme storm events.

When comparing the historical floods that occurred in Clark County, Nevada, the July 8 1999 storm event represents the most extreme flood event. This storm event had exceeded the local criteria for a 100 year flood event and caused a damage of more than $20 million (CCRFCD, 2006). During this event, a total rainfall of 1.5 to 3 inches was recorded between 60 to 90 minutes at various locations in the Las Vegas valley. This storm event is perturbed to future climatic conditions by varying the meteorological parameters which is followed by hydrological modeling that simulates the streamflow response for various climate scenarios.

5.2.5.1 Development of Climate Change Scenarios

The ensemble of climate projections available for 3 emission scenarios from WCRP CMIP3 database is utilized to develop future climate scenarios. The average monthly output from each emission scenario is used while perturbing the actual storm

event to future climatic conditions. During this process, a scaling factor is calculated between the modeled and observed monthly precipitation; this is done for the month (July 1999) when the actual storm event occurred. This factor is applied to modeled monthly (July) precipitation for different future time periods that results in an observed monthly precipitation for future. The temporal downscaling technique (Wood et al. 2004) as discussed above is followed and the change between the two observed dataset (future and present) is applied to the actual storm event.

The scenarios are constructed for each 30-year time period: 2011-2040, 2041-2070, and 2071-2100. A minimum, average and maximum precipitation for July is calculated for each 30-year period; the precipitation here represents yearly average of July precipitation from all climate projections for each emission scenario. The difference between the modeled and observed precipitation for each time period and scenarios are applied to the actual storm event to transform it into the future climatic conditions.

5.2.5.2 Extreme Value Analysis by Fitting a Distribution

An extreme value (EV) analysis is performed on the GCM data in order to identify any trend in the magnitude of the 100-year precipitation event projected by the climate models. Each of 112 climate projections from WCRP CMIP3 database is a monthly time series of precipitation (1950 – 2100). For this analysis, the baseline period is identified as 1951 - 2000, while the future projections are analyzed for 1981-2040, 2011-2070, and 2041-2100 respectively. Therefore, the number of samples used in the EV analysis for each period is more than fifty (50). Practically, it is considered that the uncertainty in forecasting could be reduced if the forecasting is done for an event that is

no more than double the observation years. Therefore, sixty (60) years of data (starting backward from 2100) are taken to forecast precipitation for a 100 year design storm.

The EV analysis is carried out by fitting each climate projection output to the Log Pearson Type III (LP3) distribution, as prescribed by the U.S. Water Resources Council (WRC, 1981), using annual maximum (AM) time series. Because the input data is measured as a monthly total precipitation, the AM series is the maximum monthly value from each year for the analysis period. Based on WRC (1981), the parameters required to fit the data to the LP3 distribution are estimated using direct method of moments (MOM). For a given data vector *x*, the log of the values in x are calculated ($y = log_{10} x$) followed by the mean, μ_y, standard deviation, σ_y and skewness, g_y of the log values for each time period and projection. In each case, a frequency factor (K_T) is calculated using a formula provided by Kite (1977) which is a function of the desired event return period (T) and the skewness of the log values. The T-year quantile is estimated from a formula proposed by Chow (1964), but used in Mays (2005) in the following form:

$$y_T = \mu_y + K_T \sigma_y \tag{5.1}$$

The magnitude of the T-year event is found by taking the anti-log of this equation:

$$x_T = 10^{y_T} \tag{5.2}$$

Because of the input data, the result of this calculation can be interpreted as the monthly rainfall total with a yearly probability of exceedance equal to 1/T.

In this case the 100 year event is selected as the “design storm” that is being projected into the future using data from multiple projections. Because all of the GCM projections from climate emission scenarios (A1B, A2, and B1) are being used individually, the result of this analysis will identify a precipitation distribution of 100-

year events for each projection at four different time periods (1951-2000, 1981-2040, 2011-2070, and 2041-2100). For each emission scenario, the mean 100-year event projected by the climate models is estimated using a bootstrap technique (Efron, 1979; 1981) with 1000 samples taken with replacement from each group of distributions. This approach provides a 95% confidence interval for the 100-year event for each emission scenario and time period.

The relative growth (ratio) of the 100-yr event is calculated on the mean, separately for each emission scenario and time period. The ratio calculation is repeated for the upper and lower confidence limits to preserve the GCM uncertainty in the streamflow simulations. The growth rate is applied to the actual storm event to transform it into the future climatic conditions for different time periods.

All constructed scenarios are forced into the hydrologic model to observe the variation in streamflow for the FT watershed. The storm duration for the actual storm event is taken as a reference period during the model simulations. The peak streamflow and total runoff volume for the actual storm event is compared with the simulated streamflows from different climate scenarios and time periods.

5.3 Climate Observations

5.3.1 Precipitation Pattern

The precipitation pattern for each climate emission scenario is compared for future time periods. Figure 5.2 displays a 10-year moving average annual precipitation during 1950-2100 with both increasing and decreasing patterns for each scenario**.** Although the precipitation magnitudes vary in between the scenarios, the change of

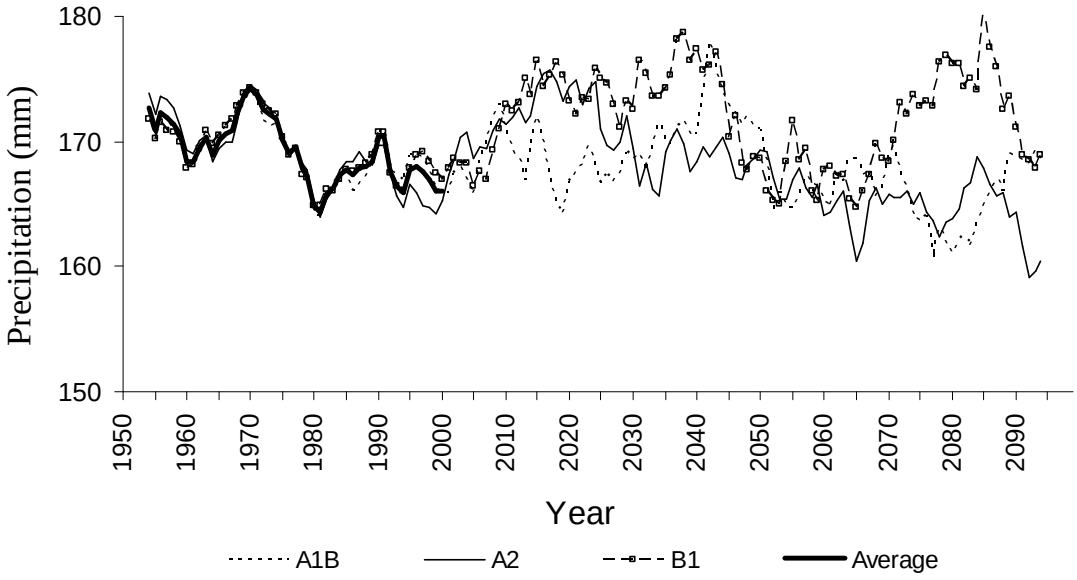

Figure 5.2 10-year moving average of total annual precipitation for each emission scenario, based on multi-model climate projections from WCRP CMIP3 data, during 1950-2100.

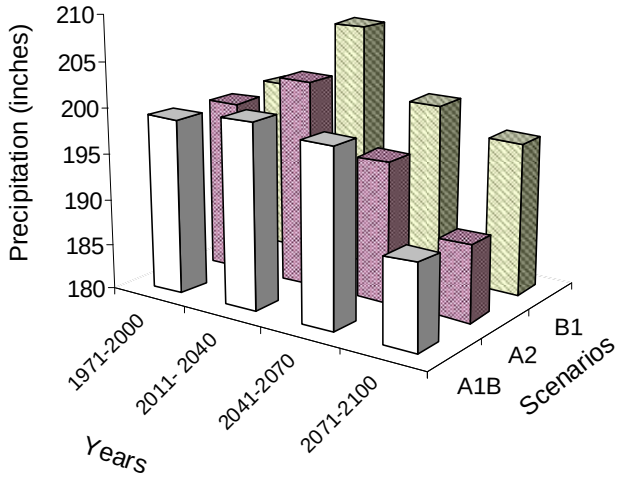

Figure 5.3 Total cumulative precipitation (measured in inches) for each emission scenario during 1971-2000, 2011-40, 2041-70, 2071-2100.

direction is similar for most future time periods (except 1995-2000 for A2; 2015-2020 and 2072-80 for A1B). Average precipitation represents an average of annual

precipitation from all scenarios for the last century. A decrease in annual precipitation is observed from 2045 until 2070 for B1, 2080 for A1B, and 2090 for A2. Higher precipitation is observed at different time periods which varies based on scenario. Maximum annual precipitation is observed for B1 during 2035-45 and 2080-2090.

The total annual precipitation (measured in inches) for each 30-year period shows a decrease while moving from 2011-2100. Figure 5.3 shows a maximum decrease in total precipitation for higher emission scenarios, similar to A2, A1B and B1. This resembles a precipitation pattern for arid regions in the future climate. This implies that the total runoff volume may decrease in the future, where B1 shows a lower decrease than A1B and A2.

The average monthly precipitation (measured in inches) during each 30-year future period is also compared with the baseline period (1971-2000) for all emission scenarios (Figure 5.4). The monthly precipitation shows an increasing pattern during Jan-Feb and July-Oct (except Sep during 2041-70), while a decreasing pattern is observed for other months with a maximum decrease during April-June. The decrease percentage varies from 12% to 46% in between the scenarios with a maximum decrease shown by A2 during all periods. The summer months (July-August) show a larger increase until 2100; an increase percentage from 5% to 21% is calculated for different time periods and scenarios. In between the scenarios, the increase percentage is higher for A1B during 2011-40, B1 during 2041-70 and maximum for A2 during 2071-2100. This indicates that the summer storm events could be more extreme in the future than at present.

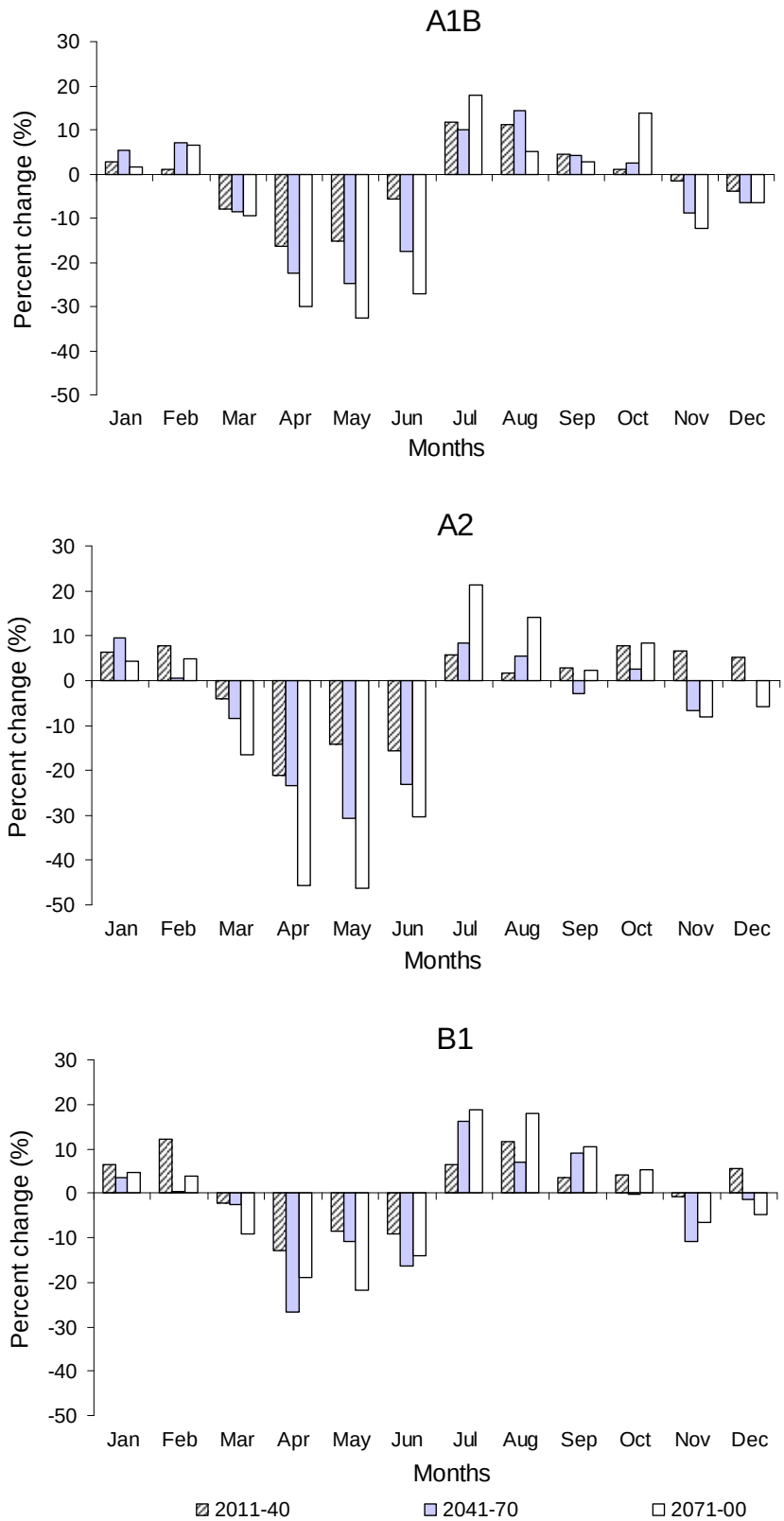

Figure 5.4 Change in average monthly precipitation (%) for each emission scenario during 30-year future period with respect to 1971 -2000.

5.3.2 Temperature Pattern

The average temperature for the Las Vegas Valley shows an increase for future periods when compared with the baseline period (1971-2000). Larger increases in temperature are shown by higher emission scenarios similar to A2, A1B and B1 (Figure 5.5). While comparing the changes in minimum and maximum temperature, an increase in temperature from 0.5 ºC to 5 ºC, 0.15 ºC to 4.5 ºC, and 0.5 ºC to 6 ºC is calculated for mean, minimum and maximum temperatures respectively. A2 shows a maximum increase in temperature (5 ºC) during 2071-2100. As mentioned earlier, the effects of temperature are not considered in this analysis since its impact on runoff is negligible for short duration extreme storm events.

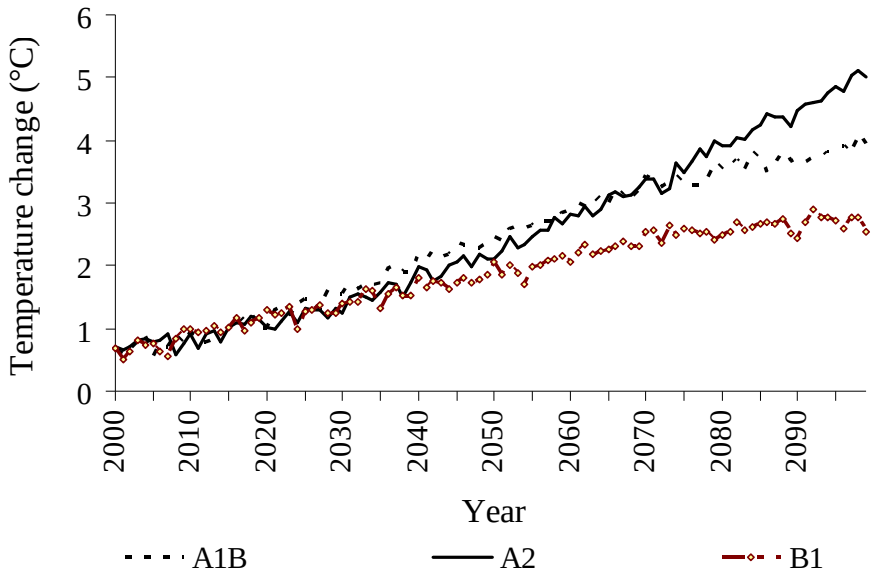

Figure5.5 Change of average annual temperature for future periods whencompared with average annual temperature for the baseline period (1971-2000) for each emission scenario (A1B, A2, B1).

5.4 Streamflow Projections

5.4.1 Inter-Model Comparison

The GCMs output for each emission scenario are utilized to observe the streamflow variation in between the GCMs; the actual storm event is perturbed into the future based on each GCM output. The actual storm event is adjusted with respect to average monthly precipitation (July) during 2011-2100 for each GCM. Figure 5.6 shows a larger variation in the simulated peak streamflows and total runoff volume between the GCMs for each emission scenario. Based on the ensemble multi-model data (only 6 model simulations shown here), the highest peak streamflows are simulated by CCCMA CGCM 3.1, while the lowest peak streamflows are simulated by GFDL CM 2.0 and MIUB ECHO-G for all three scenarios. Differences in the magnitude of peak streamflow and total runoff volume are also observed for the same GCM when simulated for different scenarios. The differences in simulated streamflows identified between the GCMs are mainly due to the type of GCMs, their origin, initial conditions, and boundary conditions for each climate projection. When the actual storm is transformed into the future climate, the precipitation intensity varies based on the GCM output. Each GCM shows only a small shift in the timing of occurrence of peak streamflow for future periods. This is due to similar hydrologic conditions and watershed characteristics that are used during model simulations for the historical and future climates. Since the simulated streamflow shows a very large variation in between the GCMs, an average precipitation from all GCMs output for each emission scenario is used to develop future climate scenarios.

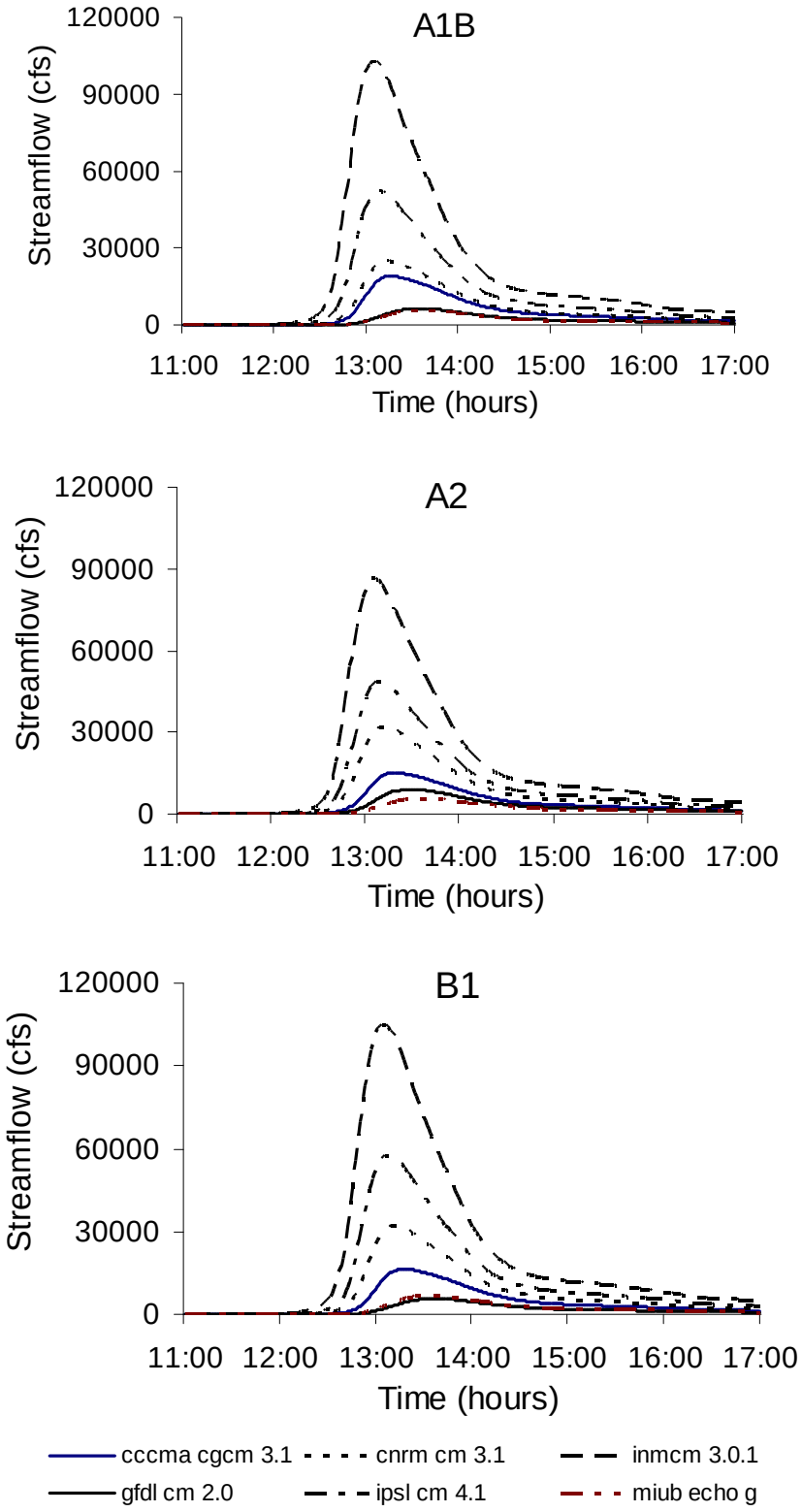

Figure 5.6 Simulated streamflow patterns for different GCMs and emission scenarios, when the actual storm event is adjusted with respect to average monthly precipitation (July) during 2011-2100 for each GCM.

5.4.2 Inter-Scenario and Multi-Decadal Comparison

5.4.2.1 Based on Ensemble of Climate Projections

A peak streamflow of 13924.4 cubic foot per second (cfs) and total runoff volume of 1791.8 acre foot are obtained, when the simulation is carried out with observed gauge data for the actual storm event (July 8 1999). Minimum, average, and maximum precipitation for July are calculated for each emission scenario during each 30-year future period (2011-40, 2041-70, 2071-2100). Each scenario shows an increase in precipitation intensity when the actual storm event is perturbed into the future climatic conditions based on average July precipitation. Figure 5.7 shows an increase in peak streamflow for all scenarios during each 30-year period up to 2100. Although the simulations are carried out for the same time period, a difference exists in the magnitude of peak streamflow in between the scenarios. Minimum and maximum peak streamflow are simulated for B1 during 2011-40 and A2 during 2071-90 respectively; the simulated peak streamflow is higher for A2 than A1B and B1 during all time periods. This indicates that the higher emission scenario simulates larger peak streamflow for an average change in precipitation in future. As discussed in section 5.4.1, no significant shift is observed in the timing of occurrence of peak streamflow for future periods.

The variation in the magnitude of peak streamflow is due to changing precipitation intensity for the actual storm event in future. The higher emission of greenhouse gases increases temperatures, evaporation rates of surface water and moisture holding capacity of the atmosphere. The increase in latent heat due to increasing radiation and surface warming causes static instability, deeper convection and vertical motion of water vapors (Gordon et al., 1992; Mitchell and Ingram, 1992; Hennessey et al, 1997).

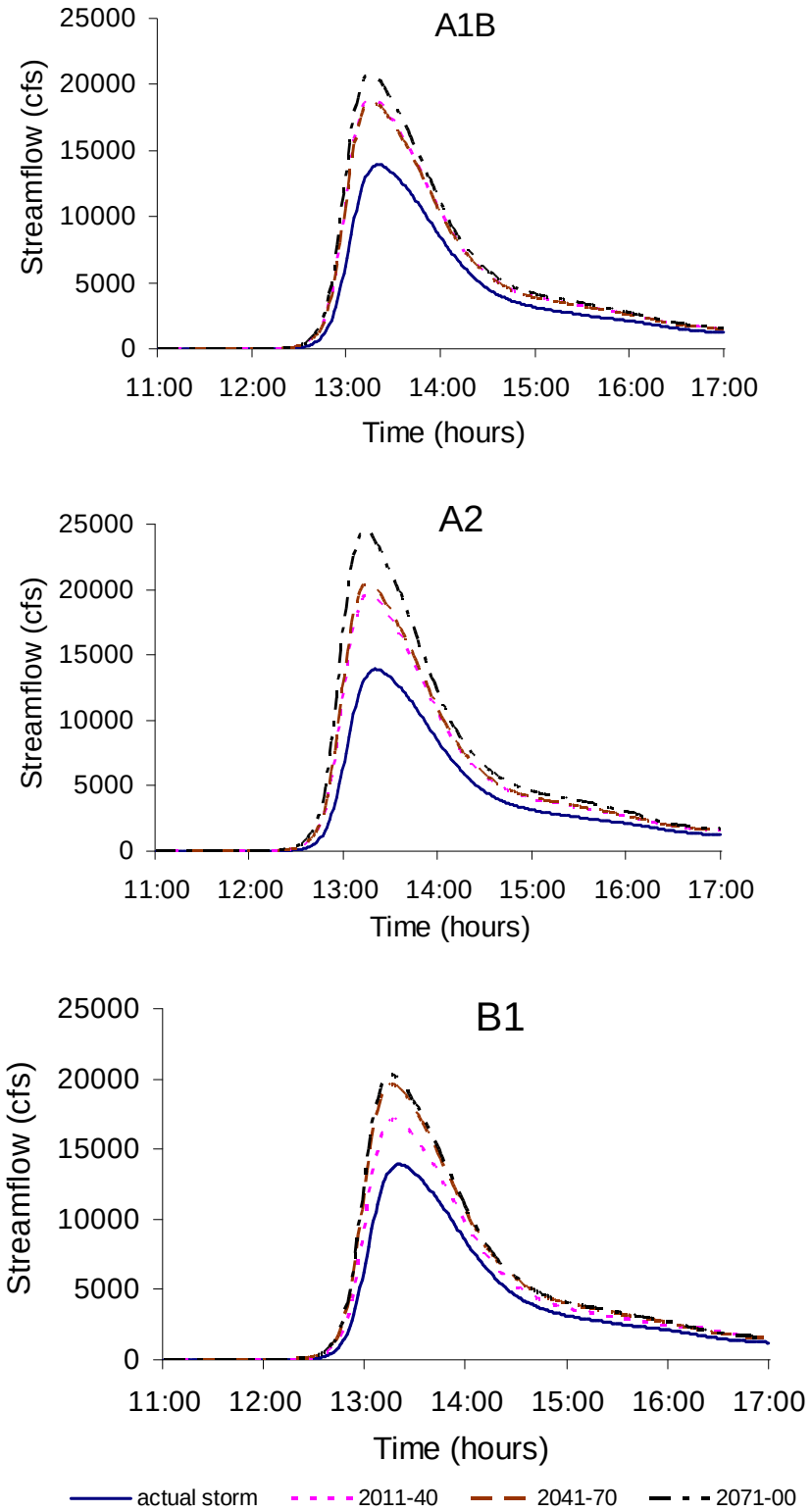

Figure 5.7 Streamflow pattern for the extreme storm when the simulations are carried out under climate emission scenarios, A1B, A2 and B1, during 2011-2040, 2041-70, and 2071-2100.

The increase in latent heat is balanced by an increase in water vapor which leads to an increase in the long wave cooling of the atmosphere. The deeper convection and increased water vapor in the atmosphere causes an increase in the precipitation intensity as well as the percentage of convective rainfall events.

Figure 5.8 shows a higher range of increase or decrease in peak streamflow and total runoff volume between the scenarios, when simulated for minimum and maximum July precipitation for future periods. The simulated peak streamflow and total runoff volume range from a decrease of 30 % to an increase of more than 150% with respect to the actual storm. As noted earlier, for an average July precipitation, a larger increase in streamflow is simulated for A2 during all future periods; it varies from 40% to 75% for peak streamflow and 30% to 65% for total runoff volume. An increase from 85% to 183% in peak streamflow and 70% to 146% in total runoff volume is simulated for the scenarios based on maximum July precipitation. A1B, B1, and A2 show larger increase during 2011-40, 2041-70, and 2071-2100 respectively. This agrees with the summer months (July-August) precipitation pattern followed by the scenarios during these time periods (Figure 5.4). A decrease from 5% to 34% in peak streamflow and 4% to 31% in total runoff volume is simulated for the scenarios based on minimum July precipitation. For these scenarios, A1B shows a larger decrease during 2011-40 and 2041-70, A2 during 2071-2100, and B1 during 2011-40 and 2071-2100; B1 shows a maximum decrease during 2071-2100.

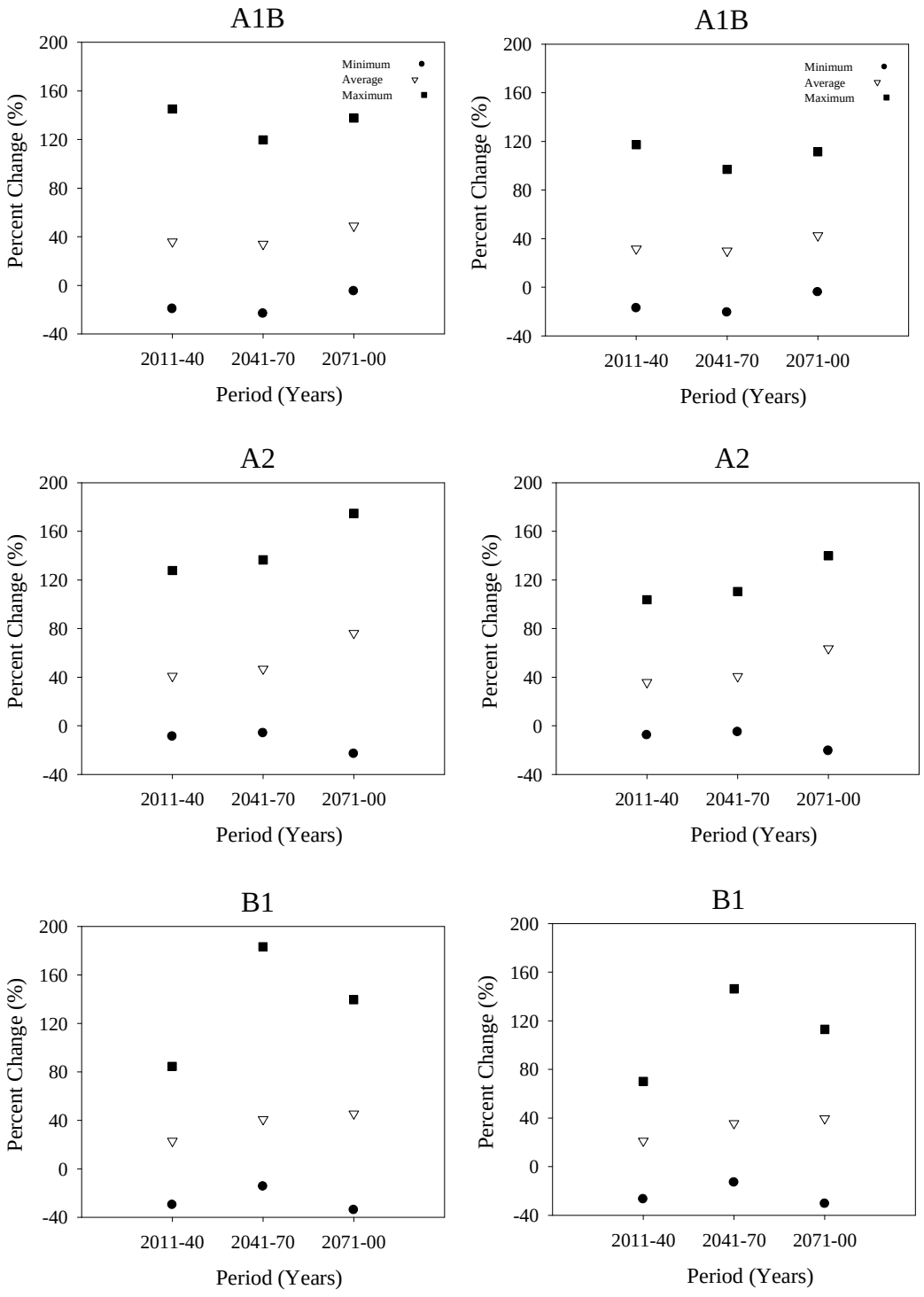

Figure 5.8 Percent change of peak runoff (left) and total runoff volume (right) for the extreme storm when the simulations are carried out for minimum, average and maximum change of precipitation for emission scenarios (A1B, A2 and B1) during each 30-year future time periods.

5.4.2.2 Extreme Value Analysis by Fitting a Distribution

Figure 5.9 shows a range of precipitation during the baseline period (1951-2000) and future periods for all emission scenarios. This precipitation represents the precipitation for a 100-year design storm. The lower dot and upper dot in the box plot represents lower 5% and upper 95% precipitation values. The calculated range of precipitation is almost equal for all scenarios during 1951-2000. An increasing precipitation pattern is observed for all scenarios over this century which is similar to the pattern shown by the summer months in Figure 4. Maximum precipitation is calculated for the higher emission scenario (A2) during 2041-2100. However, the calculated range of precipitation is similar for A1B and B1 during this period. This relative growth in precipitation, which is calculated from the modeled output for the baseline and future period, is applied to the actual storm event to transform it into the future climate. All scenarios developed for the mean and its confidence interval for future periods are forced into the MPU model to assess the impact on streamflow.

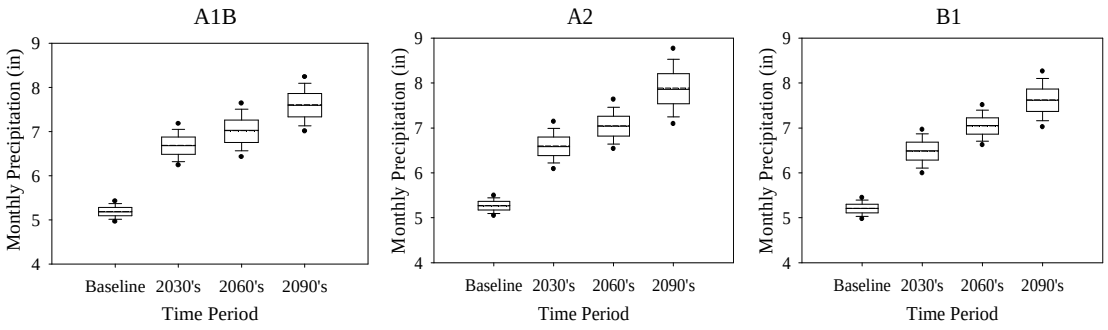

Figure 5.9 Range of modeled maximum monthly precipitation (measured in inches) for different periods and emission scenarios. The lower and upper dots in the box plot represent the lower 5% and upper 95% precipitation values (1951-2000, 1981-2040, 2011-2070, and 2041-2100 represented as baseline, 2030's, 2060's and 2090's).

Figure 5.10 shows the change in peak streamflow and total runoff volume for all scenarios during 1981-2040, 2011-2070, and 2041-2100 (represented as 2030's, 2060's, and 2090's) with respect to the baseline period (1951-2000). The average change in peak streamflow and total runoff volume is represented by the middle values while its confidence intervals (upper 95^{th} and lower 5^{th} percentile) are represented by the upper and lower values. Both peak streamflow and total runoff volume show an increasing pattern for all scenarios similar to the precipitation pattern for 100-year design storm. While considering all scenarios and an average change in precipitation, the peak streamflow shows an increase from 41% to 50%, 58% to 61%, and 83% to 90% during 1981-2040, 2011-2070, and 2041-2100 respectively. When the lower and upper percentile changes are considered, the increase percentage is larger for A2 during 2041-2100 that varies from 71% to 109%; this increase percentage is larger for A1B during 1981-2040 and 2011-2070 which varies from 44% to 55% and 51% to 72% respectively. While considering all scenarios and an average change in precipitation, the total runoff volume shows an increase from 36% to 42%, 50% to 52%, and 69% to 74% during 1981-2040, 2011-2070, and 2041-2100 respectively; however, this range varies from 30% to 90% when the lower and upper percentile changes are considered.

5.5 Discussion

This analysis has followed two different approaches which possess different assumptions and limitations. The first approach utilized data from the CCRFCD established weather stations in the watershed and average precipitation data from all climate projections for each climate emission scenario. The range of percent change

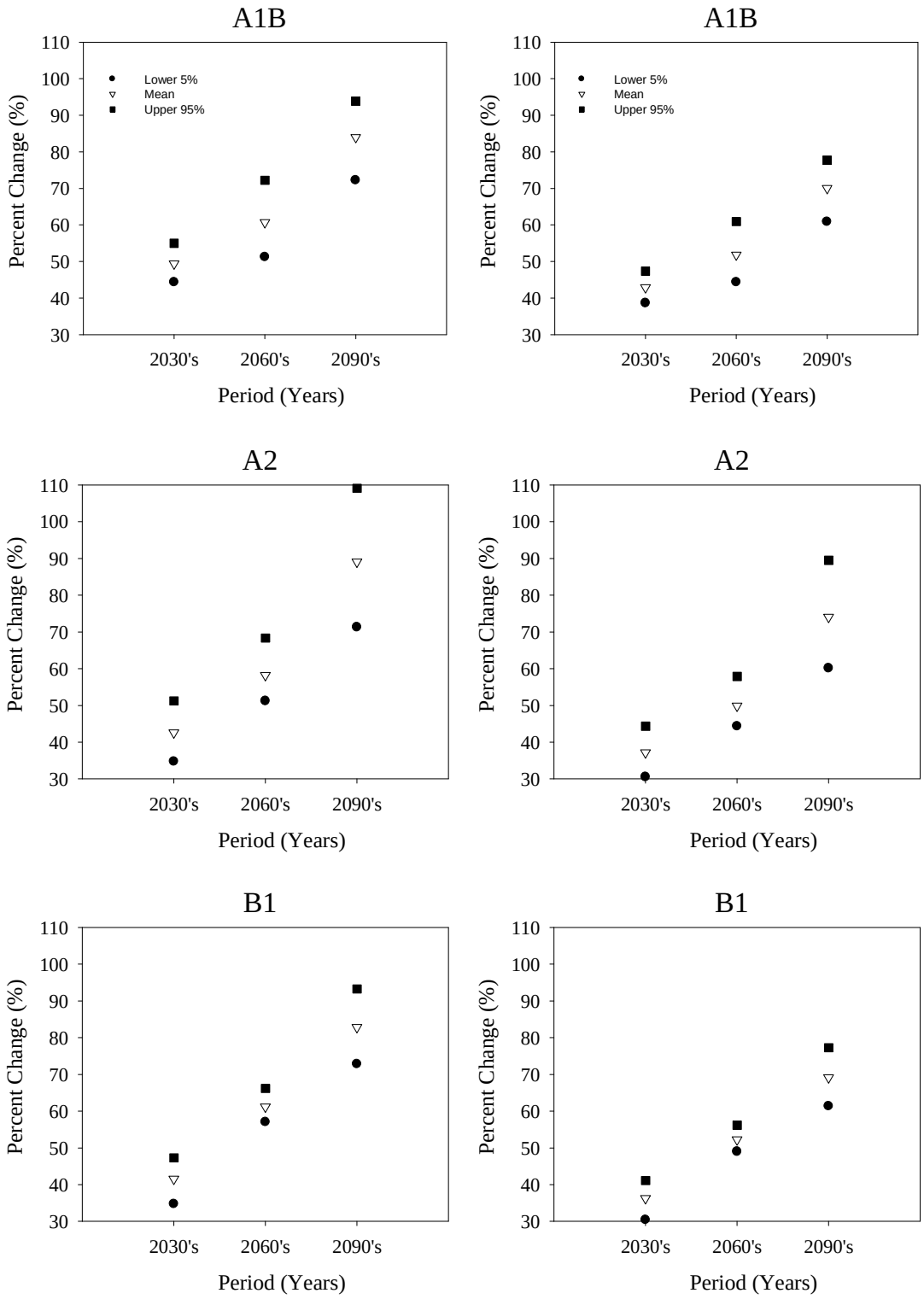

Figure 5.10 Percent change of peak runoff (left) and total runoff volume (right) for the extreme storm when the simulations are carried out for lower 5%, mean, and upper 95% change of precipitation for 30-year time periods (1981-2040, 2011-2070, and 2041-2100 represented as 2030's, 2060's and 2090's) for each emission scenario.

(max, average, and min) of streamflow is calculated with this method. The second approach utilized only GCM output to calculate relative change in current and future precipitation for a 100-year design storm, and apply that change to adjust the actual storm event. The annual maximum values are used by this method; therefore, this method is applicable to analyses focusing on maximum flows. Both approaches have shown a very high degree of change in peak streamflow and total runoff volume for the actual storm event until 2100. Higher emission scenario has shown larger changes at the end of this century. This represents the nature of extreme storm events in a changing future climate. However it should be realized that these results are limited to the ensemble of multi-model climate projections from WCRP CMIP3 dataset and the performance capacity of MPU model to simulate the future climate.

None of the multi-models could be categorized as more accurate as all of them follow some assumptions, limitations, and different levels of details intended for specific applications. The choice of multi-model and focus on mean climate in this analysis is assumed to provide a more reliable estimate of the future uncertainty. Additional analysis based on 100-year design storm and confidence interval also addresses the uncertainties associated with the impact studies related to extreme storm events. The simulated streamflow in this analysis represent streamflow from a fully developed watershed as assumed by the MPU model. Some sources of uncertainty can be attributed to the use of climate data and station data, and downscaling methods adopted in this analysis. The locally measured station data used for all stations in the watershed could be affected by many microclimatological effects (Osborn and Hulme, 1997). The downscaling method used in this analysis only considers the change in rainfall intensity for a future climate.

Therefore, land use, watershed characteristics, and variability of the extreme events remain constant. The use of other downscaling techniques may add some changes in the simulated results.

5.6 Conclusions

This paper has demonstrated the compatibility of a hydrologic model with higher resolution climate data (scenarios) incorporated to quantify the watershed level impacts of extreme storm events under anthropogenic climate change conditions. A methodology has been developed that examines the future climate and evaluates its impact in terms of corresponding changes in peak streamflow and total runoff volume. This paper has also addressed the hydrological impacts due to a 100-yr return period storm under changing climatic condition. The BCSD multi-model data used in this paper as a requirement of higher resolution data can be utilized for regional hydroclimatic studies.

The ensemble multi-model data has shown a warmer future climate and a decrease in total annual precipitation for each 30-year period up to 2100. The summer storms, which are considered as extreme storms, are expected to be more intense in future. The simulated maximum change in peak streamflow and total runoff volume ranges from 40% to more than 150% for the projected extreme storm over this century. The predicted peak streamflow for intense storms helps to evaluate the vulnerability of existing flood control facilities under anthropogenic climate change conditions. This methodology can be utilized to design a flood management tool in the Flamingo-Tropicana watershed and mitigate runoff impacts of intense storms under changing climatic conditions. Future work can be extended to a wider scale to identify the impacts

of event based changes on entire Las Vegas watersheds. Similar hydroclimatic studies can be carried out with different set of climate data, storm event, hydrologic model, and downscaling methods to increase reliability on the results obtained from this research.

CHAPTER 6

CONCLUSIONS AND RECOMMENDATIONS

6.1 Conclusions and Contributions

The research presented in this study contributes to the field of water resources engineering related to weather modification (WM), climate change and hydrology. This includes how WM programs and climate change impact the hydrologic characteristics of a non-urban watershed, and how future climate impacts extreme storm events of an urban watershed in the western United States.

6.1.1 Research Question #1 (Task 1)

In answering Research Question 1, a hydrologic model was developed (within VIC) to evaluate the impacts of WM programs on water supply. This part of research provided a proof of concept of development and application of WM scenarios for hydrologic impact evaluation. Prior to this research, no hydrologic model was developed and utilized for impact studies relating to WM operations in the North Platte watershed. The VIC model was utilized for various purposes in the watershed. A number of WM scenarios were developed and forced into the VIC model to quantify the impacts of increased precipitation on streamflow, and identify the suitable regions for cloud seeding within the watershed. The hypothesis that the anticipated increase in precipitation could augment annual and seasonal streamflow and reduce the impact during dry periods is confirmed. The centralwest and southwest regions of the watershed, which consists of higher percent coverage of woodland and evergreen broadleaf forest, were found more effective for cloud seeding operations. The present cloud seeding operations are focused on the central regions of the watershed. Based on increased streamflow, the extension of

these operations can be recommended in the southern regions of the watershed. This analysis examined the WM impact on streamflow for a range of increased precipitation in the watershed. For the proposed WM programs or programs that are claimed effective based on precipitation augmentation, the impacts on water availability can be predicted based on this analysis. The results presented here can also be utilized directly by the WM projects operating at representative watersheds.

6.1.2 Research Question #2 (Task 2)

In answering Research Question 2, a methodology was developed that incorporate downscaled climate data (projections) into a hydrologic model and derive streamflow projections to evaluate the potential impacts of climate change on water availability. The hypothesis that the higher resolution climate data and process based model can be utilized for streamflow forecasting and water availability assessment under changing climatic conditions is confirmed. The 'bias corrected and spatially disaggregated' (BCSD) multi-model data that was used as a requirement of higher resolution daily input for the VIC model can be utilized in similar regional hydroclimatic studies. Using this method, streamflow projections were developed based on forecasted multi-model multi-scenario climate projections for the North Platte watershed under anthropogenic climate change conditions. Based on the ensemble of streamflow projections, there is a possibility of increased annual streamflow for this region until 2100. An increase in streamflow was predicted for cold seasons, while projecting a higher reduction during dry seasons. Managing water in this basin under anthropogenic climate change conditions could be a challenging job, when this reduction in streamflow during summer periods coincides with increasing water demand. Prior to this research, no studies were carried out related to

long-term quantitative assessment of water availability in this basin. The streamflow projections and the range of streamflow can be utilized by decision makers in water demand management under changing climatic conditions.

The above analyses accessed water availability in the North Platte watershed under operational WM programs and anthropogenic climate change conditions. For an anticipated increase in precipitation, the WM programs are expected to increase streamflow during summer periods (June-August). Based on forecasted streamflow, the summer months are expected to get reduced streamflow, while the winter months are expected to get increased streamflow. It is not fully known at present whether an increase in streamflow (due to climate change and WM operations) could mitigate the combined impacts of reduced streamflow (during dry periods) and increasing water demand. With a known future water demand and an actual evaluation of the operational WM programs, it might be easier to conclude a more viable option- the storage of additional water during other periods and utilization during dry periods, an effective implementation of WM programs, or both.

6.1.3 Research Question #3 (Task 3)

In answering Research Question 3, a hydrological modeling approach was utilized that simulates an urban basin response to the most intense storm under anthropogenic climate change conditions. A methodology was developed that examines the future climate and corresponding changes in streamflow to quantify the watershed level hydrological impacts of extreme storm events under changing climatic conditions. Few studies (most from Europe) are available at present regarding short duration extreme events. This research performed an event based simulation for shorter duration storms in

the Flamingo Tropicana (FT) watershed in Las Vegas, Nevada. The multi-model multi-scenario BCSD data was utilized as a requirement of higher resolution data for impact studies on extreme storm events. The total annual precipitation for each 30-year period showed a continuous decrease from 2011-2100; this resembles a precipitation pattern for arid regions in the future climate. However, the summer storms, which are considered as extreme storms, were found to be more intense in the future. The simulated peak streamflow and total runoff volume showed an increase from 40% to more than 150% over this century. The hypothesis that the extreme storms could be more intense in future in arid urban areas and contribute for higher impacts on streamflow is confirmed. Based on the MPU report, the drainage facilities that are available at present in the major watersheds of Las Vegas are not able to fully convey the 100-year design flow. The outlook of these changes as a result of more intense storms under anthropogenic climate change conditions could be helpful in evaluating the vulnerability of existing flood control system. These results can be utilized for various design purposes in the watershed to mitigate runoff impacts of intense storms under changing climatic conditions.

Some sources of uncertainty in this research are attributed to the use of hydrologic models, climate data and station data, and downscaling methods adopted in this analysis. Uncertainty in a hydrologic model may arise when using the same optimized parameters for present and future climatic conditions. The measured station data (e.g. meteorological, streamflow) that are used during calibration, validation, and all other simulations in a hydrologic model are likely affected by many microclimatological effects (Osborn and Hulme 1997). The temporal downscaling method used in this analysis only considers the change in rainfall intensity for a future climate. Therefore,

land use, watershed characteristics, and variability of the extreme events remain constant. These results are limited to the ensemble of multi-model climate projections from WCRP CMIP3 dataset and the performance capacity of hydrologic models to simulate the future climate. These uncertainties could lower our confidence to some extent while concluding the reliability of the simulated results from this research. However, improvements could be achieved in the simulated results if associated uncertainties (such as perfect GCM, best scenario, method of downscaling) can be addressed in future.

This research developed methodologies for both long-term and event-based simulation to observe the potential impacts of human induced climate change on existing water resources in arid regions of the western United States. The methodology as well as hydrological models and higher resolution climate data used in this research can be utilized for other regional hydroclimatic studies. Although various uncertainties are associated with WM and climate related studies, these results can be utilized by water managers in regional water resources development and management.

6.2 Recommendations for Future Research

6.2.1 Extension of Present Research

For Task 1, more “what if” WM scenarios (such as impact of landcover from each region) can be carried out to observe the impacts on streamflow. Since the Colorado range is a future region of interest for cloud seeding operations, the impacts on streamflow can be evaluated for the entire North Platte watershed for a range of increased precipitation. Further, the impacts of WM on other hydrologic parameters such as evapo-transpiration, soil moisture, and snow water equivalent can be estimated. The routing

model of the VIC can be utilized for more precise observations of daily or sub-daily changes in streamflow. For Task 2, other downscaling techniques can be adopted to prepare the VIC daily input data from monthly meteorological data, and the results can be compared with those obtained from this research. For Task 3, calibration of the MPU (HEC-HMS) model as well as consideration of other hydrologic components (such as baseflow and local flows) may increase reliability on the simulated results. Further studies can be carried out with different set of climate data, storm event, hydrologic model, and downscaling methods, and the results can be compared with those obtained from the MPU model.

6.2.2 Other Future Studies

This research provides a basis for several other studies in the field of water resources engineering. Some of the recommendations for further study include, but not limited to, the following:

- Evaluation of the operational cloud seeding program can be carried out based on actual field observations, in this case, with respect to measured precipitation at SNOTEL stations. The actual increase in precipitation can be forced into the VIC model to quantify changes in water supply for the watershed. The comparison of actual observations and the simulated results may be helpful in estimating the uncertainties attributed to WM programs. A study on future water demand can be performed and linked with the effects of operational WM programs in the watershed. Additionally a cost benefit analysis can be carried out for these operations to conclude the programs to be financially significant. Similar impact studies can be

carried out for other operational or proposed WM programs by utilizing the methods presented in this research.

- Most uncertainties in climate related studies are attributed to the use of GCM output. An analysis that evaluates the uncertainty of GCM outputs may be helpful in drawing better conclusions for future predictability of hydroclimatic changes. Building upon the current research, future work can be performed at a regional scale to test the sensitivity of projected streamflow to changes in climate as well as landuse pattern. Streamflow projections can be developed for different emission scenarios by varying other model parameters to estimate their uncertainty under changing climatic conditions.
- The study related to impacts of climate change on extreme storm events can be extended to a wider scale covering the whole Las Vegas watersheds, and other arid or semi arid regions. These results can be utilized in identifying the storage capacity required for the watershed under changing climatic conditions. Additional research can be carried out that determines the impact of extreme storm events on storm water quality under changing climatic conditions.

APPENDIX A

DATA FOR VIC MODEL

(TASK 1, 2)

A.1.1 Important Features of Variable Infiltration Capacity Model

The important features inside the Variable Infiltration Capacity (VIC) model that are briefly discussed here is available online (http://www.hydro.washington.edu /Lettenmaier/Models/VIC). The most sensitive parameters in the VIC model are related to soil parameters. Two important features of the VIC model incorporate sub grid variability in soil moisture storage capacity and representation of drainage from the lower soil moisture zone. The two major curves are variable infiltration curve and baseflow curve. The infiltration curve accounts for sub-grid variability in infiltration and relates the infiltration with the fraction of saturated area of soil. The baseflow curve relates baseflow with soil moisture and represents baseflow as a non-linear recession.

The VIC model considers sub-grid variability in land surface vegetation processes, precipitation, topography (using elevation band), atmospheric processes, and soil moisture storage capacity as a spatial probability distribution. Elevation bands are used for more accurate estimation of mountain snowpack. All areas of same elevation range are included in one band, and fluxes and storages from each band are averaged together. Surface runoff is generated when additional precipitation to soil moisture storage at the end of the previous time step exceeds the storage capacity of the soil. The formulations that are used for surface and subsurface runoff are the Xinanjiang model and Arno non-linear baseflow respectively. The total evaporation is the sum of evaporation from canopy layer and bare soil layer, transpiration from vegetation classes, and snow sublimation. Newer versions of the VIC model incorporate several other models- snow model, routing model, excess ice and subsidence model, and lake (wetland) model. The snow algorithm inside the VIC model considers spatially

distributed snow coverage (ground snowpack, snow in vegetation canopy, snow on top of lake ice) and blowing snow sublimation. Other important features that are included in the VIC model are pointed out as follows:

- Land atmosphere exchange of moisture and energy
- No dataset allow an evaluation of interaction of water balance components over large regions for longer periods as in the VIC model.
- Sub-grid parameterization of the effects of spatial variability in soils, topography, and vegetation. Represent the non linear soil moisture dependence of the partitioning of precipitation into direct runoff and infiltration.
- VIC 4.0.1 and later versions can consider canopy energy balance separately from ground surface. They can simulate spatially distributed (laterally) soil freezing, frozen soil and permafrost processes (such as melting of excess ground ice), snow coverage and snow sublimation.

Table A1 Name of SNOTEL and stream gauge stations and their location in the North Platte Watershed.

Name of SNOTEL stations	Station ID	Number	Latitude	Longitude	Elevation	State
Columbine	06J03S	408	40.3833	-106.6000	9160	Colorado
DividePeak	07H05S	449	41.3000	-107.1500	8880	Wyoming
JoeWrite	05J37S	551	40.5167	-105.8833	10120	Colorado
NorthFork FrenchCreek	06H20S	668	41.3167	-106.3667	10130	Wyoming
OldBattle	06H10S	673	41.1500	-106.9667	10000	Wyoming
SouthBrushCreek	06H19S	772	41.3167	-106.5000	8440	Wyoming
Tower	06J29S	825	40.5333	-106.6667	10500	Colorado
Webber Springs	06hH09S	852	41.1500	-106.9167	9250	Wyoming

Name of Stream gauge Stations	Station ID	Number	Latitude	Longitude	State
Michigan river near cameron pass	6614800	4809	40.50	-105.87	CO
North Plate river near Northgate	6620000	4810	40.94	-106.34	CO
Encampment River AB Hog Park CR	6623800	4812	41.02	-106.82	WY
Encampment River at mouth near Encampment	6625000	4813	41.30	-106.72	WY
North brush creek near Saratoga	6622700	4811	41.37	-106.52	WY
N Plate River AB Seminoe Reservoir, NR Sinclair	6630000	4814	41.87	-107.06	WY

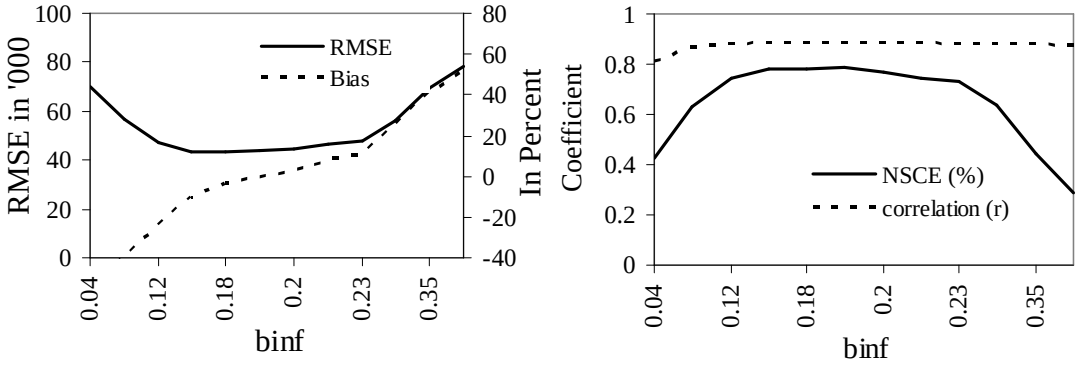

Figure A1. Sensitivity of VIC calibrated parameters (b_{inf}: infiltration parameter)

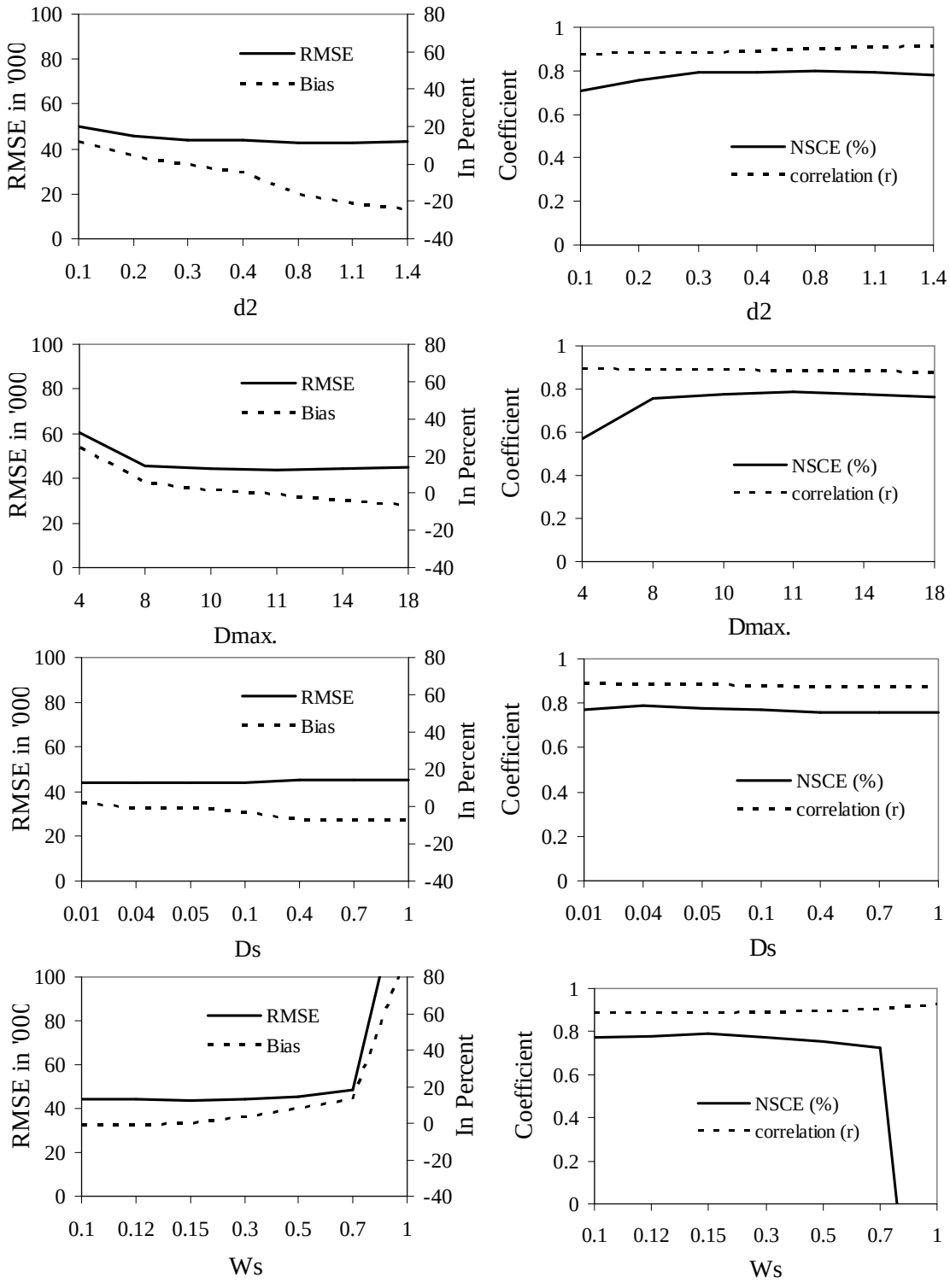

Figure A1 Sensitivity of VIC calibrated parameters (b_{inf}: infiltration parameter, d2: soil depth, D_{max}: maximum baseflow, Ds: fraction of D_{max}, Ws: fraction of maximum soil moisture)

Table A2 Grids located in the North Platte watershed

Grids considered for North Platte watershed					
Latitude	Longitude	Latitude	Longitude	Latitude	Longitude
40.3125	-105.94	40.9375	-106.19	41.4375	-107.06
40.3125	-106.06	40.9375	-106.31	41.4375	-107.19
40.3125	-106.19	40.9375	-106.44	41.4375	-107.31
40.3125	-106.31	40.9375	-106.56	41.5625	-106.44
40.3125	-106.44	40.9375	-106.69	41.5625	-106.56
40.4375	-105.81	40.9375	-106.81	41.5625	-106.69
40.4375	-105.94	41.0625	-106.19	41.5625	-106.81
40.4375	-106.06	41.0625	-106.31	41.5625	-106.94
40.4375	-106.19	41.0625	-106.44	41.5625	-107.06
40.4375	-106.31	41.0625	-106.56	41.5625	-107.19
40.4375	-106.44	41.0625	-106.69	41.5625	-107.31
40.4375	-106.56	41.0625	-106.81	41.5625	-107.44
40.4375	-106.69	41.0625	-106.94	41.6875	-106.56
40.5625	-105.81	41.1875	-106.19	41.6875	-106.69
40.5625	-105.94	41.1875	-106.31	41.6875	-106.81
40.5625	-106.06	41.1875	-106.44	41.6875	-106.94
40.5625	-106.19	41.1875	-106.56	41.6875	-107.06
40.5625	-106.31	41.1875	-106.69	41.6875	-107.19
40.5625	-106.44	41.1875	-106.81	41.6875	-107.31
40.5625	-106.56	41.1875	-106.94	41.8125	-106.44
40.5625	-106.69	41.1875	-107.06	41.8125	-106.56
40.6875	-105.94	41.3125	-106.31	41.8125	-106.69
40.6875	-106.06	41.3125	-106.44	41.8125	-106.81
40.6875	-106.19	41.3125	-106.56	41.8125	-106.94
40.6875	-106.31	41.3125	-106.69	41.8125	-107.06
40.6875	-106.44	41.3125	-106.81	41.8125	-107.19
40.6875	-106.56	41.3125	-106.94	41.8125	-107.31
40.6875	-106.69	41.3125	-107.06	41.9375	-106.94
40.8125	-106.06	41.3125	-107.19	41.9375	-107.06
40.8125	-106.19	41.4375	-106.44		
40.8125	-106.31	41.4375	-106.56		
40.8125	-106.44	41.4375	-106.69		
40.8125	-106.56	41.4375	-106.81		
40.8125	-106.69	41.4375	-106.94		

Table A3 Monthly streamflow (in acre foot): Modeled (Qm) vs. Observed (Qo)

Year	Month	Qm	Qo	Year	Month	Qm	Qo
1950	1	6382.79	16890.64	1954	9	59032.77	7747.44
1950	2	4740.48	19010.38	1954	10	48169.81	18962.78
1950	3	9006.21	26052.30	1954	11	16793.69	17244.30
1950	4	166149.60	91636.36	1954	12	1857.85	17357.95
1950	5	200350.74	172903.14	1955	1	384.31	13847.01
1950	6	272577.58	320786.78	1955	2	366.22	11801.65
1950	7	103033.99	87435.37	1955	3	5090.13	15949.88
1950	8	8986.37	22332.30	1955	4	69031.89	61527.27
1950	9	93871.98	22575.87	1955	5	120561.78	93522.64
1950	10	18346.37	23242.31	1955	6	131163.86	112462.81
1950	11	23076.35	25205.95	1955	7	47930.47	18956.63
1950	12	5645.43	25640.33	1955	8	59802.14	25455.87
1951	1	1097.83	19460.83	1955	9	10012.51	7289.26
1951	2	4222.93	18543.87	1955	10	15662.83	10803.37
1951	3	5634.23	25007.01	1955	11	7101.72	16792.07
1951	4	89149.55	66763.64	1955	12	19188.91	16601.65
1951	5	296700.36	194608.26	1956	1	3763.02	17536.26
1951	6	172512.59	275444.63	1956	2	286.75	14900.63
1951	7	234311.64	96781.49	1956	3	31094.10	31616.93
1951	8	71603.51	41743.93	1956	4	81680.09	92885.95
1951	9	11677.64	17268.10	1956	5	346388.10	226151.41
1951	10	106874.42	32483.90	1956	6	291418.88	209157.02
1951	11	7755.51	25443.97	1956	7	107484.71	35730.45
1951	12	1384.03	23303.80	1956	8	32283.77	23691.17
1952	1	492.27	22701.22	1956	9	1193.45	6961.98
1952	2	468.30	20854.21	1956	10	15640.31	9641.26
1952	3	1821.33	26556.50	1956	11	5316.13	14489.26
1952	4	148239.92	181190.08	1956	12	4395.16	16441.79
1952	5	300031.84	369110.08	1957	1	46.01	14898.45
1952	6	484111.80	419861.16	1957	2	3898.95	17832.99
1952	7	208844.24	68558.68	1957	3	17175.79	27460.36
1952	8	49973.48	38884.76	1957	4	65141.39	66882.64
1952	9	4072.41	19178.18	1957	5	351673.12	224983.14
1952	10	750.51	13496.53	1957	6	402786.87	518221.49
1952	11	1776.91	14263.14	1957	7	415382.39	308852.23
1952	12	546.79	13871.60	1957	8	56767.84	65914.71
1953	1	4968.28	21643.64	1957	9	13500.36	27520.66
1953	2	1224.76	19576.86	1957	10	67277.36	31653.82
1953	3	27982.69	28069.09	1957	11	9484.16	28121.65
1953	4	102768.07	47234.38	1957	12	1635.13	24416.73
1953	5	162410.72	76552.07	1958	1	148.76	19460.83
1953	6	247208.04	237064.46	1958	2	7330.29	22492.56
1953	7	72018.03	41713.19	1958	3	7767.95	34205.55
1953	8	46521.04	34285.49	1958	4	63322.24	66168.60
1953	9	5809.49	9984.79	1958	5	277904.24	280014.55
1953	10	11260.16	11147.70	1958	6	146468.22	238016.53
1953	11	28141.90	18862.81	1958	7	28048.86	33418.51
1953	12	798.11	15156.69	1958	8	26530.38	16054.41
1954	1	2684.28	16085.16	1958	9	27932.33	9966.94
1954	2	7183.89	17155.44	1958	10	1246.40	13668.69
1954	3	7381.12	23795.70	1958	11	10910.49	17160.99
1954	4	141511.44	63431.40	1958	12	3387.12	21619.04
1954	5	176690.56	88849.59	1959	1	1738.43	17819.11
1954	6	70115.25	49394.38	1959	2	449.12	15661.49
1954	7	32493.51	16841.45	1959	3	6240.30	19534.61
1954	8	26749.48	9819.57	1959	4	101354.60	56885.95

Year	Month	Qm	Qo	Year	Month	Qm	Qo
1970	1	3574.19	21231.67	1974	9	26580.74	14816.53
1970	2	2636.54	22375.93	1974	10	50003.15	22879.54
1970	3	3675.16	26931.57	1974	11	4241.13	25438.02
1970	4	56486.95	64919.01	1974	12	728.41	21151.74
1970	5	333491.19	264519.67	1968	9	23751.67	21486.94
1970	6	276277.43	408555.37	1968	10	39235.22	27780.10
1970	7	112128.05	138162.64	1968	11	7394.00	26830.41
1970	8	44794.29	38872.46	1968	12	2304.54	25050.05
1970	9	62820.93	30418.51	1969	1	8235.59	27251.31
1970	10	65070.51	36886.41	1969	2	949.42	20371.04
1970	11	27364.99	33530.58	1969	3	10891.87	23150.08
1970	12	1119.52	25480.46	1969	4	173676.09	117699.17
1971	1	8467.12	22510.61	1969	5	272257.98	205491.57
1971	2	2854.85	25985.85	1969	6	206301.04	213441.32
1971	3	26215.64	52731.77	1969	7	66386.25	76244.63
1971	4	106081.10	146558.68	1969	8	15607.71	23051.70
1971	5	223644.55	231377.85	1969	9	23229.93	12894.55
1971	6	267066.60	461633.06	1969	10	55071.97	30682.31
1971	7	121544.13	140007.27	1969	11	17313.35	31186.12
1971	8	13879.80	37353.72	1969	12	3849.28	22246.21
1971	9	33241.14	28770.25	1975	1	1676.65	17720.73
1971	10	19145.72	29052.89	1975	2	1068.31	16938.84
1971	11	12803.64	28716.69	1975	3	20737.59	22744.26
1971	12	10365.89	30344.13	1975	4	93902.86	62657.85
1972	1	1330.67	21102.55	1975	5	217306.61	166938.84
1972	2	6713.87	23170.12	1975	6	181739.40	295795.04
1972	3	62422.52	50764.17	1975	7	184466.81	203708.43
1972	4	86618.69	51542.48	1975	8	24592.91	41879.21
1972	5	170027.99	120515.70	1975	9	15622.41	18023.80
1972	6	174290.49	269137.19	1975	10	37335.28	21409.98
1972	7	21683.06	37716.50	1975	11	14927.48	24224.13
1972	8	21819.45	15476.43	1975	12	7204.77	15125.95
1972	9	38035.12	16774.21	1976	1	1024.45	18415.54
1972	10	106879.24	29538.64	1976	2	10654.56	20704.26
1972	11	3997.71	30436.36	1976	3	8399.80	24096.99
1972	12	3260.62	22990.21	1976	4	78542.69	68310.74
1973	1	4170.88	21760.46	1976	5	238946.00	154887.27
1973	2	222.72	19637.95	1976	6	168028.50	195709.09
1973	3	1794.85	31038.94	1976	7	73055.33	76060.17
1973	4	95753.63	98360.33	1976	8	26189.67	33523.04
1973	5	394833.67	354168.60	1976	9	26408.14	15804.30
1973	6	321867.47	325011.57	1976	10	7996.88	17800.66
1973	7	210720.41	137055.87	1976	11	1511.80	19017.52
1973	8	19284.14	47333.16	1976	12	651.13	16945.98
1973	9	55004.37	22397.36	1977	1	694.62	11848.66
1973	10	11107.30	23955.57	1977	2	3674.26	12884.63
1973	11	60481.02	31989.42	1977	3	9684.27	18606.15
1973	12	6769.47	20844.30	1977	4	143362.52	42979.83
1974	1	10756.11	21164.03	1977	5	289165.65	91309.09
1974	2	886.05	20826.45	1977	6	57148.61	79914.05
1974	3	55056.63	51852.50	1977	7	52940.39	16718.48
1974	4	103645.59	112879.34	1977	8	63211.58	14634.05
1974	5	254041.71	330311.41	1977	9	20517.57	10948.76
1974	6	297062.55	352026.45	1977	10	36196.12	14197.49
1974	7	133881.57	76675.04	1977	11	5061.90	16000.66
1974	8	10481.39	28228.96	1977	12	3030.63	20309.36

Year	Month	Qm	Qo	Year	Month	Qm	Qo
1978	1	297.76	21379.24	1982	9	85671.24	33262.81
1978	2	1749.77	18210.64	1982	10	29379.78	43010.58
1978	3	70333.11	27380.43	1982	11	4770.51	35268.10
1978	4	87326.62	65811.57	1982	12	916.18	30682.31
1978	5	310752.50	176039.01	1983	1	1225.16	22621.29
1978	6	268217.79	409566.94	1983	2	2689.31	20432.13
1978	7	136707.41	170259.17	1983	3	17729.83	29999.80
1978	8	23669.86	36308.43	1983	4	103077.39	62895.87
1978	9	22460.24	16708.76	1983	5	203786.12	195838.02
1978	10	19803.90	17603.90	1983	6	355711.03	594981.82
1978	11	4916.20	22129.59	1983	7	267099.41	323178.84
1978	12	362.33	19774.41	1983	8	52502.53	91247.60
1979	1	5.20	18126.55	1983	9	21981.64	30489.92
1979	2	5041.08	18210.64	1983	10	51512.53	39087.67
1979	3	8556.77	29046.74	1983	11	28681.95	37005.62
1979	4	156874.22	90981.82	1983	12	61.46	28770.05
1979	5	274862.82	243552.40	1984	1	634.47	26820.89
1979	6	256117.76	334770.25	1984	2	402.15	22831.34
1979	7	142761.02	123159.67	1984	3	1037.27	38946.25
1979	8	58423.24	44363.31	1984	4	47912.86	75510.74
1979	9	5089.61	17006.28	1984	5	512368.51	526825.79
1979	10	42329.20	18304.86	1984	6	266785.83	463715.70
1979	11	1513.47	21064.46	1984	7	272392.80	186737.85
1979	12	8226.56	21409.98	1984	8	70089.39	81286.61
1980	1	4550.84	27577.19	1984	9	57175.39	46395.37
1980	2	9598.70	18032.93	1984	10	22292.91	47745.12
1980	3	3188.79	33191.01	1984	11	6680.47	41135.21
1980	4	149281.02	111510.74	1984	12	703.89	28468.76
1980	5	279251.66	345191.41	1985	1	0.65	27152.93
1980	6	315417.52	278300.83	1985	2	664.05	25941.42
1980	7	116622.74	84606.94	1985	3	10776.04	47634.45
1980	8	23440.43	20985.72	1985	4	120505.67	140608.26
1980	9	37851.47	15363.97	1985	5	164387.33	279338.18
1980	10	45595.55	20948.83	1985	6	147330.05	203682.64
1980	11	20451.40	20481.32	1985	7	81230.06	69112.07
1980	12	7798.65	22123.24	1985	8	8277.88	30934.41
1981	1	1124.28	19749.82	1985	9	31948.11	18654.55
1981	2	4980.46	15944.73	1985	10	71041.51	39868.56
1981	3	14420.44	21151.74	1985	11	3061.69	33679.34
1981	4	98799.22	30251.90	1985	12	31.75	28185.92
1981	5	257426.21	74522.98	1986	1	4172.00	27054.55
1981	6	75195.48	109844.63	1986	2	18679.17	31078.61
1981	7	55953.00	35865.72	1986	3	77175.13	73170.25
1981	8	24952.22	16220.43	1986	4	91523.41	160066.12
1981	9	25532.63	11496.20	1986	5	222561.40	285363.97
1981	10	68327.04	22504.46	1986	6	441095.19	456991.74
1981	11	15068.75	21659.50	1986	7	111902.29	151382.48
1981	12	7368.99	24785.65	1986	8	30194.13	44769.12
1982	1	1035.28	23555.90	1986	9	33461.90	32703.47
1982	2	8678.02	17383.14	1986	10	63104.68	46915.04
1982	3	10048.61	31364.83	1986	11	7446.20	44282.98
1982	4	54225.36	55541.16	1986	12	611.83	27669.42
1982	5	167542.28	183724.96	1987	1	1308.57	19005.82
1982	6	195393.01	333401.65	1987	2	3545.54	25669.29
1982	7	181332.71	214714.71	1987	3	8547.14	37870.21
1982	8	36080.64	64131.57	1987	4	123592.74	83781.82

Year	Month	Qm	Qo	Year	Month	Qm	Qo
1987	5	150968.01	118425.12	1992	1	1418.07	15224.33
1987	6	73886.46	52042.31	1992	2	3398.20	19615.74
1987	7	38242.81	24066.25	1992	3	32410.30	33178.71
1987	8	26570.10	17942.08	1992	4	202435.21	49001.65
1987	9	12483.18	10675.04	1992	5	307196.16	79626.45
1987	10	45785.61	14867.70	1992	6	76368.72	78307.44
1987	11	21243.84	19975.54	1992	7	73217.88	41221.29
1987	12	3385.00	22153.98	1992	8	24679.56	17616.20
1988	1	732.29	17763.77	1992	9	25095.84	11222.48
1988	2	1258.09	20526.55	1992	10	32826.67	15261.22
1988	3	17347.91	33504.60	1992	11	3776.04	21344.13
1988	4	117458.85	127636.36	1992	12	1355.14	17419.44
1988	5	254546.00	201863.80	1993	1	214.90	19645.29
1988	6	186629.76	216773.55	1993	2	757.09	17266.51
1988	7	26034.81	44633.85	1993	3	33312.27	33762.84
1988	8	6600.68	15070.61	1993	4	97498.15	65752.07
1988	9	40389.94	10496.53	1993	5	364039.74	257264.13
1988	10	4104.25	14898.45	1993	6	320050.17	327332.23
1988	11	14330.25	19422.15	1993	7	116470.55	109140.50
1988	12	276.85	21213.22	1993	8	32039.45	38294.48
1989	1	444.87	18347.90	1993	9	54436.31	26973.22
1989	2	6152.03	17222.08	1993	10	59680.99	35220.10
1989	3	83127.41	58825.19	1993	11	5780.22	31192.07
1989	4	164865.32	70809.92	1993	12	764.18	25935.47
1989	5	138983.43	72985.79	1994	1	1587.10	23076.30
1989	6	66379.07	78009.92	1994	2	2341.98	24347.50
1989	7	39163.84	24582.74	1994	3	51665.46	49325.36
1989	8	27573.44	20463.07	1994	4	174283.40	85388.43
1989	9	57487.75	12192.40	1994	5	226149.09	178068.10
1989	10	13735.76	16570.91	1994	6	81862.99	83424.79
1989	11	8971.74	18410.58	1994	7	10246.94	19110.35
1989	12	789.91	16245.02	1994	8	13285.25	11473.59
1990	1	2724.94	15999.07	1994	9	10397.54	7324.96
1990	2	5034.24	17760.79	1994	10	32595.07	16368.00
1990	3	29121.21	36333.02	1994	11	12484.72	18481.98
1990	4	112212.67	66823.14	1994	12	2315.91	18925.88
1990	5	172270.51	70649.26	1995	1	1618.89	20131.04
1990	6	198331.41	172978.51	1995	2	12059.68	19976.73
1990	7	60476.67	62532.89	1995	3	43586.82	34377.72
1990	8	17508.79	23402.18	1995	4	81988.88	29299.83
1990	9	35524.26	13638.35	1995	5	352386.41	116826.45
1990	10	71946.54	20752.07	1995	6	383094.66	478234.71
1990	11	30294.70	24420.50	1995	7	207217.13	267840.00
1990	12	1111.99	19387.04	1995	8	30023.07	46583.01
1991	1	76.49	14154.45	1995	9	61370.80	24533.55
1991	2	4828.92	15711.47	1995	10	63898.34	35392.26
1991	3	11786.96	27515.70	1995	11	39954.57	43194.05
1991	4	59692.38	47888.93	1995	12	4156.42	33584.53
1991	5	326082.17	126111.07	1996	1	3577.95	30479.40
1991	6	184086.01	196839.67	1996	2	7933.20	36304.66
1991	7	57359.91	41639.40	1996	3	19005.95	47093.36
1991	8	25677.42	24306.05	1996	4	132080.47	142512.40
1991	9	18039.55	13894.21	1996	5	310523.91	306023.80
1991	10	8732.37	14664.79	1996	6	233193.62	309064.46
1991	11	10786.98	18095.21	1996	7	91456.82	83254.21
1991	12	553.90	15906.84	1996	8	9410.91	29895.27

Year	Month	Qm	Qo
1996	9	28339.50	17583.47
1996	10	10132.47	25726.41
1996	11	39224.65	36243.97
1996	12	4275.53	27989.16
1997	1	18754.81	30270.35
1997	2	2255.63	25724.83
1997	3	39370.95	72432.40
1997	4	113720.39	93897.52
1997	5	298774.18	311188.76
1997	6	422340.05	455980.17
1997	7	156885.39	91493.55
1997	8	86533.58	56703.87
1997	9	189730.42	71285.95
1997	10	28226.29	56648.53
1997	11	4290.57	42015.87
1997	12	334.53	34549.88
1998	1	1304.97	31653.82
1998	2	1493.98	29912.33
1998	3	41153.16	71571.57
1998	4	67608.59	74677.69
1998	5	209375.04	175239.67
1998	6	176170.08	229269.42
1998	7	89479.15	112399.34
1998	8	28875.58	50758.02
1998	9	23568.32	23182.81
1998	10	91234.52	36597.42
1998	11	26172.10	41510.08
1998	12	3183.70	29477.16
1999	1	1196.64	25566.55
1999	2	3393.94	25069.49
1999	3	48475.38	49952.53
1999	4	89568.72	71404.96
1999	5	206931.55	212378.18
1999	6	253396.07	344231.40
1999	7	100116.38	103299.17
1999	8	28270.22	41774.68
1999	9	35780.75	26187.77
1999	10	10259.34	26015.40
1999	11	11247.22	24509.75
1999	12	1334.55	25265.26
2000	1	4570.83	21342.35
2000	2	8535.25	24341.95
2000	3	17904.16	36419.11
2000	4	192495.93	81818.18
2000	5	327509.66	185385.12
2000	6	82827.41	113771.90
2000	7	14040.52	23961.72

Table A4 Modeled streamflow for an increased precipitation in the Wyoming area of the North Platte Watershed

Year	Streamflow for Wyoming area of watershed (ac ft)			
	Initial	Precipitation increase (%)		
		1%	3%	5%
1956	234844.60	235879.64	237780.78	239909.43
1957	363192.22	364641.72	367178.23	369850.50
1958	225361.65	226060.76	227329.33	228598.99
1959	224006.28	224902.57	226511.89	228152.51
1960	178005.00	178590.32	179614.88	180607.60
1961	309787.14	310514.78	311839.83	313245.52
1962	264103.48	265339.88	267567.23	269797.68
1963	217673.99	218332.22	219486.23	220637.76
1964	230399.74	231217.06	232708.84	234192.68
1965	402878.17	403849.48	405669.93	407428.50
1966	170559.08	171074.41	171967.83	172903.11
1967	340313.24	341187.95	342777.53	344364.00
1968	335825.45	337252.91	339893.17	342607.68
1969	285553.94	286394.02	287977.77	289538.41
1970	414247.32	416134.24	419791.39	423037.31
1971	298597.94	299462.96	301048.10	302701.31
1972	225943.46	226737.36	228086.72	229438.54
1973	495373.77	497196.03	500790.31	504311.70
1974	311313.89	312625.74	315011.08	317578.31
1975	272258.89	273509.89	275788.65	278122.89
1976	253763.23	254563.70	256033.63	257485.57
1977	283867.67	284560.14	285824.64	287061.93
1978	290852.60	291930.38	293923.65	295958.17
1979	279717.41	281108.67	283730.47	286428.06
1980	299812.03	301076.32	303358.40	305689.61
1981	265986.61	266435.30	267214.41	267931.37
1982	271075.60	271842.61	273041.33	274299.54
1983	319658.21	320688.64	322466.54	324369.85
1984	397648.34	399186.11	401927.29	404808.65
1985	150280.67	150905.06	151987.70	153063.81
1986	319324.25	320282.75	322248.47	324086.34
1987	181986.45	182438.92	183223.36	184012.67
1988	216741.74	217649.48	219386.94	221133.42
1989	207753.25	208583.90	210158.36	211779.45
1990	209267.78	210058.58	211490.97	212906.96
1991	276033.62	276528.34	277582.69	278682.00
1992	298014.90	298872.66	300342.77	301846.94
1993	378376.58	379706.46	382199.19	384637.58
1994	267936.51	269118.87	271253.34	273369.35
1995	445330.42	446151.52	447685.41	449203.08
1996	271482.98	272342.67	273874.62	275374.96
1997	382756.18	384002.91	386245.00	388533.58
1998	265553.00	266255.31	267573.22	268856.04
1999	333808.02	334656.04	336277.99	337954.61

Table A5 Modeled streamflow for an increase of precipitation (5%) for different regions and landcover of the North Platte Watershed

Year	Streamflow for entire North Platte Watershed (ac ft)												
	Initial	Regions						Landcover (approx. 30% coverage in each grid)					
		CE	CW	NE	NW	SE	SW	WL	WGL	EF	OS	CL	GL
1981	632230	641326	636705	636636	638095	639124	641547	637360	633897	640877	633184	633022	634422
1982	830772	841453	842322	834904	836141	840918	847005	844173	834339	857005	831556	832939	834058
1983	1060869	1073966	1077985	1064665	1066121	1074478	1076961	1080379	1066597	1095128	1061964	1063203	1066259
1984	1309055	1326744	1343059	1312979	1317042	1325628	1330676	1336454	1316848	1354979	1310426	1312467	1318329
1985	594797	601914	603592	596117	596880	604158	606206	605459	597210	612433	595183	595826	597223
1986	1104900	1119599	1123212	1108696	1110892	1120296	1121067	1126597	1110550	1144045	1106116	1107499	1110511
1987	510307	518026	514824	512518	514170	516977	518437	515844	512033	519289	510793	510997	512294
1988	721413	732334	734082	724212	725605	732262	734185	737371	725408	750725	722560	723638	726541
1989	602889	613295	609886	605861	606962	612008	612956	614168	606450	621026	604297	604808	608373
1990	656702	667023	665969	659690	660105	666800	667669	669698	660149	679331	657971	658639	661179
1991	790983	801424	797558	795676	796244	801928	803996	801158	793283	808202	791745	792229	793339
1992	766293	778764	778027	770170	771733	775526	777105	775968	769237	783353	767493	767394	770664
1993	1056776	1073435	1090269	1060832	1063144	1067885	1070974	1078918	1062547	1095483	1058646	1059218	1064332
1994	638045	651289	657705	640562	641462	644212	646451	651188	641584	659526	638965	639479	643267
1995	1220742	1236103	1237466	1227204	1228712	1233585	1235660	1233722	1224130	1246399	1221599	1222027	1223916
1996	943532	954722	954684	947389	949047	954351	960624	962146	948914	980421	945473	946287	949050
1997	1381998	1399160	1409425	1386846	1388844	1399368	1407680	1407251	1388689	1429515	1383404	1385113	1388668
1998	671880	682798	678264	675886	677476	679802	682386	682866	674601	687679	673433	673243	675651
1999	887720	902683	905441	892098	893701	898801	900537	902412	891387	913667	888719	889425	891798

(CE: centraleast, CW: centralwest, NE: northeast, NW: northwest, SE: southeast, SW: southwest; WL: woodland, WGL: wooded grassland, EF: evergreen needleleaf forest, OS: open shrublands, CL: croplands, GL: grasslands)

Table A6 Text file (.txt) format to import in ARCGIS to show the spatial distribution of precipitation for each grid (1/8 degree) in North Platte watershed (14 * 14 grids; xll: longitude lower left corner; yll: latitude lower left corner; grid size=0.125; If no value in any grid = -9999.0000)

ncols	14
nrows	14
xllcorner	-107.500000
yllcorner	40.250000
cellsize	0.125000
NODATA_value	-9999.000000

-9999.000000	-9999.000000	-9999.000000	262.399000	265.666000	-9999.000000	-9999.000000	-9999.000000	-9999.000000	-9999.0000
-9999.000000	-9999.000000	-9999.000000	-9999.000000						
-9999.000000	285.75800000	252.85300000	274.443038	233.684135	297.308596	332.049019	336.256154	354.12115096	-9999.0000
-9999.000000	-9999.000000	-9999.000000	-9999.000000						
360.22000000	357.40300000	331.49600000	290.388154	274.945346	288.285692	368.509712	622.639865	-9999.000000	-9999.0000
-9999.000000	-9999.000000	-9999.000000	-9999.000000						
484.83300000	408.85600000	303.938558	315.298269	281.911635	286.637885	381.598462	576.772558	594.268500	-9999.0000
-9999.000000	-9999.000000	-9999.000000	-9999.000000						
-9999.000000	548.0580000	472.890000	411.819500	316.387096	287.641692	380.982885	714.261615	961.620077	-9999.0000
-9999.000000	-9999.000000	-9999.000000	-9999.000000						
-9999.0000	-9999.000000	691.57800000	749.29000000	439.668346	326.574423	347.696827	594.243115	892.132038	943.259538
-9999.000000	-9999.000000	-9999.000000	-9999.000000						
-9999.000000	-9999.000000	-9999.000000	1148.9620000	888.04500000	509.5212885	444.729423	434.212673	606.184942	763.569096
620.717635	-9999.000000	-9999.000000	-9999.000000						
-9999.000000	-9999.000000	-9999.000000	-9999.000000	1080.6110000	975.8970000	1005.3248846	593.637923	499.551115	587.893808
626.233462	-9999.000000	-9999.000000	-9999.000000						
-9999.000000	-9999.000000	-9999.000000	-9999.000000	-9999.000000	1290.6490000	1292.7850000	673.857019	564.233154	419.601519
752.535250	-9999.000000	-9999.000000	-9999.000000						
-9999.000000	-9999.000000	-9999.000000	-9999.000000	-9999.000000	-9999.000000	1395.3450000	588.763000	381.049731	330.932192
412.734212	915.147269	-9999.000000	-9999.000000						
-9999.000000	-9999.000000	-9999.000000	-9999.000000	-9999.000000	-9999.000000	1395.5360000	526.67300000	402.347615	358.431904
380.276923	558.692596	1145.021000	-9999.000000						
-9999.000000	-9999.000000	-9999.000000	-9999.000000	-9999.000000	-9999.000000	1214.445000	525.545000	422.487096	408.454596
466.187000	632.941231	1110.215000	1093.411000						
-9999.000000	-9999.000000	-9999.000000	-9999.000000	-9999.000000	-9999.000000	1171.436000	640.042000	633.841019	829.954846
567.606288	703.743808	1026.379615	1039.774000						
-9999.000000	-9999.000000	-9999.000000	-9999.000000	-9999.000000	-9999.000000	-9999.000000	-9999.000000	629.6840000	803.1320000
702.095981	694.546250	783.862423	-9999.000000						

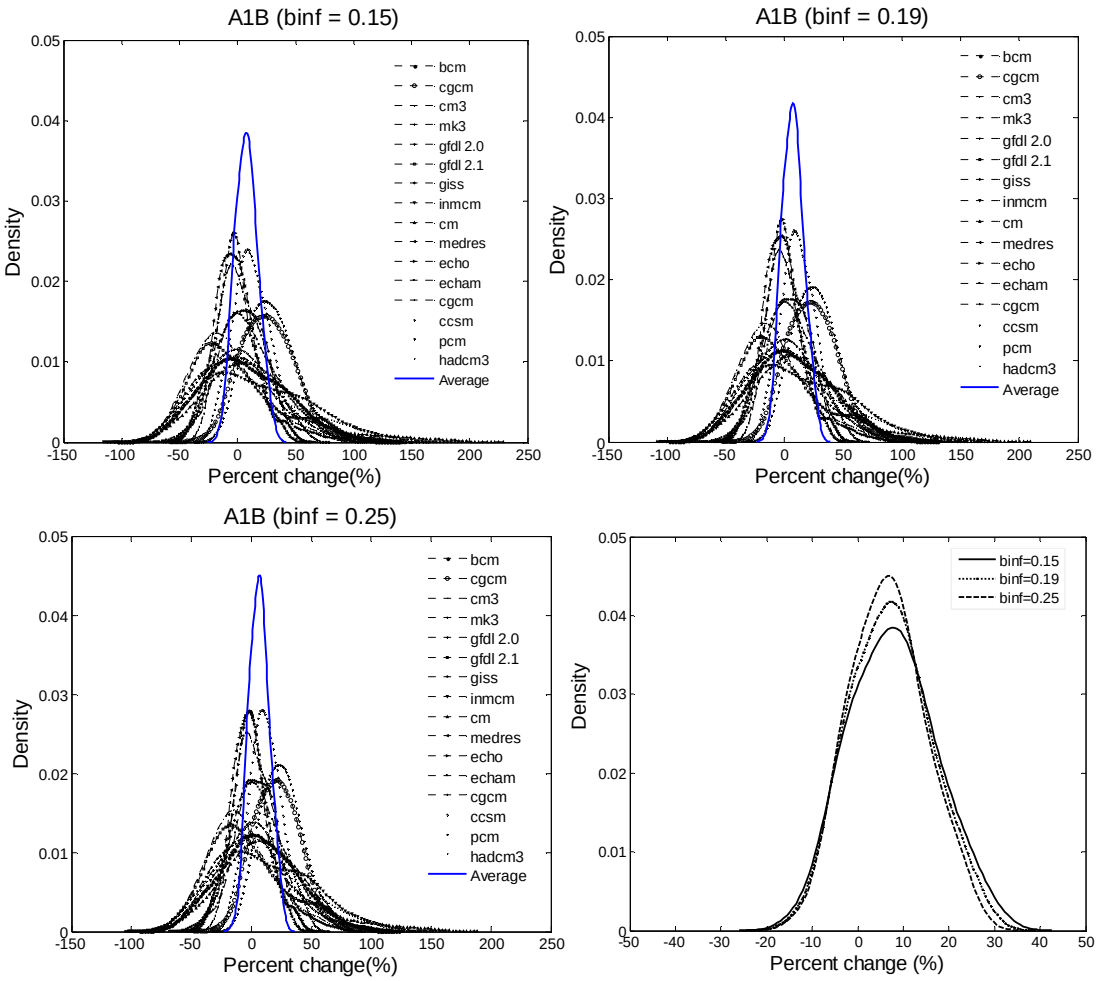

Figure A2 Probability density function plot of change in streamflow for ensemble multi-models under changing VIC calibrated parameter 'b_{inf}.' for future climate.

APPENDIX B

DOWNSCALING EXAMPLE

(TASK 3)

B.2.1 Temporal Downscaling

The BCTD technique adopted by Wood et al (2004) is extended to downscale the precipitation data from monthly to daily; and daily to hourly or actual storm event. The downscaling is performed with respect to the actual storm event. It follows four major steps which are as follows:

- Find the scaling factor (f = O1/M1) between observed (O1) and modeled (M1) monthly data for a particular storm.
- Apply this factor to future modeled data (M2) to obtain future observed data (O2= f *M2).
- Find the difference in between the future and present observed data (d = O2-O1).
- Transform present storm data to future conditions by distributing the difference in a weighted proportional method. In this case, the difference is distributed only among the wet days in a month, and only the number of hours the storm actually occurred for that particular day. ((d / O1) * observed data for the storm)

An example is presented here for better understanding of the method applied in this research.

Station Id: 4359
Station Data: July 1999

Table B1 Calculation of daily rainfall for July for future periods with respect to the actual storm event (July 8 1999)

Days	Daily rainfall (in)	Daily rainfall (d1, mm)	Total rainfall (O1, mm)	Daily rainfall from GCM, for July 1999 (m1, mm/day)	Total rainfall for July (mm) (M1= m1* 31)	Scale factor f = O1/M1	Daily rainfall from GCM, for July 2030's (d2, mm/day)	Total rainfall for July 2030's (M2= d2 * 31)
1	0.00	0.00						
2	0.00	0.00						
3	0.00	0.00						
4	0.00	0.00						
5	0.00	0.00	35.56	0.51	15.85	2.24	0.62	19.25
6	0.00	0.00						
7	0.00	0.00						
8	1.08	27.43						
9	0.16	4.06						
10	0.00	0.00						
11	0.00	0.00						
12	0.00	0.00						
13	0.00	0.00						
14	0.16	4.06						
15	0.00	0.00						

27	0.00	0.00						
28	0.00	0.00						
29	0.00	0.00						
30	0.00	0.00						
31	0.00	0.00						

Table B1 Calculation of daily rainfall for July for future periods with respect to the actual storm event (continue from previous page).

Total rainfall for July 2030's (M2= d2 * 31)	Adjusted total rainfall for July 2030's (O2= f * M2)	Difference (d3=O2-O1)	Adjusted daily rainfall for July 2030's d1+((d1/O1)*d3)	Future total rainfall for July 8 1999 (mm)
			0.00	
			0.00	
			0.00	
			0.00	**33.33**
19.25	43.20	7.64	0.00	
			0.00	
			0.00	
			33.33	
			4.94	
			0.00	
			0.00	
			0.00	
			0.00	
			4.94	
			0.00	

			0.00	
			0.00	
			0.00	
			0.00	
			0.00	
			0.00	
			0.00	
			0.00	

Table B2 Calculation of rainfall for actual storm event for future periods, based on the actual storm event on July 8 1999

Date Time	Rainfall (in)	Rainfall R1 (mm)	Observed total rainfall for July 8 1999 (Tp, mm)	Modeled total rainfall for July 8 1999 (T2030, mm)	Difference(mm) (D = T2030-Tp)	Adjusted Future Rainfall (mm) d = R1+((D/Tp)*R1)	Adjusted Future Rainfall (in) (d/25.4)
7/8/1999 11:00	0.000	0.000				0.000	0.000
7/8/1999 11:48	0.040	1.016				1.234	0.049
7/8/1999 11:49	0.080	2.032				2.469	0.097
7/8/1999 11:50	0.040	1.016	27.432	**33.328**	5.896	1.234	0.049
7/8/1999 11:50	0.040	1.016				1.234	0.049
7/8/1999 11:50	0.040	1.016				1.234	0.049
7/8/1999 11:51	0.040	1.016				1.234	0.049
7/8/1999 11:51	0.040	1.016				1.234	0.049
7/8/1999 11:52	0.040	1.016				1.234	0.049
7/8/1999 11:52	0.040	1.016				1.234	0.049
7/8/1999 11:52	0.040	1.016				1.234	0.049
7/8/1999 11:53	0.040	1.016				1.234	0.049
7/8/1999 11:54	0.040	1.016				1.234	0.049
7/8/1999 11:55	0.040	1.016				1.234	0.049
7/8/1999 11:56	0.040	1.016				1.234	0.049
7/8/1999 11:58	0.040	1.016				1.234	0.049
7/8/1999 12:01	0.080	2.032				2.469	0.097
7/8/1999 12:11	0.160	4.064				4.937	0.194
7/8/1999 12:14	0.040	1.016				1.234	0.049
7/8/1999 12:20	0.080	2.032				2.469	0.097
7/8/1999 14:20	0.080	2.032				2.469	0.097

APPENDIX C

PROGRAMMING CODES

(TASK 1, 2, 3)

```
**************************************************************************
function flux2flow(pth, outfile, infilescsv)
if nargin < 2; error('flux2flow(pth, outfile, infilescsv)');
end
% This program converts flux to flow.
gridsize=0.125;
pth='C:\cygwin\home\vicfiles\results';
if exist('infilescsv') ~= 1
        files=dir([pth 'fluxes*']);
        wt=ones(size(files));
        else
        csvd=csvread(infilescsv);
        for k=1:size(csvd, 1)
        files(k,1).name = sprintf('fluxes_%.4f_%.4f', csvd(k,1), csvd(k,2));
        end
        wt=csvd(:,3);
end
data=readASCIItable([pth files(1).name]);
fname=regexprep(files(1).name, '_', ' ');
[dum fname]=strtok(fname); [lat lon]=strtok(fname);
A=latlonGridArea(str2num(lat), str2num(lon), gridsize);
runoff=data(:,6)*A*wt(1);
for k=2:length(files)
        disp(files(k).name);
        data=readASCIItable([pth files(k).name]);
        fname=regexprep(files(k).name, '_', ' ');
        [dum fname]=strtok(fname); [lat lon]=strtok(fname);
        A=latlonGridArea(str2num(lat), str2num(lon), gridsize);
        runoff=runoff+data(:,6)*A*wt(k);            % mm x km x km = 1000 m3
end
%1 cubic meter = 0.000810713194 acre foot
runoff=runoff*1000*0.000810713194; % Convert to Acre-foot
%runoff=runoff*1000*35.3146667; % Convert to Cubic-foot
disp(['Writing... ' pth outfile '_Daily.csv']);
dlmwrite([pth outfile '_Daily.csv'], [data(:,1:3) runoff],'delimiter',',','precision', '%.6f');
return;

**************************************************************************
function data=readASCIItable(filename, FORMAT, skipheaderlines)
% Program Details:
% Reads tabulated data in a text file
% If FORMAT of the data is not given %f floating point is assumed

if (nargin == 0); error('Usage: data=readASCIItable(filename, <FORMAT def:%f>);');
end
if (exist('FORMAT') ~= 1); FORMAT='%f'; end
```

```
if (exist('skipheaderlines') ~= 1); skipheaderlines=0; end
fid=fopen(filename, 'rt');
for k=1:skipheaderlines; line=fgets(fid); end
line=fgets(fid);
data=sscanf(line, FORMAT);
cols=length(data);
fseek(fid, 0, 'bof');
for k=1:skipheaderlines; line=fgets(fid); end
data=fscanf(fid, FORMAT);
fclose(fid);
data=transpose(reshape(data, cols, [ ]));

**********************************************************************
function editmaintxtfolder
%This program is useful to read all text files in a folder, the text files starts with data-_-.
ipath='C:\Documents and Settings\anil acharya\My Documents\change of forcing
data_wed mod\change of regions_SW\';
ifiles=dir([ipath 'data*'])
length(ifiles);
opath='C:\Documents and Settings\anil acharya\My Documents\dataset for change of
regions\change of regions_SW\';
for k=1:length(ifiles);
%for k=1
        disp([ipath ifiles(k).name]);
        data=edittxtfolder([ipath ifiles(k).name]);
        ofid=fopen([opath ifiles(k).name], 'wt');
        %for n=1
        fprintf(ofid, '%6.2f %6.2f %6.2f %6.2f\n', data');
        %end
        fclose(ofid);
end

**********************************************************************
function data=edittxtfolder(filename)
%This program can read data in a text file and converts the individual column.
%if (nargin == 0); error('Usage: data=edittxtfolder(filename),<FORMAT def:%f>);');
end
if (exist('FORMAT') ~= 1); FORMAT='%f'; end
if (exist('skipheaderlines') ~= 1); skipheaderlines=0; end
fid = fopen(filename, 'rt');
data = fscanf(fid, '%f %f %f %f', [4 inf]) ;   % It has 4 rows now.
data = transpose(data);
size(data)
fclose(fid);
data(:,1)=data(:,1)*1.1; %increase first column ppt. data by 10 percent.
data(:,2)=data(:,2)+0.0;
```

```
data(:,3)=data(:,3)+0.0;
return;

**************************************************************************
function flux2annualflow_wateryear(csvfile)
% This function converts daily data into yearly data.
if nargin < 1; error('flux2annualflow(csvfile)'); end
data=csvread(csvfile);
data2=[];
for yr=1950:2000
        selm=find(data(:,1) == yr-1 & data(:,2) == 10 & data(:,3) == 1);
        seln=find(data(:,1) == yr & data(:,2) == 9 & data(:,3) == 30);
        if isempty(seln) | isempty(selm); continue; end
        data2=[data2; yr 1 1 sum(data(selm:seln,4))];
end
ocsvfile=regexprep(csvfile, '_Daily.csv', '_Annual_WY.csv');
dlmwrite(ocsvfile, data2,'delimiter',',','precision', '%.6f');
return;

**************************************************************************
function kstest(filename)
%This function is developed for two sample Kolmogorov-Smirnov (K-S) goodness of
%fit test.
filename='C:\Documents and Settings\anil acharya\Desktop\B1.xls';
x1=xlsread(filename,'Monthly streamflow_1970-2100','E482:E1549');
x2=xlsread(filename,'Monthly streamflow_1970-2100','F482:F1549');

%The following code is to perform the KS test.
[h,p,ks2stat]= kstest2(x1,x2);
% [h,p,ks2stat]= kstest2(x1,x2,0.05,'unequal')  %This is the default
% [h,p,ks2stat]= kstest2(x1,x2) % represents same as above line.
% The null hypothesis is that the two data vectors are from the same continuous
distribution % while the alternative hypothesis is that they are from different continuous
distributions. the % result h is 1 if the test rejects the null hypothesis at the 5%
significance level; 0 otherwise. % The p value is less than 0.05 while rejecting the null
hypothesis.
end

**************************************************************************
function pcpgrid2avgpcpgrid(pth, outfile, infilescsv)
% This function calculates the average of precipitation, minimum and maximum
%temperature, and wind speed for a number of grid cells in a watershed.
if nargin < 2; error('pcpgrid2avgpcpgrid(pth, outfile, infilescsv)');
end
pth='C:\cygwin\home\vicfiles\results';
if exist('infilescsv') ~= 1
```

```
        files=dir([pth 'data*']);
        wt=ones(size(files));
        else
        csvd=csvread(infilescsv);
        for k=1:size(csvd, 1)
                files(k,1).name = sprintf('data_%.4f_%.4f', csvd(k,1), csvd(k,2));
        end
        wt=csvd(:,3);
end
data=readASCIItable([pth files(1).name]);
fname=regexprep(files(1).name, '_', ' ');
[dum fname]=strtok(fname); [lat lon]=strtok(fname);
precip=data(:,1);
maxtmp=data(:,2);
mintmp=data(:,3);
windspeed=data(:,4);
for k=2:length(files)
        disp(files(k).name);
        data=readASCIItable([pth files(k).name]);
        fname=regexprep(files(k).name, '_', ' ');
        [dum fname]=strtok(fname); [lat lon]=strtok(fname);
        precip=precip+data(:,1);
        maxtmp=maxtmp+data(:,2);
        mintmp=mintmp+data(:,3);
        windspeed=windspeed+data(:,4);
end
precip=precip/length(files);
maxtmp=maxtmp/length(files);
mintmp=mintmp/length(files);
windspeed=windspeed/length(files);
dlmwrite([pth outfile '_avgpptmpwindDaily.csv'], [precip maxtmp mintmp
windspeed],'delimiter',',','precision', '%.6f');

return;

**********************************************************************
function pdfplot
%This plots the probability density function for the data from 16 models using Kernels
density function.
filename='C:\Documents and Settings\anil acharya\Research\North Plate\Main
Files\results_GCM\all binf comparison.xlsx';

y1=xlsread(filename,'modelcomparison','BY3:BY91');
y2=xlsread(filename,'modelcomparison','BZ3:BZ91');
y3=xlsread(filename,'modelcomparison','CA3:CA91');
y4=xlsread(filename,'modelcomparison','CB3:CB91');
```

```
y5=xlsread(filename,'modelcomparison','CC3:CC91');
y6=xlsread(filename,'modelcomparison','CD3:CD91');
y7=xlsread(filename,'modelcomparison','CE3:CE91');
y8=xlsread(filename,'modelcomparison','CF3:CF91');
y9=xlsread(filename,'modelcomparison','CG3:CG91');
y10=xlsread(filename,'modelcomparison','CH3:CH91');
y11=xlsread(filename,'modelcomparison','CI3:CI91');
y12=xlsread(filename,'modelcomparison','CJ3:CJ91');
y13=xlsread(filename,'modelcomparison','CK3:CK91');
y14=xlsread(filename,'modelcomparison','CL3:CL91');
y15=xlsread(filename,'modelcomparison','CM3:CM91');
y16=xlsread(filename,'modelcomparison','CN3:CN91');
Avg=xlsread(filename,'modelcomparison','CO3:CO91');

[f1,x1] = ksdensity(y1);
        plot(x1,f1,'k.:','LineWidth',1,'MarkerSize',1.5);
hold on
[f2,x2] = ksdensity(y2);
        plot(x2,f2,'ko:','LineWidth',1,'MarkerSize',1.5);
hold on
[f3,x3] = ksdensity(y3);
        plot(x3,f3,'kx:','LineWidth',1,'MarkerSize',1.5);
hold on
[f4,x4] = ksdensity(y4);
        plot(x4,f4,'k+:','LineWidth',1,'MarkerSize',1.5);
hold on
[f5,x5] = ksdensity(y5);
        plot(x5,f5,'k*:','LineWidth',1,'MarkerSize',1.5);
hold on
[f6,x6] = ksdensity(y6);
        plot(x6,f6,'ks:','LineWidth',1,'MarkerSize',1.5);
hold on
[f7,x7] = ksdensity(y7);
        plot(x7,f7,'kd:','LineWidth',1,'MarkerSize',1.5);
hold on
[f8,x8] = ksdensity(y8);
        plot(x8,f8,'kv:','LineWidth',1,'MarkerSize',1.5);
hold on
[f9,x9] = ksdensity(y9);
        plot(x9,f9,'k^:','LineWidth',1,'MarkerSize',1.5);
hold on
[f10,x10] = ksdensity(y10);
        plot(x10,f10,'k<:','LineWidth',1,'MarkerSize',1.5);
hold on
[f11,x11] = ksdensity(y11);
        plot(x11,f11,'k>:','LineWidth',1,'MarkerSize',1.5);
```

```
hold on
[f12,x12] = ksdensity(y12);
        plot(x12,f12,'kp:','LineWidth',1,'MarkerSize',1.5);
hold on
[f13,x13] = ksdensity(y13);
        plot(x13,f13,'kh:','LineWidth',1,'MarkerSize',1.5);
hold on
[f14,x14] = ksdensity(y14);
        plot(x14,f14,'k+','LineWidth',1,'MarkerSize',1.5);
hold on
[f15,x15] = ksdensity(y15);
        plot(x15,f15,'k*','LineWidth',1,'MarkerSize',1.5);
hold on
[f16,x16] = ksdensity(y16);
        plot(x16,f16,'kx','LineWidth',1,'MarkerSize',1.5);
hold on
[f17,x17] = ksdensity(Avg);
        plot(x17,f17,'LineWidth',2,'MarkerSize',3);
hold on
        legend('bcm','cgcm','cm3','mk3','gfdl 2.0','gfdl
        2.1','giss','inmcm','cm','medres','echo','echam','cgcm','ccsm','pcm','hadcm3','Averag
        e')
hold off
title(['Density estimate for A1B'],'Fontsize',11,'color','k');
xlabel('Percent change(%)');
ylabel ('Density');
end

**********************************************************************
function snotel2csv;
%This function is used to process the snotel precipitation and temperature %data (.txt file
from National Resource Conservation Service, NRCS) and write it in a .csv format.
filename='C:\Documents and Settings\Anil\snotel\OldBattle_pcp.txt';
fid=fopen(filename, 'rt');
str=textscan(fid, '%s', 'delimiter', '\n', 'whitespace', '');
fclose(fid);
marks=[];
for k=1:size(str{1}, 1);
        if (strcmp(str{1}{k}, '----------') == 1); marks=[marks; k]; end;
end
marks=marks-35;

Data=[];
[M,D]=meshgrid([10:12 1:9], 1:31);
Y=M;
for k=1:length(marks)
```

```
        [d, um]=strtok(str{1}{marks(k)-7}); [yr, um]=strtok(um);
        yr=str2num(yr); if (yr < 50); yr=yr+2000; else; yr=yr+1900; end;
        Y(:,1:3)=yr-1;Y(:,4:end)=yr;
        data=strvcat(str{1}{marks(k):(marks(k)+30)});
        bars=strvcat(str{1}{marks(k)-1});
        for n=1:size(data,1)
                sel=(fix(bars) == 45 & fix(data(n,:)) == 32);
                data(n,sel)='-';
                data(n,:)=regexprep(data(n,:), '---', 'Nan');
                data(n,:)=regexprep(data(n,:), '-', ' ');
        end
        data=transpose(reshape(sscanf(transpose(data), '%f'), [], 31));
        data=data(:, 2:end);
        Data=[Data; [Y(:) M(:) D(:) data(:)]];
end
% If its a pcp or swq data then convert to mm
if (strcmp(filename((end-2):end), 'pcp') | strcmp(filename((end-2):end), 'swq'))
        Data(:,4)=Data(:,4)*25.4; % Convert inches to mm
end
ofile=regexprep(filename, '\.', '');
csvwrite([ofile '.csv'], Data(:,1:4));
return;

**************************************************************************
function metData_bin2asc
% The program converts binary forcing data into ascii format
ipath='E:\vic411files\forcing data\A1B_binary\sresa1b.mri_cgcm2_3_2a.5\';
ifiles=dir([ipath 'data*']);
opath='E:\vic411files\forcing data\A1B_ascii\sresa1b.mri_cgcm2_3_2a.5\';
for k=1:length(ifiles)
        disp([ipath ifiles(k).name])
        r=readmetBINARYdata([ipath ifiles(k).name], datenum(1950, 1, 1, 2099, 12,
        31));
        ofid=fopen([opath ifiles(k).name], 'wt');
        for n=1:length(r.year)
        fprintf(ofid, '%6.2f %6.2f %6.2f %6.2f\n', r.prcp(n), r.tmax(n), r.tmin(n),
        r.wind(n));
        end
        fclose (ofid);
end

**************************************************************************

function r = readmetBINARYdata(filename, startJD)
% This function loads the binary met data
if (nargin == 0); error('r=readmetBINARYdata(filename, startJD)'); end
```

```
disp('The variables are to be set manually');
fid=fopen(filename, 'r');
fseek(fid, 0, 'eof');
Nrec=ftell(fid)/8;
fseek(fid, 0, 'bof');
r.prcp = fread(fid, Nrec, '1*uint16', 6)/40.0;
fseek(fid, 2, 'bof');
r.tmax = fread(fid, Nrec, '1*int16', 6)/100.0;
fseek(fid, 4, 'bof');
r.tmin = fread(fid, Nrec, '1*int16', 6)/100.0;
fseek(fid, 6, 'bof');
r.wind = fread(fid, Nrec, '1*int16', 6)/100.0;
dvec=datevec(datenum(1949, 1, 1, 0, 0, 0):datenum(2000, 7, 31, 0, 0, 0));
dvec=datevec(startJD:startJD+length(r.prcp)-1);
r.year=date2fyear(dvec);
fclose(fid);
return;

*************************************************************************
function fyear=date2fyear(dvec)
% This function converts date to fyear
%         fyear=date2fyear([yr, mon, day, <hr, min, sec>])
if (nargin < 1); error('fyear=date2fyear([yr, mon, day, <hr, min, sec>])'); end;
if (size(dvec,2) > 3 & size(dvec,2) < 6); error('fyear=date2fyear([yr, mon, day, <hr, min,
sec>])'); end;
[fdoy, yr]=date2fdoy(dvec);
sel=frac(fdoy) == 0;
fdoy(sel)=fdoy(sel)+1/60/24/366;
fyear=yr+fdoy/366;

*************************************************************************
function [fdoy, yr]=date2fdoy(dvec)
% This function converts date to floating point day of year
% fdoy=date2fdoy([yr, mon, day, <hr>, <min>, <sec>])
if (nargin < 1); error('fdoy=date2fdoy([yr, mon, day, <hr, min, sec>])'); end;
if (size(dvec,2) > 3 & size(dvec,2) < 6); error('fdoy=date2fdoy([yr, mon, day, <hr, min,
sec>])'); end;
[idoy, yr]=date2idoy(dvec);
% Start of year is 0
% End of year is 364.99999 or 365.999999
idoy=idoy-1;
if (size(dvec, 2) == 3)
  error('Date vector doesn''t have time-of-day entries');
else
  fdoy=idoy+tod2fday(dvec(:,4:6));
end
```

```
**************************************************************************
function [idoy, yr]=date2idoy(dvec)
% This function converts date to integer day of year
%  idoy=date2idoy([yr, mon, day, <hr>, <min>, <sec>])
if (nargin < 1); error('idoy=date2idoy([yr, mon, day, <hr, min, sec>])'); end;
if (size(dvec,2) > 3 & size(dvec,2) < 6); error('idoy=date2idoy([yr, mon, day, <hr, min,
sec>])'); end;
yr=fix(dvec(:,1));
mn=fix(dvec(:,2));
dy=fix(dvec(:,3));
monthly_days=[0 cumsum([31 28 31 30 31 30 31 31 30 31 30 31])];
monthly_days_leap=[0 cumsum([31 29 31 30 31 30 31 31 30 31 30 31])];
idoy=dy*0;
for i=1:length(yr)
        if (isleap(yr(i)))
        idoy(i)=dy(i)+monthly_days_leap(mn(i));
        else
        idoy(i)=dy(i)+monthly_days(mn(i));
        end
end
return;

**************************************************************************
function x=isleap(yy)
% This function returns 1 if input is a leap year
%       x=isleap(yy)
if (nargin == 0); error('x=isleap(yy)'); end;
x=(~mod(yy, 4) & mod(yy, 100)) | ~mod(yy, 400);

**************************************************************************
function [month, day, year] = date2mdy(d)
% This function converts a Matlab date format to month, day, year
%  [month, day, year] = date2mdy(Date)
%  Date is the date format is in the matlab function DATE

if nargin == 0
    d = date;
end

i = 1;
while d(i) ~= '-'
        day(1,i) = d(i);
        i = i + 1;
end

day = str2num(day);
```

```
 i = i + 1;
while d(i) ~= '-'
        month = [month d(i)];
        i = i + 1;
 end

if month == 'Jan'
        month = 1;
        elseif month == 'Feb'
        month = 2;
        elseif month == 'Mar'
        month = 3;
        elseif month == 'Apr'
        month = 4;
        elseif month == 'May'
        month = 5;
        elseif month == 'Jun'
        month = 6;
        elseif month == 'Jul'
        month = 7;
        elseif month == 'Aug'
        month = 8;
        elseif month == 'Sep'
        month = 9;
        elseif month == 'Oct'
        month = 10;
        elseif month == 'Nov'
        month = 11;
        elseif month == 'Dec'
        month = 12;
        else
        error('Problem identifying the month')
 end

 i = i + 1;
 year = d(1,i:size(d,2));
 year = str2num(year);

**************************************************************************
function A=latlonGridArea(lat, lon, gridsize)
% A=latlonGridArea(lat, lon, gridsize)
% This function returns area in square kilometers
A=zeros(size(lat));
dln=[-gridsize -gridsize gridsize gridsize]/2;
dlt=[-gridsize gridsize gridsize -gridsize]/2;
```

```
for k=1:length(A(:))
        [x, y]=ll2km(lat(k), lon(k), lat(k)+dlt, lon(k)+dln);
        A(k)=polyarea(x, y); % Area in square kilometers
end
return;
lon=readASCIIimg([gfolder 'longitude.txt'], '%f');
lat=readASCIIimg([gfolder 'latitude.txt'], '%f');
A=latlonGridArea(lat, lon, 1/8);
%subplot(2,1,1);plot(lon+dln, lat+dlt, 'ro-', lon, lat, 'x');
%subplot(2,1,2);plot(x, y);

**************************************************************************
function [x,y]=ll2km(lat0, long0, lat, long)
% LL2KM Compute distance between two geographical locations
%       [x y]=ll2km(lat0, long0, lat, long)
%       x: Distance along longitude
%       y: Distance along latitude
if (nargin < 3); error('[x,y]=ll2km(lat0, long0, lat, long)'); end;
dtr=pi/180;
rtd=180/pi;
Ra=6378.1363;
Kflat=1/298.257;

RE=(1-Kflat*(sin(dtr*lat0))^2)*Ra;
R2=RE*cos(dtr*lat);
A=RE*sin(dtr*(lat-lat0));
B=R2.*(1-cos(dtr*(long-long0)))*sin(dtr*lat0);
C=R2.*sin(dtr*(long-long0));
x=C;
y=A+B;

**************************************************************************
% Calculates the 100-yr Precipitation value for each climate change
% projection scenario
clear all
clc
load mod_all
load obs_all
[mmon outs] = size(mod_all); %mmon - number of months in model data
omon = length(obs_all); %omon - number of months in observed data
myrs = mmon/12;
oyrs = omon/12;
%Reshape matrix to calculate the Annual Maximum (AM) series easier.
re_mod_all = reshape(mod_all,12,(mmon*outs)/12);
re_obs_all = reshape(obs_all,12,(omon)/12);
re_mam_all = max(re_mod_all);
```

```
re_oam_all = max(re_obs_all);

%Reshape max matrix so that years are on the rows and each column is a
%different model output.
mam_all = reshape(re_mam_all,myrs,outs);
oam_all = reshape(re_oam_all,oyrs,1);
%-----------------------------------------------------
%   LOG PEARSON TYPE III - CURRENT CONDITIONS ANALYSIS
% %-----------------------------------------------------
ystart = 1971;
yend = 2000;
years = 1950:1:2099;
curstart = find(years == ystart);
curend = find(years == yend);
f1s = 2011; f1start = find(years == f1s);
f1e = 2040; f1end = find(years == f1e);
f2s = 2041; f2start = find(years == f2s);
f2e = 2070; f2end = find(years == f2e);
f3s = 2071; f3start = find(years == f3s);
f3e = 2099; f3end = find(years == f3e);

%Step 1) Calc the log of all the values
log_mam = log10(mam_all);
log_oam = log10(oam_all);%--observed data

%Step 2) Calculate the column moments from model data to represent the
%'current' conditions analysis
mlog_mam = mean(log_mam(curstart:curend,:)); slog_mam =
std(log_mam(curstart:curend,:));
sklog_mam = skewness(log_mam(curstart:curend,:));
%--observed data
mlog_oam = mean(log_oam); slog_oam = std(log_oam);
sklog_oam = skewness(log_oam);

%Step 3) Calculate K after Kite (1977) as referenced by Mays (2005), pg 321
km = sklog_mam/6;
ko = sklog_oam/6;%--observed data

z = 2.58; %From z table using p = 0.0995 = 1-(1/(2*T))
        %where T is return period for event (in this case T = 100)

for i = 1:outs;
   K(i) = z+(z^2-1)*km(i)+(1/3)*(z^3-6*z)*km(i)^2-(z^2-1)*km(i)^3+z*km(i)^4+
   (1/3)*km(i)^5;
%--observed data
   Ko = z+(z^2-1)*ko+(1/3)*(z^3-6*z)*ko^2-(z^2-1)*ko^3+z*ko^4+(1/3)*ko^5;
```

```
end

%Step 4) Calculate the log precipitation value for the T-year event
for j = 1:outs;
   logxtm(j) = mlog_mam(j)+K(j)*slog_mam(j);
end
%--observed data
logxto = mlog_oam+Ko*slog_oam;

%Step 5) Calculate the T-year precipitation
for e = 1:outs
        xtm(e) = 10^(logxtm(e));
end
xto = 10^(logxto);%--observed data

%Convert output into inches to compare with standard storms of US
xtm_in = xtm/25.4;
xto_in = xto/25.4;%--observed data

% Repeat process for 2011 - 2040
f1mlog_mam = mean(log_mam(f1start:f1end,:));
f1slog_mam = std(log_mam(f1start:f1end,:));
f1sklog_mam = skewness(log_mam(f1start:f1end,:));
f1km = f1sklog_mam/6;
for i = 1:outs;
        f1K(i) = z+(z^2-1)*f1km(i)+(1/3)*(z^3-6*z)*f1km(i)^2-...
        (z^2-1)*f1km(i)^3+z*f1km(i)^4+(1/3)*f1km(i)^5;
end
for j = 1:outs;
         f1logxtm(j) = f1mlog_mam(j)+f1K(j)*f1slog_mam(j);
end
for f = 1:outs;
        f1xtm(f) = 10^(f1logxtm(f));
end
f1xtm_in = f1xtm/25.4;

% Repeat process for 2041 - 2070
f2mlog_mam = mean(log_mam(f2start:f2end,:));
f2slog_mam = std(log_mam(f2start:f2end,:));
f2sklog_mam = skewness(log_mam(f2start:f2end,:));
f2km = f2sklog_mam/6;
for i = 1:outs;
        f2K(i) = z+(z^2-1)*f2km(i)+(1/3)*(z^3-6*z)*f2km(i)^2-...
         (z^2-1)*f2km(i)^3+z*f2km(i)^4+(1/3)*f2km(i)^5;
end
for j = 1:outs;
```

```
        f2logxtm(j) = f2mlog_mam(j)+f2K(j)*f2slog_mam(j);
end
for g = 1:outs;
        f2xtm(g) = 10^(f2logxtm(g));
end
f2xtm_in = f2xtm/25.4;

% Repeat process for 2071 - 2099
f3mlog_mam = mean(log_mam(f3start:f3end,:));
f3slog_mam = std(log_mam(f3start:f3end,:));
f3sklog_mam = skewness(log_mam(f3start:f3end,:));
f3km = f3sklog_mam/6;
for i = 1:outs;
        f3K(i) = z+(z^2-1)*f3km(i)+(1/3)*(z^3-6*z)*f3km(i)^2-...
        (z^2-1)*f3km(i)^3+z*f3km(i)^4+(1/3)*f3km(i)^5;
end
for j = 1:outs;
        f3logxtm(j) = f3mlog_mam(j)+f3K(j)*f3slog_mam(j);
end
for h = 1:outs
        f3xtm(h) = 10^(f3logxtm(h));
end
f3xtm_in = f3xtm/25.4;

**************************************************************************
%Code estiamtes the 95% CI of the projected mean 100-yr storm event and
%compiles results from LP3.m into a table.

%Organize output data
xtm = [xtm_in; f1xtm_in; f2xtm_in; f3xtm_in];

for alt = 1:4
        A1B_samples(:,alt) = bootstrp(1000,@mean, xtm(alt,1:39));
        A2_samples(:,alt) = bootstrp(1000,@mean, xtm(alt,40:76));
        B1_samples(:,alt) = bootstrp(1000,@mean, xtm(alt,77:112));
        A1B_ci(:,alt) = bootci(1000,@mean, xtm(alt,1:39));
        A2_ci(:,alt) = bootci(1000,@mean, xtm(alt,40:76));
        B1_ci(:,alt) = bootci(1000,@mean, xtm(alt,77:112));
end
sample_all = [A1B_samples A2_samples B1_samples];
xlswrite('100yr_mean.xls',sample_all,'Sheet1','A3');

A1B_mean = mean(A1B_samples);
A2_mean = mean(A2_samples);
B1_mean = mean(B1_samples);
```

```
A1B = [A1B_mean; A1B_ci];
A2 = [A2_mean; A2_ci];
B1 = [B1_mean; B1_ci];
out_all = [A1B; A2; B1];
xlswrite('100yr_mean.xls',out_all,'Sheet2','C2');

box_all = [A1B_samples A2_samples B1_samples];
boxmax = max(max(box_all));
boxmin = min(min(box_all));
titles = {'1971-2000' '1981-2040' '2011-2070' '2041-2100'...
   '1951-2000' '1981-2040' '2011-2070' '2041-2100'...
   '1951-2000' '1981-2040' '2011-2070' '2041-2100'};
yaxes = {'A1B' ' ' ' ' ' 'A2' ' ' ' ' ' 'B1' ' ' ' ' ' '};
for p = 1:12
        subplot(3,4,p); boxplot(box_all(:,p));
        title(titles(p));
        axis([0 2 boxmin-2 boxmax])
        ylabel(yaxes(p));
end
%[fi,xi]=ksdensity(A1_samples);
%plot(xi,fi)
```

****

% Program to determine the data dependency and perform random permutation test and Kolmogorov Smirnov (KS) test for temporally dependent data series (Using ‘R’)

```
data <- read.csv("data.csv", header=T)

y <- data[1:360,3]
z <- data[1:360,4]

ks.obs <- ks.test(y,z)
ks.obs

ks.obs <- ks.obs$stat

D <- cbind(y,z)
N <- nrow(D)

iter <- 1000

KS <- rep(0, iter)

for(it in 1:iter){

print(it)
```

```
y.sim <- rep(0, N)
z.sim <- rep(0, N)

for(i in 1:N){
pick <- rbinom(1, 1, 0.5)+1

if(pick==1){
y.sim[i] <- D[i,1]
z.sim[i] <- D[i,2]
}

if(pick==2){
y.sim[i] <- D[i,2]
z.sim[i] <- D[i,1]
}

}

KS[it] <- ks.test(y.sim,z.sim)$stat

}

hist(KS, col="yellow")
abline(v=ks.obs, lwd=3, col="red")

p.value <- mean(KS>ks.obs)
p.value

ks.obs

acf(y)
plot(acf(y),xlab="Lag", ylab="Auto Correlation", main="Data Visualization for
Dependency")
**********
```

APPENDIX D

DATA FOR HEC-HMS MODEL

(TASK 3)

Table D1 List of historical major flood events in Clark County, Nevada

Event Date	Total Rainfall	No. of gauges / Storm period/ Max. rainfall	Location/ Other remarks
August 27 2007	>1”	9 / 3 am – 5 am 2” in 30 min period 2.67” in 1 hour period	Near Lakes Detention basin 4359 (3.11”). Peak flow recorded in Flamingo wash (1000 cfs.) and Las Vegas Wash at Pabco Rd. (2700 cfs.)
August 2 2007	>2” in 90 min	1 pm - 2pm 2.50” in 90 min period	Brownstone Canyon in West Las Vegas valley (4329) (2.68”)
August 19 2003	>2” in 90 min		Mainly in Gowan watershed, Historic event
July 8 1999	1.5” – 3” in 60-90 min	9:15 am -11 am 2 gauges 3”, 5 gauges 2”, 12 gauges >1.5”	Very big flood event. 100 year return period. Over 20 million damages. Flow significant in Flamingo, DC & LV Wash.
Sep 11 1998	1” or more	11:30 am	Low flows in DC and PW. Significant flows in FT, Sloan and LV Wash. May be a 100 years flood for some reaches.
July 20-24 1998	>1” July 23 >1” in 20 min		Max flow in Flamingo Wash
Sep 1 to 3 1997	>1.25”		
August 9 to 10 1997	2.83” and 2.56” in Henderson and Boulder city	1.26” in 15 min.	Heavy rain in LV, worst condition in Henderson and Boulder city (very high damage). Exceeded the 100 yr flood event
July 28 1996	0.8”	2pm	Not so heavy
August 22-23 1995		4:30 pm 0.75” in 15 min	No damage. Large flow in Spring Mountain road and Flamingo road
August 8 1994	Max 1.57” 0.60” <1 hour	6:15 pm	Mainly in Gowan No damage, lasted for an hour
Feb 8 1993	>1.5” for whole day	Henderson (2.40”) >1” in Flamingo	Limited damages only.
Feb 12 1992	1” for whole day.	4 pm-1:30 am	Not so heavy
Sep 6-8 1991		6 am and through the whole weekend. Las Vegas -10:30 am to 2 pm	Significant flows in Flamingo wash. Most of the valley received little or no rain
August 10 1991	1.25” in an hour and 1.65” in 3 hours	7 pm	Light/moderate intensity in valley. Higher in CalNevari and Laughlin.

(Note: All of these data are compiled from the annual reports obtained from Clark County Regional Flood Control District. DC: Duck Creek, PW: Pittman Wash).

Table D2 List of Stations in the Flamingo Tropicana Watershed in Las Vegas, Nevada

Basins	Stations Id	Station Name	Station Type	Latitude	Longitude	Elevation
St 4084	4084	Las Vegas Wash near Sahara Avenue	Water Level	36° 8' 34"	115° 3' 11"	1637
St 4274	4274	Downtown Las Vegas	Full Weather Station	36° 9' 57"	115° 8' 44"	2102
St 4304	4304	Blue Diamond Ridge South	Full Weather Station	36° 5' 2"	115° 23' 9"	4833
St 4309	4309	Desert Inn Detention Basin	Water Level	36° 7' 47"	115° 14' 32"	2370
St 4314	4314	Blue Diamond Ridge North	Precipitation	36° 6' 27"	115° 23' 52"	4823
St 4319	4319	Beltway Channel at Town Center	Water Level	36° 7' 12"	115° 19' 27"	2800
St 4324	4324	Red Rock Canyon	Precipitation	36° 7' 50"	115° 25' 41"	3625
St 4329	4329	Brownstone Canyon	Precipitation	36° 10' 50"	115° 25' 3"	4423
St 4334	4334	Upper Flamingo 1	Precipitation	36° 3' 29"	115° 19' 20"	2979
St 4339	4339	Beltway Channel at Peace Way	Water Level	36° 6' 26"	115° 17' 49"	2625
St 4344	4344	Red Rock DB	Water Level	36° 9' 9"	115° 21' 17"	3136
St 4349	4349	Upper Flamingo DB	Water Level	36° 5' 24"	115° 16' 14"	2388
St 4354	4354	The Lakes	Full Weather Station	36° 7' 28"	115° 17' 8"	2541
St 4359	4359	The Lakes Detention Basin	Water Level	36° 7' 40"	115° 16' 42"	2527
St 4364	4364	Flamingo Wash at Torrey Pines	Water Level	36° 6' 10"	115° 14' 3"	2218
St 4369	4369	Flamingo Wash at Decatur Blvd	Water Level	36° 6' 8"	115° 12' 29"	2159
St 4374	4374	Flamingo Wash at Eastern	Water Level	36° 7' 23"	115° 7' 9"	1790
St 4379	4379	VanBuskirk DB	Water Level	36° 6' 30"	115° 6' 41"	1834
St 4384	4384	Desert Inn Super Arterial	Water Level	36° 7' 47"	115° 9' 50"	
St 4394	4394	Flamingo Wash at Nellis Blvd	Water Level	36° 8' 32"	115° 3' 60"	1673
St 4399	4399	Flamingo Wash near Mojave	Water Level	36° 7' 59"	115° 6' 12"	1783
St 4404	4404	F-1 Debris Basin	Water Level	36° 5' 50"	115° 20' 20"	2842
St 4409	4409	F-2 Debris Basin	Water Level	36° 4' 48"	115° 19' 44"	2716
St 4414	4414	Blue Diamond Detention Basin	Water Level	36° 1' 55"	115° 19' 1"	2899
St 4424	4424	F-1 Channel	Water Level	36° 5' 14"	115° 18' 48"	2621
St 4434	4434	Beltway Channel at Buffalo	Water Level	36° 3' 58"	115° 15' 15"	2520
St 4444	4444	R-4 Detention Basin	Water Level	36° 6' 46"	115° 21' 13"	2981
St 4449	4449	R-4 Channel	Water Level	36° 7' 14"	115° 19' 54"	2789
St 4454	4454	Warm Springs/Jones	Precipitation	36° 3' 24"	115° 13' 24"	2440
St 4474	4474	Tropicana Wash DB	Water Level	36° 4' 54"	115° 11' 59"	2290
St 4484	4484	Tropicana Wash at Swenson	Water Level	36° 6' 51"	115° 8' 49"	2030
St 4574	4574	Flamingo Wash near Spencer	Water Level	36° 7' 11"	115° 7' 44"	1828

Table D3 Modeled streamflow and volume for an average, minimum and maximum change in precipitation for future climate. Precipitation here represents an average of precipitation from all climate projections for each emission scenario (A1B, A2, B1).

	Modeled Streamflow					
	Peak Streamflow (cfs)			Total Volume (ac ft)		
For flood event on July 8 1999	13924.4			1791.8		
	Streamflow for average change in precipitation					
	A1B	A2	B1	A1B	A2	B1
2011-2040	18930.6	19608	17115	2357.7	2431.9	2172
2041-2070	18653.1	20439	19603	2327.4	2520.9	2431.4
2071-2100	20738.3	24536	20261	2552.6	2932.1	2501.9
	Streamflow for maximum change in precipitation					
	A1B	A2	B1	A1B	A2	B1
2011-2040	34133.4	31693	25712	3892.5	3650	3047.6
2041-2070	30593.6	32922	39447	3527.6	3771.6	4413.9
2071-2100	33101.6	38255	33361	3789	4296.9	3816.7
	Streamflow for minimum change in precipitation					
	A1B	A2	B1	A1B	A2	B1
2011-2040	11229	12708	9782.9	1482.8	1653.6	1312.8
2041-2070	10690.6	13102	11890	1420.1	1699.5	1559.2
2071-2100	13261.6	10725	9196.2	1717.9	1424.1	1243.7

Table D4 Range of precipitation (inches) for 100 year return period storm based on modeled maximum monthly precipitation. The lower 5% and upper 95% represents its confidence intervals.

Scenarios	Confidence Interval	Monthly Precipitation (inches)			
		1951-2000	1981-2040	2011-2070	2041-2100
A1B	Mean	5.18	6.71	7.01	7.63
	Lower 5	4.93	6.16	6.30	6.93
	Upper 95	5.47	7.32	7.74	8.42
A2	Mean	5.27	6.61	7.05	7.92
	Lower 5	5.00	6.12	6.44	7.06
	Upper 95	5.55	7.34	7.77	8.97
B1	Mean	5.21	6.49	7.03	7.59
	Lower 5	4.98	5.93	6.54	6.98
	Upper 95	5.50	7.09	7.57	8.38

Table D5 Modeled streamflow and volume for a mean change in annual maximum precipitation (mm/month). The lower 5% and upper 95% represents its confidence intervals.

	Modeled Streamflow					
	Peak Streamflow (cfs)			Total Volume (ac ft)		
	Mean					
	A1B	A2	B1	A1B	A2	B1
2011-2040	20804	19854	19704	2560.1	2457.5	2441.7
2041-2070	25615	22029	22447	3046.8	2685.5	2728.1
2071-2100	22373	26330	25454	2720.5	3118.1	3030.7
	Lower 5%					
	A1B	A2	B1	A1B	A2	B1
2011-2040	20095	18763	18765	2483.9	2338.8	2336.8
2041-2070	23983	21059	21869	2883.1	2586.6	2669.5
2071-2100	21059	23851	24066	2586.6	2869.7	2891.3
	Upper 95%					
	A1B	A2	B1	A1B	A2	B1
2011-2040	21579	21059	20509	2640.1	2586.6	2528.4
2041-2070	26992	23441	23140	3184.3	2829	2798.5
2071-2100	23983	29119	26909	2883.1	3395.7	3176.3

REFERENCES

Aguado, E., D. R. Cayan, L. Riddle, and M. Roos (1992). Climatic fluctuations and the timing of west coast streamflow. *Journal of Climate,* 5:1468–1483.

Aizen, V.B., E.M. Aizen, J.M. Melack and J. Dozier (1997). Climatic and hydrologic changes in the Tien Shan, Central Asia. *Journal of Climate,* 10:1393:1404.

Alder, H.L. and E.B. Roessler (1975). *Introduction to Probability and Statistics*. 6th edition, W.H. Freeman and Co. Ltd, U.S.A.

AMS (American Meteorological Society) (1998). Planned and inadvertent weather modification. *B. American Meteorological Society,* 73:331-337.

Arnell, N.A. (1999). Climate change and global water resources. *Global Environmental Change,* 9:31-49.

Arnell, N.W. and N.S. Reynard (1996). The effects of climate change due to global warming on river flows in Great Britain. *Journal of Hydrology,* 183:397-424.

Arnell, N.W., D.A. Hudson and R.G. Jones (2003). Climate change scenarios from a regional climate model: Estimating change in runoff in southern Africa. *Journal of GeophysicalResearch Atmospheres,* 108(D16), 4519, doi:10.1029/2002JD002782.

Arora and Boer (2001). Effects of simulated climate change on the hydrology of major river basins. *Journal of Geophysical research,* 106(D4):3335-3348.

ASCE, American Society of Civil Engineers (2004). Standard practice for the design and operation of precipitation enhancement projects. ASCE/EWRI Standard 42-04, Reston, VA.

_____ (2006). *Guidelines for Cloud Seeding to Augment Precipitation*. 2nd edition, ASCE Manuals and Reports on Engineering Practice No. 81, (ASCE)/EWRI, Reston, VA.

Barker, R. (2009), NAIWMC news. Idaho Power's cloud seeding efforts keep water flowing over dams and may save you money. Idaho Statesman, (www.idahostatesman.com) published 11/19/2009.

Barlow, M., S. Nigam, and E. H. Berbery (2001). ENSO, Pacific decadal variability, and U.S. summertime precipitation, drought and streamflow. *Journal of Climate,* 14:2105–2128.

Barnett, T.P., D.W. Pierce, H.G. Hidalgo, C. Bonfils, B.D. Santer, T. Das, …. M.D. Dettinger (2008). Human-induced changes in the hydrology of the Western United States. *Science,* 319:1080-1083, doi: 10.1126/science.1152538.

Barontini, S., G. Grossi, N. Kouwen, S. Maran, P. Scaroni and R. Ranz (2009). Impacts of climate change scenarios on runoff regimes in the Southern Alps. Hydrology and Earth System Sciences Discussion, HESSD, 6:3089-3141.

Bates, B.C., S.P. Charles, N.R. Sumner and P.M. Fleming (1994). Climate change and its hydrological implications for South Australia. *Trans. of the R. S. of S Australia*, 118(1):35-43.

Beebee, R.A. and M. Manga (2004). Variation in the relationship between snowmelt runoff in Oregon and ENSO and PDO. *Journal of the American Water Resources Association*, 40(4):1011-1024.

Beniston, M., D.B. Stephenson, O.B. Christensen, C.A.T. Ferro, C. Frei, K. Halsnaes….K. Woth (2007). Future extreme events in European climate: An exploration of regional climate model projections. *Climate Change*, 81(1):81– 95.

Benjamini, Y. and Y. Harpez (1986). Observational rainfall—Runoff analysis for estimating effects of cloud seeding on water resources in Northern Israel. *Journal of Hydrology,* 83:299-306.

Bergstrom, S., B. Carlsson, M. Gardelin, G. Lindstrom, A. Pettersson and M. Rummukainen (2001). Climate change impacts on runoff in Sweden assessments by global climate models, dynamical downscaling and hydrological modeling. *Climate Research,*16:101-112.

Bigg, E.K. (1997). An independent evaluation of a South African hygroscopic cloud seeding experiment, 1991–1995. *Atmospheric Research,* 43:111-127.

Boe, B.A. (2008). Operational aspects of the Wyoming Weather Modification Pilot Project: An update. Section 5.2, Access http://ams.confex.com/ams/17WModWMA/techprogram/ paper_139288.htm.

Bonfils, C., B.D. Santer, D.V. Pierce, H.G. Hidalgo, G. Bala, T. Das….A.W. Wood (2008). Detection and attribution of temperature changes in the western U.S. *Journal of Climate*, 21:6404-6424.

BOR (Bureau of Reclamation), (2006). Drought Conditions in the West. Online feature from the Upper Colorado Regional Office of Reclamation, Access www.usbr.gov/uc/feature/drought.html.

Braun, L.N., M. Weber and M. Schulz (2000). Consequences of climate change for runoff from Alpine regions. *Annals of Glaciology,* 31:19-25.

Breed, D. (2008). Cloud seeding to enhance snowfall. Colorado Water. Newsletter of the water center of Colorado State University, 25(6):1-37.

Bronstert, A., D. Niehoff and G. Burger (2002). Effects of climate and land-use change on storm runoff generation: present knowledge and modeling capabilities. *Hydrologic Processes,* 16(2):509–529

Bronstert, A., G. Burger, M. Heidenreich and B. Kohler (1999). Impact of climate change on flooding and sustainable river management. *Proceedings of the two International Riband Workshop,* 26-27 Feb 1998.

Brown, B.G. and R.W. Katz (1995). Regional analysis of temperature extremes: Spatial analog for climate change? *Journal of Climate*, 8:108–119.

Bruintjes, R.T. (1999). A review of cloud seeding experiments to enhance precipitation and some new prospects. *B. of the American Met. Society*, 80(5):805-820.

Bultot, F., A. Coppens, G.L. Dupriez, D. Gellens and F. Meulenberghs (1988a). Repercussions of a CO_2 doubling on the water cycle and on the water balance_ a case study for Belgium. *Journal of Hydrology,* 99:319-347.

Buonomo, E., R. Jones, C. Huntingford, and J. Hannaford (2007). On the robustness of changes in extreme precipitation over Europe from two high resolution climate change simulations. *Q. J. R. Meteorological Society,* 133: 65– 81.

Cameron, D., K. Beven and P. Naden (2000). Flood frequency estimation by continuous simulation under climate change (with uncertainty). *Hydrology and Earth Science System,* 4(3):393-405.

Cavazos, T. and B. Hewitson (2002). Relative performance of empirical predictors of daily precipitation. In *Integrated Assessment and Decision Support, Proceedings of the First Biennial Meeting of the International Environmental Modelling and Software Society*,Vol.1, RizzoliAE, JakemanAJ (eds). Manno, Switzerland. iEMSs; 334–339.

Cayan, D., A.L. Luers, G. France and B. Croes (2006). Scenarios of climate change in California: An overview. White Paper, A report from California Climate Change Center, Feb 2006.

Chao, Y., M. Ghil and J.C. Mcwilliams (2000). Pacific interdecadal variability in the century's sea surface temperatures. *Geophysical Research Letter*, 27:2261-2264.

Cherkauer, K. A., and D. P. Lettenmaier (2003). Simulation of spatial variability in snow and frozen soil. *Journal of Geophysical Research*, 108, 8858, doi:10.1029/2003JD003575.

Chen, B. and H. Xiao (2010). Silver iodide seeding impact on the microphysics and dynamics of convective clouds in the high plains. *Atmospheric Research*, 96(2-3):186-207.

Chiew, F.H.S, P.H. Whetton, T.A. McMahon and A.B. Pittock (1995). Simulation of the impacts of climate change on runoff and soil moisture in Australian catchments. *Journal of Hydrology*, 167:121-147.

Chow, V.T. (1964). Editor-in-Chief, *Handbook of Applied Hydrology*. McGraw-Hill.

Christensen, J. H., and O. B. Christensen (2003). Severe summertime flooding in Europe. *Nature*, 421:805– 806.

Clark County Regional Flood Control District (CCRFCD), (2006). History of flooding in Clark County. Access http://www.ccrfcd.org/03-history.htm (cited Nov. 1, 2007)

Cooper, C.F. and W.C. Jolly (1970). Ecological effects of silver iodide and other weather modification agents: A review. *Water Resources Research*, 6:88-98.

Coquard, J., P.B. Duffy, K.E. Taylor and J.P. Iorio (2004). Present and future surface climatein the western U.S.A. as simulated by 15 global climate models. *Climate Dynamics*, 23:455–472.

Cotton, W.R. (2007). Basic cloud seeding concept. *Southwest Hydrology*, 16-17, Mar/Apr. 2007.

Cotton, W.R. (2008). Weather and climate engineering. Position paper for a workshop "Perturbed Clouds in the Climate System" in Frankfurt, Germany, March 2008.

Covey, C., K.M. AchutaRao, U. Cubasch, P. Jones, S.J. Lambert, M.E. Mann, T.J. Phillips and K.E. Taylor (2003). An overview of results from the coupled model intercomparison project. *Global Planet Change*, 37:103–133.

Cubasch, U., G.A. Meehl, G.J. Boer, R.J. Stouffer, M. Dix, A. Noda, C.A. Senior, S. Raper and K.S. Yap (2001). Projections of future climate change. In: Houghton JT et al. (eds) Climate Change 2001. Cambridge University Press, Cambridge, UK, pp 525-582.

Cubasch, U., J. Waszkewitz, G. Hegerl and J. Perlwitz (1995). Regional climate changes as simulated in time-slice experiments. *Climate Change*, 31: 273-304

Cubasch, U. et al. (2000). The Scientific Basis: Contribution of working group I to the third assessment report of the Intergovernmental Panel on Climate Change, J.T. Houghton et al., Eds. (Cambridge Univ. Press, Cambridge, 2001), pp. 525-582

Curie, M., D. Janc and V. Vuckovic (2007). Cloud seeding impact on precipitation as revealed by cloud-resolving mesoscale model. *Meteorology and Atmospheric Physics,* 95:179-193.

Dankers, R. and L. Feyen (2009). Flood hazard in Europe in an ensemble of regional climatescenarios. *Journal of Geophysical Research,* 114(D16108), doi:10.1029/2008JD011523

Dankers, R., L. Feyen and O. B. Christensen (2009). On the benefit of high resolution climatesimulations in impact studies of hydrological extremes. *Hydrol. Earth Syst. Sci. Discuss.*, 6:2573–2597.

Dennis, A. S. (1980). *Weather Modification by Cloud Seeding*. International Geophysics Series, 24, Academic Press, New York, NY, 21-22.

Dettinger, M. D., and D. R. Cayan (1995). Large-scale atmospheric forcing of recent trends toward early snowmelt runoff in California. *Journal of Climate,* 8**:** 606–623.

Diffenbaugh, N.S., J.S. Pal, R.J. Trapp and F. Giorgi (2005). Fine-scale processes regulate the response of extreme events to global climate change. *Proceedings of the National Academy of Sciences of the United States of America*, 102:15774-15778.

Duffy, P.B. and CoAuthors (2003). High resolution simulations of global climate, Part 1: simulations of the present climate. *Climate Dynamics*, 21:371–390

Durman, C.F., J.M. Gregory, D.C. Hassell, R.G. Jones and J.M. Murphy (2001). A comparison of extreme European daily precipitation simulated by a global and a regional climate model for present and future climates. *Quarterly Journal of the Royal Meteorological Society,* 127:1005–1015.

Easterling, D.R., G.A. Meehl, C. Parmesan, S.A. Changnon, T.R. Karl and L.O. Mearns (2000).Climate Extremes: Observations, Modeling and Impacts. *Science*, 289:2068-2074.

Efron, B (1979). Bootstrap Methods: Another Look at the Jackknife. *The Annals of Statistics,* 7(1):1–26.

Efron, B. (1981). Nonparametric estimates of standard error: The jackknife, the bootstrap and other methods. *Biometrika*, 68:589-599.

Eisler, R. (1996). Silver hazards to fish, wildlife, and invertebrates: A synoptic review. *Contaminant Hazard Reviews*, 32, Patuxent Wildlife Research Center, U.S. National Biological Service, Laurel, MD.

Ekstro¨m, M., H. J. Fowler, C. G. Kilsby and P. D. Jones (2005). New estimates of future changes in extreme rainfall across the UK using regional climate model integrations. 1. Future estimates and use in impact studies. *Journal of Hydrology*, 300:234–251.

EPA (2009). Past climate change. Last updated on Monday, September 28, 2009. Access http://www.epa.gov/climatechange/science/pastcc.html

Fowler, A.M. and K.J. Hennessey (1995). Potential impacts of global warming on the frequency and magnitude of heavy precipitation. *Natural Hazards*, 11:283–303.

Fowler, H. J. and C. G. Kilsby (2003a). A regional frequency analysis of United Kingdom extreme rainfall from 1961 to 2000. *Int. J. Climatology*, 23:1313– 1334.

Fowler, H. J. and C. G. Kilsby (2003b). Implications of changes in seasonal and annual extreme rainfall. *Geophysical Research Letters*, 30(13), 1720, doi:10.1029/2003GL017327.

Fowler, H. J. and M. Ekstro¨m (2009). Multi-model ensemble estimates of climatechange impacts on UK seasonal precipitation extremes. *Int. J. Climatology*, 29:385– 416.

Fowler, H. J., M. Ekstro¨m, C. G. Kilsby and P. D. Jones (2005). New estimates of future changes in extreme rainfall across the UK using regional climate model integrations.1. Assessment of control climate. *Journal of Hydrology*, 300:212–233.

Fowler, H. J., S. Blenkinsop and C. Tebaldi (2007). Linking climate change modeling to impacts studies: recent advances in downscaling techniques for hydrological modeling. *Int. J. Climatology* 27: 1547–1578.

Fowler, T.L., B.G. Brown and R.T. Bruintjes (2001). Statistical evaluation of a cloud seeding experiment in Coahuila, Mexico. Preprints, *15th Conf. on Planned and Inadvertent Weather Modification*, Albuquerque, NM, *American Meteorological Society*, 49-53.

Frei, C., R. Scho¨ ll, S. Fukutome, J. Schmidli and P. L. Vidale (2006). Future change of precipitation extremes in Europe: An intercomparison of scenarios from regional climate models. *Journal of Geophysical Research*, 111, D06105, doi:10.1029/2005JD005965

Frich, P., L. V. Alexander, P. Della-Marta, B. Gleason, M. Haylock, A. M. G. K. Tank and T. Peterson (2002). Observed coherent changes in climatic extremes during the second half of the twentieth century. *Journal of Climate Research,* 19:193–212.

Gao, X., G. Zheng and D. Jin (2006). A numerical comparison study of cloud seeding by silver iodide and liquid carbon dioxide. *Atmospheric Research,* 79:183-226.

Gellens, D. and E. Roulin (1998). Streamflow response of Belgian catchments to IPCC climate change scenarios. *Journal of Hydrology,* 210:242-258.

Georgakakos, K.P., D.J. Seo, H. Gupta, J. Schaake and M.B. Butts (2004). Towards the characterization of streamflow simulation uncertainty through multimodel ensembles. *Journal of Hydrology,* 298:222–241.

Gerbaux, M., N. Hall, N. Dessay and I. Zin (2009). The sensitivity of Sahelian runoff to climate change. *Journal–des Sciences Hydrologiques,* 54(1):5-16.

Gibbons, J. D. (1985). *Nonparametric Statistical Inference*. 2nd. edition, M. Dekker, U.S.A.

Giorgi, F., C. Shields, L.O. Mearns and L. McDaniel (1998). Regional nested model simulations of present day and $2 \cdot CO_2$ climate over the Central Plains of the United States. *Climate Change,* 40:457–493.

Giorgi, F. and L. O. Mearns (2003). Probability of regional climate change based on the Reliability Ensemble Averaging (REA) method. *Geophysical Research Letters,* 30(12):1629.

Giorgi, F., S.C. Brodeur and G.T. Bates (1994). Regional climate change scenarios over the United States produced with a nested regional climate model. *Journal of Climate,* 7:375-399.

Givati, A. and D. Rosenfeld (2004). Quantifying precipitation suppression due to air pollution. *Journal of Applied Meteorology,* 43:1038-1056.

Gleick, P.H. (1986). Methods for evaluating the regional hydrologic impacts of global climatic changes. *Journal of Hydrology,* 88:97-116.

Gordon, H.B., P.H. Whetton, A.B. Pittock, A.M. Fowler and M.R. Haylock (1992). Simulated changes in daily rainfall intensity due to the enhanced greenhouse effect: implications for extreme rainfall events. *Climate Dynamics,* 8:83–102.

Goswami, B.N., V. Venugopal, D. Sengupta, M. S. Madhusoodanan and K. Xavier (2006). Increasing trend of extreme rain events over India in a warming environment. *Science,* 314:1442:1444.

Govindasamy, B., P.B. Duffy, J. Coquard (2003). High resolution simulations of global climate, Part 2: effects of increased greenhouse gases. *Climate Dynamics,* 21:391-404

Grant, L.O. (1983). Utilization and assessment of operational weather modification programs for augmenting precipitation. *Agricultural Water Management,* 7:23-35.

Griffith, D.A. and M.E. Solak (1999). A cloud seeding program to enhance hydroelectric power production from the El Cajon drainage, Honduras. Proceedings of the s*eventh conference on Weather Modification,* Chiang Mai, Thailand, February 17-22, 1999.

Griffith D.A. and M.E. Solak (2006). The potential use of winter cloud seeding programs to augment the flow of the Colorado River. Colorado White Paper, A report prepared for the Upper Colorado River Commission, March 2006.

Griffith, D.A., M.E. Solak and D.P. Yorty (2005a). Summary and evaluation of the winter 2004-2005 cloud seeding program in the Boise River drainage. North American Weather Consultants Report No. WM 05-3 to Boise Project Board of Control.

Griffith, D.A., M.E. Solak and D.P. Yorty (2007). A level II weather modification feasibility study for winter snowpack augmentation in the Salt River and Wyoming ranges in Wyoming. *Journal of Weather Modification,* 39: __ Access, www.nawcinc.com/WYOMING JWM Paper.pdf

Griffith, D.A., M.E. Solak and D.P. Yorty (2009). 30+ winter seasons of operational cloud seeding in Utah. *Journal of Weather Modification,* 41:23-37.

Griffith, D.A., M.E. Solak, R.B. Almy and D. Gibbs (2005b). The Santa Barbara cloud seeding project in coastal Southern California: Summary of results and their implications. *85th AMS Annual Meeting, American Meteorological Society -Combined Preprints*, pp. 2855-2860.

Groisman, P.Y. and CoAuthors (1999). Changes in the probability of heavy precipitation: important indicators of climatic change. *Climate Change,* 42:243-283.

Groisman, P.Y., R. W. Knight, T. R. Karl, D. R. Easterling, B. Sun, and J. H. Lawrimore (2004). Contemporary changes of the hydrological cycle over the contiguous United States: Trends derived from in situ observations. *Journal of Hydrometeorology,* 5: 64-85.

Gutzler, D.S., D.M. Khan and C. Thornbrugh (2002). Modulation of ENSO-based long lead outlooks of Southwestern U.S. winter precipitation by the Pacific Decadal Oscillation. *American Meteorological Society,* 17:1163-1172.

Hamlet, A. F. and D.P. Lettenmaier (1998). Effects to Columbia basin water resources associated with climate variability and operating system design. Summary of Hydrology Results, Year 3 Rep., JISAO Climate Impacts Group, University of Washington, Seattle.

Hamlet, A.F. and D.P. Lettenmaier (1999). Effects of climate change on hydrology and water resources in the Columbia River basin. *JAWRA,* 35(6):1597-1623.

Hamlet, A.F., P. W. Mote, M. P. Clark, and D. P. Lettenmaier (2005). Effects of temperature and precipitation variability on snowpack trends in the western United States. *Journal of Climate,* 18**:**4545–4561.

Hastay, M. and J.S. Gladwell (1969). Statistical evaluations of a cloud-seeding program at the streamflow control level. *Journal of Hydrology,* 9:117-135.

Hayhoe, K., C.P. Wake, T.G. Huntington, L. Luo, M.D. Schwartz, J. Sheffield, E. Wood…D. Wolfe (2007). Past and future changes in climate and hydrological indicators in the U.S. Northeast. *Climate Dynamics,* 28:381-407.

Heggli, M., B. Dunn, A. Huggins, J. Denholm, L. Angri and T. Luker (2007). The snowy precipitation enhancement research project. *AMS Conf. Weather Mod.,* 2007. Access http://www.radiometrics.com/Snowy Hydro.pdf

Held, I. M. and B. J. Sodden (2006). Robust responses of the hydrological cycle to global warming. *Journal of Climate*, 19:5686-5699.

Hennessey, K.J., J.M. Gregory and J.F.B. Mitchell (1997). Changes in daily precipitation under enhanced greenhouse conditions. *Climate Dynamics,* 13:667-680.

Hidalgo, H.G. and J.A. Dracup (2003). ENSO and PDO effects on hydroclimatic variations of the Upper Colorado River. *American Meteorological Society,* 4:5-23.

Hidalgo, H.G. and CoAuthors (2009). Detection and attribution of streamflow timing changes to climate change in the western United States. *J. of Climate,* 22:3838-3855.

Holroyd E.W., J.A. Heimbach and A.B. Super (1995). Observations and model simulation of AgI seeding within a winter storm over Utah's Wasatch Plateau. *Journal of Weather Modification,* 27:35-56.

Houghton, J.T., G.J. Jenkins and J.J. Ephraums (1990). *Climate Change: The IPCC Scientific Assessment.* Cambridge University Press, 364 pp.

Huggins, A.W. (2007). Another wintertime cloud seeding case study with strong evidence of seeding effects. *Journal of Weather Modification*, 39:9-36.

Huggins, A.W., S.L. Kelyon, L. Warren, A.D. Peace, S.P. Bilish, J. Denholm and S.K. Chai (2008). Recent results from a randomized wintertime cloud seeding experiment in the snowy mountains of Australia. Access, http://ams.confex.com/ams/17WModWMA /techprogram/paper 139167.htm. (cited 02/21/2010)

Hunter, S.M. (2007). Optimizing cloud seeding for water and energy in California. A pierfinal project report for California Energy Commission, March 2007.

Hunter, S.M., S. Meyer and R. Aman (2005). Water augmentation from cloud seeding in the Colorado River Basin. Bureau of Reclamation Technical Service Center, 9p.

Huntingford, C., R.G. Jones, C. Prudhomme, R. Lamb, J.H.C. Gash and D.A. Jones (2003).Regional climate—model predictions of extreme rainfall for a changing climate. *Q. J.R. Meteorological Society,* 129:1607–1621.

Iorio, J.P., P.B. Duffy, B. Govindasamy, S.L. Thompson, M. Khairoutdinov and D. Randall (2004). Effects of model resolution and subgrid-scale physics on the simulation of precipitation in the continental United States. *Climate Dynamics,* 23:243–258.

IPCC (Intergovernmental Panel on Climate Change) (2001). Climate Change 2001: Impacts, Adaptation, and Vulnerability. Contribution of working group II to the third assessment report to the IPCC. Cambridge: Cambridge University Press, U.K., and New York. (pp. 191-234)

IPCC (2007a). Climate change 2007: The physical science basis. Contribution of Working Group I to the Fourth Assessment Report of the Intergovernmental Panel on Climate Change. Cambridge: Cambridge University Press, U.K., and New York.

IPCC (2007b). Climate change 2007: Synthesis report. Summary for Policymakers, Fourth Assessment Report of the Intergovernmental Panel on Climate Change. Cambridge: Cambridge University Press, U.K., and New York.

Jian, W. and L. Shuo (2006). Effect of climate change on snowmelt runoffs in mountainous regions of inland rivers in Northwestern China. *Science in China*, 49(8):881-888.

Johnson, H.L. (1985). An evaluation of the North Dakota cloud modification project. A final report to the North Dakota Weather Modification Board, 1985.

Jones, P. D. and P. A. Reid (2001). Assessing future changes in extreme precipitation over Britain using regional climate model integrations. *Int. J. Climatology,* 21:1337–1356.

Jones, R.G., J.M. Murphy, M. Noguer and A.B. Keen (1997). Simulation of climate change over Europe using a nested regional-climate model. 11. Comparison of driving and regional model responses to a doubling of carbon dioxide. *Quarterly Journal of the Royal Meteorological Society,* 123:265-292.

Joubert A.M. and B.C. Hewitson (1997). Simulating present and future climate of southern Africa using general circulation models. *Progress in Phy. Geography,* 21(1):51-78.

Kahan, A.M. (1972). Reclamations Great Plains weather modification program. *American Meteorological Society,* Rapid City, South Dakota, 222-225.

Kang, B. and J.A. Ramirez (2007). Response of streamflow to weather variability under climatechange in the Colorado Rockies. *J. of Hydrologic Engineering,* 12(1):63-72.

Karl, T.R. and R.W. Knight (1998). Secular trends of precipitation amount, frequency, and intensity in the USA. *B. American Meteorological Society,* 79:231-241.

Karl, T.R., R.W. Knight, D.R. Easterling and R.G. Quayle (1996). Indices of climatic change for the United States. *B. American Meteorological Society,* 77: 279-292.

Kauser, R., A. Bari and U. Rafique (2008). A case study of cloud seeding experiments conducted in Pakistan. *The International Journal of Meteorology,* 33(331):238-247.

Kay, A.L., R.G. Jones and N.S. Reynard (2006). RCM rainfall for UK flood frequency estimation. II. Climate change results. *Journal of Hydrology,* 318:163-172.

Kendon, E.J., D.P. Rowell, R.G. Jones and E. Buonomo (2008). Robustness of future changes in local precipitation extremes. *Journal of Climate,* 21: 4280–4297.

Kethley, L.I. (1970). Weather modification and the hydrologic cycle. *Presented at the 50th annual meeting of the American Geophysical Union* in April 1969.

Kharin, V. V. and F. W. Zwiers (2000). Changes in the extremes in an ensemble of transient climate simulations with a coupled atmosphere ocean GCM. *Journal of Climate*, 13: 3760–3788.

Kiktev, D., D. M. H. Sexton, L. Alexander, and C.K. Folland (2003). Comparison of modeled and observed trends in indices of daily climate extremes. *Journal of Climate*, 16: 3560-3571.

Kim, J., T.K. Kim, R.W. Arritt and N.L. Miller (2002). Impacts of increased atmospheric CO_2 on the hydroclimate of the western United States. *Journal of Climate*, 15:1926–1942

Kite, G.W. (1977). *Frequency and Risk Analysis in Hydrology*. Water Resources Publications, Fort Collins, CO.

Knowles, N., M. D. Dettinger and D. R. Cayan (2006). Trends in snowfall versus rainfall in the western United States. *Journal of Climate*, 19**:**4545–4559.

Krause, P., D.P. Boyle and F. Base (2005). Comparison of different efficiency criteria for hydrological models. *Advances in Geosciences*, 5: 89-97.

KWO (Kansas Water Office), (2001). Weather Modification Program, Fact Sheet No. 18, 2001: Kansas Water Office, 1p. (Access NAIWMC FAQs).

Kyselý, J. and R. Beranová (2009). Climate-change effects on extreme precipitation in central Europe: uncertainties of scenarios based on regional climate models. *Th. Applied Climatol*ogy, 95:361–374.

Lambert, S.J. and G.J.Boer (2001). CMIP1 evaluation and intercomparison of coupled climate. *Climate Dynamics*, 17:83-106.

Leung, L.R. and M.S. Wigmosta (1999). Potential climate change impacts on mountain watersheds in the Pacific Northwest. *Journal of the American Water Resources Association*, 35(6): 1463-1471.

Leung, L.R. and S.J. Ghan (1999). Pacific Northwest climate sensitivity simulated by a regional climate model driven by a GCM. Part II: 2 $\cdot CO_2$ simulations. *Journal of Climate*, 12: 2031–53.

Leung, R.B., Y. Qian, X. Bian, W.M. Washington, J. Han and J.O. Roads (2004). Mid centuryensemble regional climate change scenarios for the western United States. *Climatic Change*, 62: 75–113.

Levin, Z. (2009). On the state of cloud seeding for rainfall enhancement. A Report prepared by the Cyprus Institute, EEWRC, May 2009.

Levin, Z., N. Halfon and P. Alpert (2010). Reassessment of rain enhancement experiments and operations in Israel including synoptic considerations. *Atmospheric Research,* doi:10.1016/j.atmosres.2010.06.011 (Article in Press).

Li, L., Z.C. Hao, J.H. Wang, Z.H. Wang and Z.B. Yu (2008). Impact of future climate change on runoff in the head region of the Yellow River. *Journal of Hydrologic Engineering,* 13(5):347-354.

Liang, X., D. P. Lettenmaier, E. F. Wood and S. J. Burges (1994). A simple hydrologically based model of land surface water and energy fluxes for general circulation models. *Journal of Geophysical Research,* 99(14):415– 428.

Liu, J., S. Wang and Y. Huang (2007). Effect of climate change on runoff in a basin with mountain permafrost, Northwest China. *Permafrost and Periglacial Processes, 18:367-377.*

Lohmann, D., R. Nolte-Holube and E. Raschke (1996). A large scale horizontal routing model to be coupled to land surface parameterization schemes. *Tellus,* 48A:708-721.

Lopez, A., C. Tebaldi, M. New, D. Stainforth, M. Allen and J. Kettleborough (2006). Two approaches to quantifying uncertainty in global temperature changes. *Journal of Climate,* 19:4785– 4796.

Loukas, A., L. Vasiliades and N.R. Dalezios (2002). Potential climate change impacts on flood producing mechanisms in southern British Columbia, Canada using the CGCMA1 simulation results. *Journal of Hydrology,* 259:163-188.

Mailhot, A., A. Kingumbi, G. Talbot and A. Poulin (2010). Future changes in intensity and seasonal pattern of occurrence of daily and multi-day annual maximum precipitation over Canada. *Journal of Hydrology,* 388: 173-185.

Mantua, N.J., S.R. Hare, Y. Zhang, J.M. Wallace and R.C. Francis (1997). A Pacific interdecadal climate oscillation with impacts on salmon production. *B. of American Meteorological Society,* 78 (6): 1069-1079.

Mather G. K., D. E. Terblanche, F. E. Steffens and L. Fletcher (1997). Results of the South African cloud-seeding experiments using hygroscopic flares. *Journal of Applied Meteorology,* 36:1433–1447.

Maurer, E.P. (2007). Uncertainty in hydrologic impacts of climate change in the Sierra Nevada, California, under two emissions scenarios. *Climate Change,* 82:309–325.

Maurer, E. P., A.W. Wood, J.C. Adam, D.P. Lettenmaier and B. Nijssen (2002). A long term hydrologically based dataset of land surface fluxes and states for the conterminous United States. *Journal of Climate,* 15:3237-3251.

Maurer E. P. and H. G. Hidalgo (2008). Utility of daily vs. monthly large-scale climate data: an intercomparison of two statistical downscaling methods. *Hydrology and Earth System Sciences Discussion,* 4:3413–3440.

Maurer, E. P., L. Brekke, T. Pruitt and P. B. Duffy (2007). Fine-resolution climate projections enhance regional climate change impact studies. *Eos Trans. AGU,* 88(47):504.

Mays, L.W. (2005). *Water Resources Engineering,* 2005 edition. John Wiley & Sons, Hoboken, N.J.

May, L.W., R. Voss and E. Roeckner (2002). Changes in the mean and extremes of the hydrological cycle in Europe under enhanced greenhouse gas conditions in a global time slice experiment. *Adv. in Global Change Research*, 10:1–29.

McCabe, G.J. and M.A. Ayers (1989). Hydrologic effects of climate change in the Deleware River basin. *Water Resources Bulletin,* 25(6):1231-1242.

McGuffie, K., A.H. Sellers, N. Holbrook, Z. Kothavala, O. Balachova and J. Hoekstra (1999). Assessing simulations of daily temperature and precipitation variability with global climate models for present and enhanced greenhouse climates. *International Journal of Climatology,* 19:1–26.

McGurty, B. M. (1999). Turning silver into gold: Measuring the benefits of cloud seeding. *HydroReview,* 18:2-6.

Mearns, L.O., L. Giorgi, L.R. McDaniel and C. Shields (1995). Analysis of daily variability of precipitation in a nested regional climate model: comparison with observations and doubled CO_2 results. *Global Change,* 10:55-78

Mearns, L.O., R.W. Katz and S.H. Schneider (1984). Extreme high temperature events: changes in their probabilities with changes in mean temperature. *Journal of Applied Meteorology and Climatology,* 23:1601-1613

Mearns, L.O., S.H. Schneider, S.L. Thompson and L.R. McDaniel (1990). Analysis of climatevariability in general circulation models: Comparison with observations and changes in variability in $2XCO_2$ experiments. *J. Geophysical Research,* 95(20):469-490.

Medina, J.G. (2000). The feasibility of operational cloud seeding in the North Platte River Basin headwaters to increase mountain snowfall. Reclamation Technical ServiceCenter Report, Bureau of Reclamation, May 2000.

Meehl, G. A., J. M. Arblaster, and C. Tebaldi (2005). Understanding future patterns of increased precipitation intensity in climate model simulations. *Geophysical Research Letter*, 32, L18719, doi:10.1029/2005GL023680.

Meehl G.A. and CoAuthors (2007). The WCRP CMIP3 multimodel dataset – A new era in climate change research. *B. of American Meteorological Society*, 88:1383–1394.

Merritt, W.S., Y. Alila, M. Barton, B. Taylor, S. Cohen and D. Neilsen (2006). Hydrologic response to scenarios change in sub watersheds of the Okanagan basin, British Columbia. *Journal of Hydrology*, 326: 79–108.

Middelkoop, H., K. Daamen, D. Gellens, W. Grabs, J.C.J. Kwadijk, H. Lang, B.W.A.H. Parmet, B. Schadler, J. Schulla and K. Wilke (2001). Impact of climate change on hydrological regimes and water resources management in the Rhine Basin. *Climate Change*, 49:105-128.

Miller, N.L., J. Kim, R.K. Hartman and J. Fararra (1999). Downscaled climate and stream flow study of the southwestern U.S. *JAWRA*, 35(6):1525-1537.

Miller, W.P. and T.C. Piechota (2008). Regional analysis of trend and step changes observed in hydroclimatic variables around the Colorado River basin. *Journal of Hydrometeorology*, 9(5):1020-1034.

Milly, P.C.D., K.A. Dunne and A.V. Vecchia (2005). Global pattern of trends in streamflow and water availability in a changing climate. *Nature*, 438:347-350.

Milly, P. C. D., R. T. Wetherald, K. A. Dunne and T. L. Delworth (2002). Increasing risk of great floods in a changing climate. *Nature*, 415:514–517.

Minville, M., F. Brissette and R. Leconte (2008). Uncertainty of the impact of climate change on the hydrology of a Nordic watershed. *Journal of Hydrology*, 358:70-83.

Mitchell J.F.B. and W.J. Ingram W.J. (1992). Carbon dioxide and climate: mechanisms of changes in cloud. *Journal of Climate*, 5:5-21.

Morrison, A.E., S.T. Siems, M.J. Manton and A. Nazarov (2009). On the analysis of a cloud seeding dataset over Tasmania. *Journal of Applied Meteorology and Climatology*, 48:1267-1280.

Mote, P. W. (2003). Trends in snow water equivalent in the Pacific Northwest andtheir climatic causes. *Geophysical Research Letter*, 30**,** 1601, doi:10.1029/2003GL017258.

Mote, P. W. (2006). Climate-driven variability and trends in mountain snowpack in western North America. *Journal of Climate*, 19:6209– 6220.

Mote, P.W., A.F. Hamlet, M.P. Clark and D.P. Lettenmaier (2005). Declining mountain snowpack in western North America, *B. of American Meteorological Society*, 39-49, doi:10.1175/BAMS-86-1-39.

Murty, A.S.R., and CoAuthors (2000). 11-year warm cloud seeding experiment in Maharashtra State, India. *Journal of Weather Modification*, 32:10-20.

NAIWMC (North American Interstate Weather Modification Council) (2010). Cloud seeding Frequently Asked Questions (FAQs) (Access online 2010, www.naiwmc.org).

NASA news (2008). Access http://geology.com/nasa/human-linked-climate change.shtml

Newmann, M., G.P. Compo and M.A. Alexander (2003). ENSO-forced variability of the Pacific Decadal Oscillation. *Journal of Climate*, 16(23):3853-3857.

Noda, A. and T. Tokioka (1989). The effect of doubling the CO_2 concentration on convective and non-convective precipitation in a general circulation model coupled with a simple mixed layer ocean model. *J. Meteorological Society Japan*, 67:1057–1069.

NRC (National Research Council) of the National Academy of Sciences (2003). *Critical issues in weather modification research.* Board on Atmospheric Sciences and Climate, Division on Earth and Life Studies, National Academy Press, 123 pp.

Osborn, H.B. (1972). Comments by a hydrologic engineer on cloud seeding in Arizona. *Thirdconference on weather modification,* American meteorological Society, Rapid City, South Dakota, 146-151.

Osborn, T. J. and M. Hulme (1997). Development of a relationship between station and grid box rain day frequencies for climate model evaluation. *J. of Climate*, 10**:**1885-1908.

Osborn, T.J., M. Hulme, P.D. Jones and T.A. Basnett (2000). Observed trends in the daily intensity of United Kingdom precipitation. *Int. Journal of Climatology*, 20:347–364.

Palmer, T. and J. Ra¨isa¨nen (2002). Quantifying the risk of extreme seasonal precipitation events in a changing climate. *Nature*, 415:512–514.

Pandil, W. (2009). NAIWMC news. Study: Big impact with cloud seeding. Local News, August 29, 2009. Access http://www.minotdailynews.com/page/content.detail/id/531595.html?nav=5010

Papineu, J.M. (2001).Wintertime temperature anomalies in Alaska correlated with ENSO and PDO. *Int. Journal of Climatology*, 21:1577-1592.

Pfister, L., J. Kwadijk, A. Musy, A. Bronstert and L. Hoffmann (2004). Climate change, land use change and runoff prediction in the Rhine-Meuse basins. *River Research and Applications*, 20:229-241.

Pierce, D.W., T.P. Barnetta, B.D. Santer and P.J. Glecklerb (2009). Selecting global climate models for regional climate change studies. *PNAS*, 106(21):8441-8446.

Pierce, D.W., and CoAuthors (2008). Attribution of declining western U.S. snowpack to human. *American Meteorological Society*. doi: 10.1175/2008JCLI2405.1.

Pilgrim, D. H., Chapman, T. G. & Doran, D. G. (1988). Problems of rainfall–runoff modeling in arid and semiarid regions. *Hydrologic Sciences Journal*, 33(4):379–400.

Prudhomme, C., D. Jakob and C. Svensson (2003). Uncertainty and climate change impact on the flood regime of small UK catchments. *Journal of Hydrology*, 277:1-23.

Prudhomme, C., N. Reynard and S. Crooks (2002). Downscaling of global climate models for flood frequency analysis: where are we now? *Hydrologic Processes*, 16:1137-1150.

Pupacko, A. (1993). Variations in northern Sierra Nevada streamflow: Implications of climatechange. *Water Resources Bulletin*, 29:283–290.

Ra¨isa¨nen, J. (2005). Impact of increasing CO_2 on monthly to annual precipitation extremes: Analysis of the CMIP2 experiments. *Climate Dynamics*, 24:309–323.

Ra¨isa¨nen, J. and R, Joelsson (2001). Changes in average and extreme precipitation in two regional climate model experiments. *Tellus*, 53A:547–566

Rasch, P.J., J. Latham and C. C. Chen (2009). Geoengineering by cloud seeding: influence on sea ice and climate system. *Environmental Research Letters*, 4, (2009), doi:10.1088/1748-9326/4/4/045112

Regonda, S.K., B. Rajagopalan, M. Clark and J. Pitlick (2005). Seasonal cycle shifts in hydroclimatology over the western United States. *Journal of Climate*, 18(2): 372-384.

Reynard, N.S., C. Prudhomme and S.M. Crooks (2001). The flood characteristics of large U.K. Rivers: Potential effects of changing climate and land use. *Climate Change,* 48:343-359.

Rind, D., R. Goldberg and R. Ruedy (1989). Change in climate variability in the 21st century. *Climate Change,* 14:5-37.

Robson, A.J. (2003). Evidence for trends in UK flooding. Royal society meeting and Philosophical Transaction Journal. *Proceedings of flood risk in a changing climate.* Statistical Royal Society, 21-22 Nov 2001, London.

Rodbell, D. T., Seltzer, G. O., Anderson, D. M., Abbott, M. B., Enfield, D. B. & Newman, J. H. (1999). An ~15,000-Year Record of El-Niño Alluviation in Southwestern Ecuador. *Science,* 283:516–520

Roos, M. (1987). Possible changes in California snowmelt patterns. *Proceedings of the Fourth Pacific Climate Workshop,* Pacific Grove, CA, PACLIM, 22–31.

Roos, M. (1991). A trend of decreasing snowmelt runoff in Northern California. *Proceedings of the 59th Western Snow Conference, Juneau, AK,* Western Snow Conference, 29–36.

Rosenfeld, D., and W.L. Woodley (1989). Effects of cloud seeding in West Texas. *J. Applied Meteorology*, 28:1050–1080.

Rosenfeld, D., and W.L. Woodley (1993). Effects of cloud seeding in West Texas: Additional results and new insights. *J. Applied Meteorology*, 32:1848-1866.

Ryan, T., J. Busto, A.W. Huggins and S.M. Hunter (2005). Weather modification for precipitation augmentation and its potential usefulness to the Colorado River Basin States. A Report, October 2005.

Sanchez, J. L., J. Dessens, J.L. Marcos, J.T. Fernández (1999). Comparison of rain water silver concentrations from seeded and non-seeded days in Leon (Spain). *J. of Weather Modification*, 31:87-90.

Schoennagel, T., T. T. Veblen, W.H. Romme, J.S. Sibold and E. R. Cook (2005). ENSO and PDO variability affect drought-induced fire occurrence in Rocky mountain subalpine forest. *Ecological Applications,* 15(6):2000-2014.

Schreider, S. Y., D.I. Smith and A.J. Jakeman (2000). Climate change impacts on urban flooding. *Climate Change*, 47:91-115.

Seager, R. and CoAuthors (2007). Model projections of an imminent transition to a more arid climate in Southwestern North America. *Science,* 316:1181-1184.

Seely, E.H. and D.G. DeCoursey (1975). Hydrologic impact of weather modification. *Water Resources Bulletin*, 11(2):365-369.

Segal, Y., A. Khain, M. Pinsky and D. Rosenfeld (2004). Effects of hygroscopic seeding on raindrop formation. *Atmospheric Research*, 71:3-34.

Sell, R.S. and F.L. Leistritz (1998). Economic impact of reducing hail and enhancing rainfall in North Dakota. 29 p., (Access NAIWMC FAQs).

Semenov, V. A., and L. Bengtsson (2002). Secular trend in daily precipitation characteristics:Greenhouse gas simulation with a coupled AOGCM. *Climate Dynamics*, 19:123–140.

Sharon, D., A. Kessler, A. Cohen and E. Doveh (2008). The history and recent revision of Israel's cloud seeding program. *Israel Journal of Earth Sciences*, 57(1):65-69.

Shaw, H. (2006). California has an expensive thirst. *Stockton Record*, 15 February 2006. Access www.recordnet.com/apps/pbcs.dll/article?AID=/20060215/NEWS01/602150336/1001/ NEWS01

Silverman, B.A. (2001). A critical assessment of glaciogenic seeding of convective clouds for rainfall enhancement. *B. of American Meteorological Society*, 82(5):903-923.

Silverman, B.A. (2003). A critical assessment of hygroscopic seeding of convective clouds for rainfall enhancement. *B. of American Meteorological Society*, 1219-1230, doi:10.1175/BAMS-84-9-1219.

Silverman, B.A. (2010). An evaluation of eleven operational cloud seeding programs in the watersheds of the Sierra Nevada Mountains. *Atmospheric Research*, doi: 10.1016/j.atmosres.2010.06.013 (Article in Press).

Silverman, B.A. and W. Sukarnjanaset (2000). Results of the Thailand warm-cloud hygroscopic particle seeding experiment. *Journal of Applied Meteorology*, 39:1160-1175.

Smith, P.L., H.D. Orville, B.A. Boe and J.L. Stith (1992a). A status report on weather modification research in the Dakotas. *Atmospheric Research*, 28:271-298.

Smith, P.L., Jr., L.R. Johnson, D.L. Priegnitz, B.A. Boe and P.W. Mielke (1997). An exploratory analysis of crop hail insurance data for evidence of cloud seeding effects in North Dakota. *Journal of Applied Meteorology*, 36:463-473.

Smith, P.L., Jr., L.R. Johnson, D.L. Priegnitz, and P.W. Mielke, Jr., (1992b). A target control analysis of wheat yield data for the North Dakota cloud modification project region. *Journal of Weather Modificatio*n, 24:98-105.

Snyder, M.A., J.L. Bell, L.C. Sloan, P.B. Duffy and B. Govindasamy (2002). Climate responses to a doubling of atmospheric CO_2 for a climatically vulnerable region. *Geophysical Research Letters*, 29:1–4.

Spak, S., T. Holloway, B. Lynn, and R. Goldberg (2007). A comparison of statistical and dynamical downscaling for surface temperature in North America. *Journal of Geophysical Research*, 112, D08101, doi:10.1029/2005JD006712.

Stephens, M. A. (1970). Use of the Kolmogorov–Smirnov, Cramer– von-Mises and related statistics without extensive tables. *J. Royal Statistical Society,* 32B:115–122.

Stauffer, N.E., Jr., (2001). Cloud seeding – the Utah experience. WMA, *Journal of Weather Modification*, 33:70-73.

Stauffer, N.E. and K. Williams (2000). Utah cloud seeding program, increased runoff/cost analysis. Technical Report, Utah Department of Natural Resources, Division of Water Resources.

Stewart, I. T., D. R. Cayan, and M. D. Dettinger (2005). Changes toward earlier streamflow timing across western North America. *Journal of Climate*, 18:1136–1155.

Strzepek, K.M. and D.N. Yates (1997). Climate change impacts on the hydrologic resources of Europe: A simplified continental scale analysis. *Climate Change*, 36:79-92.

Stute, M., A. Clement and G. Lohmann (2001). Global climate models: Past, Present and future. From the Academy, *PNAS*, 98(19):10529-10530.

Super, A.B. and J.A. Heimbach, Jr., (2005). Propane cloud seeding experiment overview: Wasatch Plateau, Utah, during winter of 2003/04, *Journal of Weather Modification*, 37, 32 pp, May 2005.

Tebaldi, C., K. Hayhoe, J. M. Arblaster, and G. A. Meehl (2006). Going to the extremes: An intercomparison of model-simulated historical and future changes in extreme events. *Climate Change*, 79:185– 211.

Tebaldi, C., L. O. Mearns, D. Nychka, and R. L. Smith (2004). Regional probabilities of precipitation change: A Bayesian analysis of multimodel simulations. *Geophysical Research Letter*, 31, L24213, doi:10.1029/2004GL021276.

Tebaldi, C., R. L. Smith, D. Nychka, and L. O. Mearns (2005). Quantifying uncertainty in projections of regional climate change: A Bayesian approach to the analysis of multi model ensembles. *Journal of Climate*, 18:1524–1540.

Terblanche, D.E., F.E. Steffens, L. Fletcher and M.P. Mittermaier (2000). Towards the operational application of hygroscopic flares for rainfall enhancement in South Africa. *Journal of Applied Meteorology*, 39:1811-1821.

Timilsena, J., T. Piechota, G. Tootle and A. Singh (2009). Associations of interdecadal/interannual climate variability and long-term Colorado River basin streamflow. *Journal of Hydrology*, 365(3-4):289-301.

Tootle, G.A. and T.C. Piechota (2006). Relationships between Pacific and Atlantic Ocean sea surface temperatures and U.S. streamflow variability. *Water Resources Research*, 42, W07411, doi:10.1029/2005WR004184.

Tootle, G.A., T.C. Piechota and F. Gutierrez (2008). The relationships between Pacific and Atlantic Ocean Sea surface temperatures and Colombian streamflow variability. *Journal of Hydrology*, 349:268-276

Tripathi, S., V.V. Srinivas and R.S. Nanjundiah (2006). Downscaling of precipitation for climate change scenarios: A support vector machine approach. *Journal of Hydrology*, 330(3-4):621-640.

Tsiouris E.S., A.F. Aravanopoulos, N.L. Papadoyiannis, K.M. Sofoniou, N. Polyzopoulos, M.M. Christodoulou, F.V. Samanidou, A.G. Zachariadis, H. I.A. Constantinidou (2002a). Soil silver content of agricultural areas subjected to cloud seeding with silver iodide. *Fresenius Environmental Bulletin*, 11:697-702.

Tsiouris E.S., A.F. Aravanopoulos, N.L. Papadoyiannis, K.M. Sofoniou, F.V. Samanidou, A.G. Zachariadis, H.-I.A. Constantinidou (2002b). Soil silver mobility in areas subjected to cloud seeding with AgI. *Fresenius Environmental Bulletin*, 12:1059-1063.

Tucker, G.E. and R. Slingerland (1997). Drainage basin response to climate change. *Water Resources Research*, 33(8): 2031-2047

Udall, B. and G. Bates (2007). Climatic and hydrologic trends in the Western U.S.: A review of recent peer reviewed research. Intermountain West Climate Summary, Jan. 2007.

U.S. DoI (Department of Interior), Bureau of Reclamation (2003). Water 2025: Preventing crises and conflict in the West, May 2003. Access http://www.doi.gov/water2025/index.html

U.S. Geological Survey, USGS (2004). Climatic fluctuations, drought, and flow in the Colorado River Basin. USGS Fact Sheet 2004-3062, August 2004. Access http://pubs.usgs.gov/fs/2004/3062/

U.S. Global Change Research Program (2009). Great Plains climate change. Access http://geology.com/climate-change/great-plains/

U.S. Water Resources Council (1981). Guidelines for determining flood flow frequency. Bulletin 17B (revised), Hydrology committee, *Water Resources Research Council*, Washington.

Utah Department of Natural Resources (Division of Water Resources), (2005). Utah cloud seeding program: Increased runoff/cost analysis. Salt Lake, UT, 15 p.

Vanrheenen, N.T., A.W. Wood, R.N. Palmer and D.P. Lettenmaier (2004). Potential implications of PCM climate change scenarios for Sacramento San Joaquin River Basin hydrology and resources. *Climatic Change,* 62**:**257–281

Vicuna, S., E.P. Maurer, B. Joyce, J.A. Dracup and D. Purkey (2007). The sensitivity of California water resources to climate change scenarios. *JAWRA,* 43(2):482–498.

Voss, R., W. May and E. Roeckner (2002). Enhanced resolution modeling study on anthropogenic climate change: changes in the extremes of the hydrologicalcycle. *International Journal of Climatology,* 22:755–777.

Wahl, K. L. (1992). Evaluation of trends in runoff in the western United States: Managing water resources during global change. *JAWRA,* 701–710.

Walsh, K. and A.B. Pittock (1998). Potential changes in tropical storms, hurricanes, and extreme rainfall events as a result of climate change. *Climate Change*, 39:199-213.

Wang, J., Y. Hong, J. Gourley, P. Adhikari, L. Li and F. Su (2009). Quantitative assessment of climate change and human impacts on long term hydrologic response. *Int. Journal of Climatology*, doi: 10.1002/joc.2023.

Warburton, J. A., S. K. Chai, and L. G. Young (1995). A new method for assessing snowfall enhancement by silver iodide seeding using physical and chemical techniques, *Journal of Applied Meteorology*, 35:1569-1573.

Warburton, J.A., S.K. Chai, R.H. Stone, L.G. Young (1996). The assessment of snowpack enhancement by silver iodide cloud-seeding using the physics and chemistry of the snowfall. *Journal of Weather Modification*, 28:19-28.

Watterson, I. G. and M. R. Dix (2003). Simulated changes due to global warming in daily precipitation means and extremes and their interpretation using the gamma distribution. *Journal of Geophysical Research*, 108(D13), 4379, doi:10.1029/2002JD002928.

Watterson, I.G., M.R. Dix, H.B. Gordon and J.L. McGregor (1995). The CSIRO nine level atmospheric general circulation model and its equilibrium present and doubled CO_2 climates. *Australian Meteorological Magazine*, 44:111-125

Wehner, M. F. (2004). Predicted twenty-first-century changes in seasonal extreme precipitation events in the parallel climate model. *Journal of Climate*, 17:4281– 4290.

Westerling, A. and T. Swetnam (2003). Interannual to decadal drought and wildfire in the western United States. *EOS*, 84: 545–560.

Wetterhall F., S. Halldin and C. Xu (2005). Statistical precipitation downscaling in central Sweden with the analogue method. *Journal of Hydrology*, 306(1-4):174-190.

Widmann, M., C.S. Bretherton and E.P. Salathe (2002). Statistical precipitation downscaling over the Northwestern United States using numerically simulated precipitation as a predictor. *Journal of Climate*, 16:799-816.

Wilby R. L., T. Wigley, D. Conway, P.D. Jones, B.C. Hewitson and D.S. Wilks (1998). Statistical downscaling of general circulation model output: a comparison of methods. *Water Resources Research*, 34(11):2995–3008.

Wilks D.S. (1999). Multisite downscaling of daily precipitation with a stochastic weather generator. *Climate Research*, 11:125-136.

Williams, B.D. and J.A. Denholm (2009). Assessment of the environmental toxicity of silver iodide with reference to a cloud seeding trial in the snowy mountains of Australia. *J. Weather Modification*, 41:75-96.

WMA (Weather Modification Association), (2005). *Weather Modification Association Capability Statement.* Access www.weathermodification.org/capabilities.htm.

WMA, (2009). Weather Modification Association position statement on the environmental impact of using silver iodide as a cloud seeding agent. WMA, July 2009.

WMO (World Meteorological Organization) (2000). Register of weather modification projects 2000 (TD No. 1094): World Meteorological Organization, 2000.

Wood, A.W., D.P. Lettenmaier and R.N. Palmer (1997). Assessing climate change implications for water resources planning. *Climate Change,* 37(1):203-228.

Wood, A. W., E. P. Maurer, A. Kumar and D. P. Lettenmaier (2002). Long-range experimental hydrologic forecasting for the eastern United States. *Geophysical Research Atmospheres*, 107(D20), 4429, doi:10.1029/2001JD000659.

Wood, A. W., L.R. Leung, V. Sridhar and D.P. Lettenmaier (2004). Hydrologic implications of dynamical and statistical approaches to downscaling climate model outputs.*Climatic Change*, 15:189-216.

Woodley, W.L. and D. Rosenfeld (2008). Evaluation of the effectiveness of cloud seeding in Texas from 2002 through 2006. Access ams.confex.com/ams/pdfpapers/138761.pdf

Woodley, W.M., D. Rosenfeld and A. Strautins (2000). Identification of a seeding signature in Texas Using Vlulti Spectral Satellite. *Journal of Weather Modification*, 32:37-53.

WWDC (Wyoming Water Development Commission) (2005). Wyoming level II weather modification feasibility study: Executive summary. Prepared by Weather Modification Inc for the WWDC, March 2005.

WWDC, (2010). Wyoming Weather Modification Pilot Project. Access http://www.ral.ucar.edu/projects/wyoming/ (cited March 2010)

Xu, C. (1999). From GCMs to river flow: a review of downscaling methods and hydrological modeling approaches. *Progress in Physical Geography,* 23(2):229-249.

Yin, Y., Z. Levin, T. Reisin and S. Tzivion, (2000). Seeding convective clouds with hygroscopic flares: Numerical simulations using a cloud model with detailed microphysics. *J. Applied Meteorology*, 39:1460–1472.

____, (2001). On the response of radar-derived properties to hygroscopic flare seeding. *J. Applied Meteorology*, 40:1654–1661.

Yu, B. and F.W. Zwiers (2007). The impact of combined ENSO and PDO on the PNA climate: a 1000 year climate modeling study. *Climate Dynamics,* 29:837-851.

Zhang, C., M. A. Nearing, J. D. Garbrecht and J. L. Steiner (2005). Downscaling monthly forecasts to simulate impacts of climate change on soil erosion and wheat production. *Soil Science Society of America Journal*, 68:1376-1385.

Zovne, J.J. and J.K. Koelliker (1979). Hydrologic and economic impact of added rainfall in Kansas. For presentation at the 1979 summer meeting of American Society of Agricultural Engineers and Canadian Society of Agricultural Engineering.

Zvi, A.B. (1988). Enhancement of runoff from a small watershed by cloud seeding. *Journal of Hydrology,* 101:291-303.

Zvi, A.B. and A. Fanar (1997). The effect of randomized cloud seeding on runoff depth from a small watershed in central Israel. *Journal of Hydrology,* 191:161-178.

Zvi, A.B. and M. Langerman (1993). Assessment of runoff enhancement by randomized cloud seeding in case of a carry-over flow. *Journal of Hydrology,* 142:391-408.

Zwiers, F.W. and V.V. Kharin (1998). Changes in the extremes of the climate simulated by CCC GCM2 under CO_2 doubling. *Journal of Climate,* 11:2200-2222.

http://gdo-dcp.ucllnl.org/downscaled_cmip3_projections/ (Download link for bias corrected and spatially downscaled 1/8º climate projections derived from WCRPs CMIP3 data)

VITA

Graduate College
University of Nevada, Las Vegas

Anil Acharya

Degrees:

Bachelor of Science, Civil Engineering, 2003
Institute of Engineering, Tribhuvan University, Nepal

Master of Science, Water Engineering and Management, 2006
Asian Institute of Technology, Thailand

Dissertation Title: Impacts of Climate Change and Weather Modification on Hydrologic Characteristics of Watersheds in the Western United States.

Dissertation Examination Committee:

Chairperson, Thomas C. Piechota, Ph.D, P.E.
Committee Member, Sajjad Ahmad, Ph.D, P.E.
Committee Member, Jacimaria Batista, Ph.D, P.E.
Committee Member, Kumud Acharya, Ph.D.
Graduate Faculty Representative, Anton Westveld, Ph.D.